

INVESTIGATION OF THE DYNAMIC PROPERTIES OF PLATE-LIKE
STRUCTURES

A THESIS SUBMITTED TO
THE GRADUATE SCHOOL OF NATURAL AND APPLIED SCIENCES
OF
MIDDLE EAST TECHNICAL UNIVERSITY

BY

ENGİN KAHRAMAN

IN PARTIAL FULFILLMENT OF THE REQUIREMENTS
FOR
THE DEGREE OF MASTER OF SCIENCE
IN
AEROSPACE ENGINEERING

SEPTEMBER 2011

Approval of the thesis:

INVESTIGATION OF THE DYNAMIC PROPERTIES OF PLATE-LIKE STRUCTURES

Submitted to **ENGİN KAHRAMAN** in partial fulfillment of the requirements for the degree of **Master of Science in Aerospace Engineering, Middle East Technical University** by,

Prof. Dr. Canan Özgen

Dean, Graduate School of **Natural and Applied Sciences**

Prof. Dr. Ozan TEKİNALP

Head of Department, **Aerospace Engineering**

Assist. Prof. Dr. Melin ŞAHİN

Supervisor, **Aerospace Engineering Dept., METU**

Examining Committee Members

Prof. Dr. Yavuz YAMAN

Aerospace Engineering Dept., METU

Assist. Prof. Dr. Melin ŞAHİN

Aerospace Engineering Dept., METU

Prof. Dr. Serkan ÖZGEN

Aerospace Engineering Dept., METU

Assist. Prof. Dr. Ercan GÜRSES

Aerospace Engineering Dept., METU

Dr. Muvaffak HASAN

Chief Engineer, TAI

Date:

08/09/2011

I hereby declare that all information in this document has been obtained and presented in accordance with academic rules and ethical conduct. I also declare that, as required by these rules and conduct, I have fully cited and referenced all material and results that are not original to this work.

Name, Last name : Engin Kahraman

Signature :

ABSTRACT

INVESTIGATION OF THE DYNAMIC PROPERTIES OF PLATE-LIKE STRUCTURES

Kahraman,Engin

M.Sc., Department of Aerospace Engineering

Supervisor: Assist. Prof. Dr. Melin Şahin

September 2011, 123 Pages

This study presents the investigation and the verification of the modal parameters of a plate-like structure by using different modal analysis methods. A fin-like structure which is generally used in aircraft is selected as a subcategory of a plate-like test structure.

In the first part of the thesis, the natural frequencies and the corresponding mode shapes of the fin are extracted by Finite Element Analysis method. Classical Modal Analysis and Testing methods comprising both impact hammer and modal shaker applications are then applied in order to obtain the modal parameters such as; resonance frequencies, mode shapes and damping ratios.

In the second part, a recent modal analysis technique, Operational Modal Analysis, is also applied in the laboratory environment. Since Operational Modal Analysis method does not require any information of input forcing, the fin structure is tested under both mechanical and acoustical types of excitations without measuring the given input forces.

Finally, Operational Modal Analysis and Testing is also performed under various flow conditions generated in the wind tunnel which may simulate the real operating environment for the fin structure. The modal parameters extracted under these flow conditions are then compared with the previously obtained Finite Element, Classical and Operational Modal Analyses results.

Keywords: Plate-like Structures, Finite Element Modelling and Analysis, Modal Analysis and Testing, Operational Modal Analysis, Vortex-induced Vibration

ÖZ

PLAKA BENZERİ YAPILARDA DİNAMİK ÖZELLİKLERİN ARAŞTIRILMASI

Kahraman,Engin

Yüksek Lisans, Havacılık ve Uzay Mühendisliği Bölümü

Tez Yöneticisi: Yrd. Doç. Dr. Melin Şahin

Eylül 2011, 123 Sayfa

Bu çalışma, farklı modal analiz yöntemleriyle plaka benzeri bir yapının modal parametrelerinin araştırılmasını ve doğrulanmasını sunmaktadır. Genel olarak uçaklarda kullanılan ve plaka benzeri yapıların bir alt kategorisi olan fin benzeri yapı test yapısı olarak seçilmiştir.

Tezin ilk bölümünde, sonlu elemanlar yöntemi kullanılarak finin doğal frekansları ve bu frekanslara karşılık gelen biçim şekilleri çıkarılmıştır. Daha sonra, rezonans frekansları, biçim şekilleri ve sönümlenme oranları gibi modal parametreleri bulmak için darbe çekici ve modal titreştirici uygulamalarını içeren Klasik Modal Analiz ve Testler de uygulanmıştır.

İkinci bölümde, yeni bir yöntem olan Operasyonel Modal Analiz yöntemi laboratuvar koşullarında uygulanmıştır. Operasyonel Modal Analiz yöntemi girdi kuvvet bilgisine ihtiyaç duymadığından fin yapı mekanik ve akustik tipte uyarım altında girdi kuvvetleri ölçülmeden de test edilmiştir.

Son olarak, Operasyonel Modal Analiz ve Testler finin gerçek çalışma ortamını temsil edecek şekilde rüzgar tüneline oluşturulmuş çeşitli akış durumlarında da

gerçekleştirilmiştir. Bu akış durumlarından elde edilen modal parametreler daha önceden sonlu elemanlar, klasik ve operasyonel modal analizlerden bulunan sonuçlarla da karşılaştırılmıştır.

Anahtar Kelimeler: Plaka Benzeri Yapılar, Sonlu Elemanlar Yöntem ve Analizi, Modal Analiz ve Testler, Operasyonel Modal Analiz, Girdap Uyarımlı Titreşimler

To my mother...

'annem'e...

ACKNOWLEDGEMENTS

I would like to express my deepest gratitude and thanks to my supervisor Assist. Prof. Dr. Melin Şahin for his guidance, support and criticism. I will never forget his encouragement that motivated me to introduce this study.

I also would like to thank Prof. Dr. Yavuz Yaman, Prof. Dr. Serkan Özgen and Assist. Prof. Dr. Ercan Gürses for their helpful criticism and valuable comments.

I would like to thank my company TAI and my chief Dr. Muvaffak Hasan for his support and understandings throughout my study.

My special thanks are for my leader Derya Gürak and my colleague Fatih Karadal who always supported me and share their valuable experiences in helpful discussions.

I would also thank my friends for their friendship and understandings. Özge Polat deserves more by being the fellow friend of me during this challenging period.

I am grateful to the precious lady Dilcu Keleş for her understanding and endless support before and during this study.

Finally, I would express my deepest thanks to my father for his encouragements and support throughout my whole life. I would like to thank my sister, Gülçin for her understanding and her warm motivation. And my greatest thanks go to my mother for her patience and love in all moments of my life. It would be never possible without her fondness and wishes.

TABLE OF CONTENTS

ABSTRACT	iv
ÖZ.....	vi
ACKNOWLEDGEMENTS	ix
TABLE OF CONTENTS	x
LIST OF TABLES	xiii
LIST OF FIGURES	xvi
CHAPTERS	1
1. INTRODUCTION	1
1.1 Motivations of the study	1
1.2 Objectives of the study	2
1.3 Limitations of the study	2
1.4 Outline of the study	3
2. LITERATURE SURVEY	5
2.1 Introduction	5
2.2 Finite Element Modelling and Analysis	5
2.3 Classical Modal Analysis and Testing	6
2.4 Operational Modal Analysis and Testing	7
2.4.1 Types of Operational Modal Analysis techniques.....	7
2.4.2 Harmonic excitation detection and elimination in OMA	8
2.4.3 Mode shapes and Operating Deflection Shapes in OMA.....	9
2.4.4 Operational Modal Analysis applications.....	10
2.5 Vortex-Induced Vibrations	12
2.5.1 Analytical studies	13
2.5.2 Experimental studies	13
2.6 Summary	14
3. FINITE ELEMENT MODELLING AND ANALYSIS OF PLATE-LIKE STRUCTURE ...	15
3.1 Introduction	15
3.2 General information on plate-like test structure	15
3.2.1 General properties of fin-like structures.....	15
3.2.2 Geometrical and material properties of fin-like structure	17

3.3	Finite element analysis of fin-like structure	18
3.4	Summary	22
4.	MODAL TESTING OF FIN-LIKE STRUCTURE VIA CLASSICAL MODAL ANALYSIS.....	23
4.1	Introduction	23
4.2	Classical Modal Analysis theory	23
4.3	Test setup and software for Classical Modal Analysis tests.....	25
4.4	Classical Modal Analysis tests	29
4.4.1	Impact hammer tests	29
4.4.2	Shaker tests with random noise input.....	37
4.4.3	Shaker tests with sine sweep input signal	43
4.5	Summary	48
5.	MODAL TESTING OF FIN-LIKE STRUCTURE VIA OPERATIONAL MODAL ANALYSIS IN IN-VACUO CONDITIONS.....	49
5.1	Introduction	49
5.2	Operational Modal Analysis Theory	49
5.3	Test setup and software for Operational Modal Analysis tests.....	54
5.4	Operational Modal Analysis tests in in-vacuo conditions.....	58
5.4.1	Operational Modal Analysis by using shaker excitation with random noise input signal.....	59
5.4.2	Operational Modal Analysis by using acoustic noise excitation	65
5.5	Summary	73
6.	MODAL TESTING OF FIN-LIKE STRUCTURE VIA OPERATIONAL MODAL ANALYSIS IN WIND TUNNEL CONDITIONS	75
6.1	Introduction	75
6.2	Wind tunnel and test setup	75
6.3	Operational Modal Analysis tests in wind tunnel.....	78
6.3.1	Tests by OMA in wind tunnel without vortex generator	79
6.3.2	Tests by OMA in wind tunnel with vortex generator	96
6.4	Summary	108
7.	CONCLUSIONS	109
7.1	General conclusions	109
7.2	Recommendations for future works	111
	REFERENCES.....	112
	APPENDICES	117
	APPENDIX A.....	118
A.	ADDITIONAL ANALYSES.....	118

A.1. Mesh independency check for Finite Element Analysis(FEA).....	118
A.2. Finite Element Analysis(FEA) for the fixture bar used in Classical Modal Analysis tests	119
A.3. Finite Element Analysis(FEA) for the test base used in Operational Modal Analysis tests	121
APPENDIX B.....	122
B. ADDITIONAL INFORMATIONS	122
B.1. Wind tunnel radial blower rotational speed vs. flow speeds	122

LIST OF TABLES

TABLES

Table 3.1.	Material properties for aluminium	17
Table 3.2.	Natural frequencies of fin-like structure obtained from FEA	19
Table 3.3.	Natural frequencies of fin-like structure by adding the mass effects of accelerometers	21
Table 4.1.	FFT Analysis Settings.....	30
Table 4.2.	Resonance frequencies and damping ratios of fin-like structure from impact hammer test	34
Table 4.3.	MAC table for impact hammer test and FEA results	36
Table 4.4.	FFT analysis setup parameters for random noise shaker test.....	37
Table 4.5.	Resonance frequencies and damping ratios of the fin from random noise shaker test.....	39
Table 4.6.	MAC table for random noise shaker test and FEA results.....	42
Table 4.7.	FFT analysis setup parameters for sine-sweep shaker test	43
Table 4.8.	Resonance frequencies and damping ratios of the fin from sine-sweep shaker test	45
Table 4.9.	MAC table for sine-sweep shaker test and FEA results	47
Table 4.10.	Comparison of FEA and Classical Modal Analysis tests results for the fin-like structure.....	48
Table 5.1.	Resonance frequencies by OMA-FDD method and differences from CMA random noise shaker test	61
Table 5.2.	Damping ratios by OMA and CMA for shaker test with random noise input	62
Table 5.3.	MAC table for OMA and CMA with random noise shaker input	64
Table 5.4.	MAC table OMA with random noise shaker input and FEA	65
Table 5.5.	Resonance frequencies by OMA-FDD method with acoustic noise input and differences from impact hammer test result	67
Table 5.6.	Damping ratios by OMA with acoustic noise input and impact hammer test	68

Table 5.7.	Resonance frequencies extracted by OMA-FDD method using different number of accelerometers	71
Table 5.8.	MAC table for OMA acoustic noise (five accelerometers case) and impact tests results	73
Table 6.1.	Automatic Mode Extraction parameters for OMA wind tunnel tests ...	79
Table 6.2.	Resonance frequencies and damping ratios extracted from OMA wind tunnel test with flow speed=4.78 m/s	81
Table 6.3.	Resonance frequencies extracted by OMA for different flow speeds in wind tunnel.....	82
Table 6.4.	Damping ratios extracted by OMA for different flow speeds in wind tunnel.....	82
Table 6.5.	Standard deviations of damping ratios extracted by OMA-EFDD for different flow speed conditions.....	83
Table 6.6.	Resonance frequencies and damping ratios extracted from OMA wind tunnel test with flow speed=14.79 m/s.....	84
Table 6.7.	Standard deviations for damping ratios extracted by OMA-EFDD for the wind tunnel test with flow speed=14.79 m/s.....	85
Table 6.8.	Damping ratios of impact hammer test and OMA test in wind tunnel with high speed and their differences	86
Table 6.9.	Resonance frequencies extracted from OMA wind tunnel test for different angle of attacks with flow speed=4.78 m/s	88
Table 6.10.	Damping ratios extracted from OMA wind tunnel test for different angle of attacks with flow speed=4.78 m/s.....	88
Table 6.11.	Resonance frequencies and damping ratios of the fin extracted from the tunnel tests with different flow speed and angle of attack combinations	92
Table 6.12.	MAC table for OMA in wind tunnel and FEA results	95
Table 6.13.	Circular cylinder positions for the vibration levels investigation.....	99
Table 6.14.	Resonance frequencies extracted by OMA for different positions of vortex generator 1	101
Table 6.15.	Damping ratios extracted by OMA for different positions of vortex generator 1.....	102
Table 6.16.	Resonance frequencies extracted from the OMA tests with and without vortex generators.....	105

Table 6.17.	Damping ratios extracted from the OMA tests with and without vortex generators	106
Table 6.18.	MAC table for the condition with vortex generator 1 in wind tunnel and FEA results (For reduced measurement point set)	107
Table 6.19.	MAC table for the condition with vortex generator 2 in wind tunnel and FEA results (For reduced measurement point set)	107
Table A.1.	First five natural frequencies of the fin for different mesh densities	118
Table B.1.	Blower motor rotational speed vs. flow speed table	122

LIST OF FIGURES

FIGURES

Figure 3.1.	Vertical stabilizer of Turkish Stars Northrop NF-5.....	16
Figure 3.2.	Antennas of KT-1T Aircraft.....	16
Figure 3.3.	(a) Geometry of fin-like structure (b) Dimensions of fin-like structure.....	17
Figure 3.4.	Finite element model of the fin-like structure	18
Figure 3.5.	First five mode shapes of the fin-like structure extracted from FEA...20	
Figure 4.1.	Analysis of a system	23
Figure 4.2.	Test setup for the classical modal analysis tests	25
Figure 4.3.	Text fixture bar and fixed fin.....	26
Figure 4.4.	Shaker stringer attachment.....	27
Figure 4.5.	Impulse shapes (left) and force spectrums (right) on an aluminium plate for different impact hammer tips [62].	28
Figure 4.6.	Sample screen of PULSE™ Labshop Software.....	29
Figure 4.7.	A sample acceleration-time history via impact hammer test	31
Figure 4.8.	Measurement/excitation points over the fin and hammer roving direction	32
Figure 4.9.	Frequency Response Functions from impact hammer test results	32
Figure 4.10.	Composite FRF curve from the impact hammer test results.....	33
Figure 4.11.	First five mode shapes of the fin extracted from impact hammer test	35
Figure 4.12.	MAC diagram for impact hammer test and FEA results.....	36
Figure 4.13.	FRF plots for shaker test with random noise	38
Figure 4.14.	Composite FRF plot for shaker test with random noise.....	39
Figure 4.15.	First five mode shapes of the fin extracted from shaker test with random noise.....	41
Figure 4.16.	MAC diagram for random noise shaker test and FEA results.....	42
Figure 4.17.	FRF plots for shaker test with sine-sweep input.....	44
Figure 4.18.	Composite FRF plot for shaker test with sine-sweep input.....	44
Figure 4.19.	First five mode shapes of the fin extracted from shaker test with sine-sweep input.....	46

Figure 4.20.	MAC diagram for sine-sweep shaker test and FEA results	47
Figure 5.1.	Sample SVD Plot	51
Figure 5.2.	Inverse Discrete Fourier Transform(IDFT) process for EFDD method.....	52
Figure 5.3.	Natural frequency(left) and damping ratio(right) calculation in EFDD method.....	52
Figure 5.4.	Acoustic noise excitation equipments and placements	55
Figure 5.5.	OMA Software analysis options screen.....	56
Figure 5.6.	Sample screen for mode extraction in OMA software	58
Figure 5.7.	Average SVD plot from shaker random noise OMA test.....	60
Figure 5.8.	First five mode shapes of the fin extracted from shaker test with random noise input by OMA.....	63
Figure 5.9.	MAC diagram for OMA and CMA with random noise shaker input	64
Figure 5.10.	Reduced set of measurement points for OMA tests.....	66
Figure 5.11.	Average SVD plot for OMA test with acoustic noise input	67
Figure 5.12.	A sample position for five accelerometers	69
Figure 5.13.	Average SVD plot for OMA acoustic noise test with 5 accelerometers set	70
Figure 5.14.	The first three mode shapes of the fin extracted from OMA test with acoustic noise input (five accelerometer case).....	72
Figure 5.15.	MAC diagram for OMA acoustic noise (five accelerometers case) and impact tests results	73
Figure 6.1.	Wind tunnel sections and dimensions	76
Figure 6.2.	Fin mounting frame location for wind tunnel tests	77
Figure 6.3.	(a) Test base location on mounting frame (b) Test base top view	78
Figure 6.4.	SVD plot for OMA test in tunnel with flow speed=4.78 m/s.....	80
Figure 6.5.	SVD plot for the OMA test in wind tunnel with flow speed=14.79m/s.....	84
Figure 6.6.	Output PSD curves for the fin under different flow speed conditions in wind tunnel.....	87
Figure 6.7.	Output PSD curves for the fin for changing angle of attack (a) All modes (b) First mode	90
Figure 6.8.	First five mode shapes of the fin extracted from OMA in wind tunnel for the condition $V_{\text{flow}} = 4.78 \text{ m/s}$ and $\text{AOA} = 5^\circ$	94
Figure 6.9.	MAC diagram for OMA in wind tunnel and FEA results	95

Figure 6.10.	Reynolds Number (Re) vs Strouhal Number (St) [75]	97
Figure 6.11.	Position of the vortex generator and the fin	98
Figure 6.12.	Coordinate definition for the vortex generator position in wind tunnel....	98
Figure 6.13.	Average PSD functions from reference accelerometer for different positions of the vortex generator 1 (a) For all modes (b) For the first mode.....	100
Figure 6.14.	Average PSD functions for first and second mode excitation by vortex generators (a) For all modes (b) For the first two modes.....	104
Figure A.1.	Test fixture bar cross-section	119
Figure A.2.	Text fixture bar FEA result for the first mode	120
Figure A.3.	Dimensions of the test base	121
Figure A.4.	The first mode shape of the test base	121
Figure B.1.	Blower motor rotational speed vs. flow speed graph and fitted curve.....	123

CHAPTER 1

INTRODUCTION

1.1 Motivations of the study

Modal parameters define the dynamic behaviour of a structure. Having the information of these dynamic behaviours are important for an optimum structural design. Modal testing methods are the ways to validate the mathematical models for the dynamic characteristics of the structures. Classical modal analysis and testing methods use both the excitation and the response of the system for modal parameter extraction. Being a traditional and reliable way of modal analysis, Classical Modal Analysis (CMA) is limited when the input excitation is not known or not able to be measured.

Aircraft are subjected to various aerodynamic loads during their flights which are sometimes difficult to estimate. Operational Modal Analysis (OMA), on the other hand, is the technique to extract modal parameters of the structures during their operations (i.e. during the flight of an aircraft) which do not need the information about the input excitations. In this particular study, OMA is applied to a plate-like structure which is actually a fin, under the simulated real operating conditions where the input forces are not known. The modal parameters extracted from these analyses are then compared with the results obtained from traditional modal analysis/testing techniques and numerical models such as Finite Element Models (FEM).

1.2 Objectives of the study

The objectives of this study can be listed as follows:

- Developing a numerical model (i.e. FEM) of the test structure (i.e. the fin) comprising the modal properties,
- Validating the obtained FEM of the fin structure via different traditional modal analysis and testing methods,
- Investigating the differences in extracting of modal parameters of various types of modal testing methods,
- Applying OMA technique to the fin structure under different excitations and extracting modal parameters and comparing then with the ones obtained from traditional modal testing methods,
- Simulating different flow conditions over the fin structure in the wind tunnel and investigating the effects of these conditions on the extraction of modal properties of the fin via OMA and testing.

1.3 Limitations of the study

The main limitations of this study can be listed as follows:

- The numerical (FE) models are constructed only to get general information on the dynamic properties of the fin before starting modal testing. Therefore no updating of the FEM is performed.
- In the modal testing part of the study, the measuring devices (i.e. accelerometers) are attached to the fin and that apparently brings extra mass to the structure. In this study, the effects of these additional masses are also examined but instead of performing a correction/tuning study they are taken as negligible.
- In the wind tunnel testing part of this study, no measuring devices (i.e. pressure tabs etc.) are used in the determination of the flow properties.

- No analysis is conducted to examine the aeroelastic effects on the fin in wind tunnel tests.

1.4 Outline of the study

The organisation of this thesis can be given as follows:

In Chapter 2, the literature survey about Finite Element Analysis (FEA) and the modal testing applications are given briefly. Types and properties of OMA techniques and recent OMA applications are given in following sections. Analytical and experimental studies focusing on Vortex-Induced Vibration (VIV) are also provided in this chapter.

Chapter 3 is devoted to the general information on the fin-like structures and their usage on the aircraft. Geometrical properties of the particular test structure (i.e. the fin) used in this study and the preliminary studies regarding Finite Element Analysis of it are also given in this chapter.

In Chapter 4, general information about the theory of Classical Modal Analysis (CMA) is given. Then, the test setup and the software used for the CMA of the fin are introduced. In the following sections of this chapter impact hammer testing application of the fin is explained. Finally, shaker tests with both random noise and sine sweep inputs are also given in this chapter.

Chapter 5 is devoted to the OMA applications on the fin structure in in-vacuo conditions. First, the theory of OMA is given and then, the software and test setup used for the tests are introduced. Finally, the OMA tests of the fin performed via shaker random noise input and acoustic excitation are detailed.

Chapter 6 provides the modal testing of the fin in wind tunnel conditions. First, brief information is given about the test setup and the wind tunnel used in the thesis. Afterwards, the tests performed in wind tunnel with and without vortex generator are given in a detailed way.

Chapter 7 includes the general conclusions drawn from this study. Recommendations for the future works are also given in this particular chapter.

CHAPTER 2

LITERATURE SURVEY

2.1 Introduction

In this chapter, studies conducted related to the subject of this thesis are summarised. First, general information about Finite Element Modelling and Analysis is given. Secondly, for the widely used technique, Classical Modal Analysis and testing, is briefly explained. Afterwards, the literature about the Operational Modal Analysis (OMA) which may be considered to be a new method for modal testing is given in a more detailed way. Following these, the definition and the various types of Operational Modal Analysis (OMA) are provided. The harmonic input signal detection and elimination methods are also mentioned. Mode Shapes and Operating Deflection Shapes (ODS) are also defined. In the following parts, applications of OMA in aerospace engineering and other fields are presented. The studies making the use of OMA in structural health monitoring and numerical model updating of the structures are also summarised. In the second part of this study, the vortex-induced vibration phenomenon is defined and both numerical and experimental studies on vortex-induced vibration are given as final sections of this chapter.

2.2 Finite Element Modelling and Analysis

Finite Element Analysis (FEA) is a mathematical procedure which uses computer sources for the analysis of structures. FEA has the ability to make wide range of

structural analyses such as; static stress and displacement, transient dynamic response and normal mode analysis. From modal analysis point of view, FEA is used to extract dynamic properties of structures, including mode shapes and corresponding natural frequencies [1]. The advantage of FEA is the ability to solve large number of structural dynamics problems with high speed digital computers. On the other hand, the non-linear problems need to be examined case by case and solution strategies should be developed for each of them [1]. Since FEA is a mathematical method for analysis, the results of FEA should be validated by some tests. Buehrle et al. [2] performed normal mode analysis for the aircraft fuselage structures by different modelling techniques. As the second step, these results are compared with the test results to validate the Finite Element Model (FEM). Finite element models updating is sometimes a compulsory process (i.e. for flutter analysis of aircraft) if a validated model is needed for the further analysis and investigations [3].

2.3 Classical Modal Analysis and Testing

Modal analysis is the name of the process for determining the inherent dynamic characteristics of a system. Natural frequencies, damping ratios and mode shapes are these dynamic characteristics. Modal analysis uses these characteristics to formulate a mathematical model for the system [4]. Modal testing is the process involved in testing the structures in order to have the mathematical model of them which describes their dynamic or vibration behaviour [5]. In Classical Modal Analysis (CMA) both the input and output of a system are used to determine the dynamic characteristics. There are wide ranges of application areas of the CMA in different types of industries. Aerospace industry is one the main fields where the applications of CMA and modal testing are used. Ground Vibration Testing (GVT) is a classical modal testing application on an aircraft which is performed very late in the development process. Experimental results are used for validating the structural dynamic models. Predicting the flutter behaviour of the aircraft is the main outcome of this test which is used to plan the safety-critical in-flight tests [6]. In-flight flutter testing is another application of modal testing which is applied to an aircraft during its flight in order to enlarge its flight envelope [7].

2.4 Operational Modal Analysis and Testing

Operational Modal Analysis (OMA) is a technique for modal analysis by using only the outputs of a system. It has the types based on frequency and time domain techniques. OMA has broad application areas in modal identification.

2.4.1 Types of Operational Modal Analysis techniques

In literature, there are OMA techniques based on time domain or frequency domain.

Frequency domain based techniques

As a frequency domain based technique, Frequency Domain Decomposition (FDD) technique was introduced by Brincker et al. [8]. In this method, the output Power Spectral Density (PSD) functions are calculated at each frequency to form a PSD matrix. By decomposing this matrix via Singular Value Decomposition (SVD) technique this method separates the response spectra into single degree of freedom systems and then simple peak picking is applied on SVD function plots for modal parameter estimation. By this method, the ability to identify the close modes in case of signals containing strong noise can be achieved. Resonance frequency and mode shape information can also be extracted by the simple peak picking technique within this method. Subsequently, Brincker et al. improved the FDD by transforming the single degree of freedom systems into time domain [9]. By this new method, so called, Enhanced Frequency Domain Decomposition (EFDD), in addition to resonance frequency and mode shape information damping values for the systems could also be obtained. Damping values are estimated by the logarithmic decrement method applied on the obtained correlation functions in time domain and the resonance frequencies are obtained by counting the zero crossings of these correlation functions [10]. Like the EFDD technique, Curve-fit Frequency Domain Decomposition (CFDD) technique was also improved as another extension of FDD which also enables damping estimation [11]. This method is based on fitting the appropriate curves on single degree of freedom systems which are calculated by

decomposing the spectral density functions and extracting modal parameters from those curves. Compared to EFDD technique, CFDD technique improved the modal parameter estimation on a noisy SVD plot by using curve-fitting in frequency domain instead of back-transforming the SVD functions to time domain.

Time domain based techniques

As a time domain based technique Natural Excitation Technique (NExT) is improved by James III et al. [12] and applied on operating wind turbines to extract model parameters. Stochastic Subspace Identification (SSI) technique is one of the most commonly used techniques based on time domain which has three kinds as Unweighted Principal Components (UPC), Principal Components (PC) and Canonical Variate Analysis (CVA) [11]. A full modal model is fitted to the data in time domain by these techniques. The input to the modal model is assumed as stationary force signal. So the method works with broadband excitation. AR-ARMA, Eigensystem Realization Algorithm, Polyreference Time Domain, Least Squares Complex Exponential, Ibrahim Time Domain and Instrumental Variables can be called as the other commonly used methods in Operational Modal Analysis [13].

2.4.2 Harmonic excitation detection and elimination in OMA

The techniques mentioned above are appropriately applied on the systems in case of pure stochastic excitation. However, for the condition of deterministic signals are present on stochastic excitation, this signal perturbs the method and it can be treated as a structural mode. Consequently, the above methods are improved for better modal parameter estimation. Brincker et al. also recommended investigating the peaks at SVD plots at same frequency [8]. It was stated as a decisive parameter for a harmonic component in input signal if the peak exists in all SVD plots. If a structural mode is close to the harmonic component mode shape estimate is not affected in this method. On the other hand, frequency and damping estimates can be heavily biased while using inverse Fourier transform. Jacobsen introduced several easy-to-use techniques to identify harmonics in OMA [14]. Examining Short Time Fourier Transform (STFT) contour plots, checking SVD matrices, comparing mode

shapes visually and in terms of Modal Assurance Criterion (MAC) values are some of these techniques. Later on, in addition to these easy-to-use techniques Jacobsen implemented "Kurtosis checking" to the prior EFDD technique to eliminate the influence of harmonic components in OMA [15]. Jacobsen et al. also implemented a method to eliminate harmonic components that is based "Fast Kurtosis checking" in EFDD and applying a novel CFDD technique [16]. They also checked the applicability of this method on a ship and gravity dam ambient modal testing. In literature, several studies made as the applications of harmonic component determining and eliminating are also present [17], [18].

2.4.3 Mode shapes and Operating Deflection Shapes in OMA

The deflection shapes of a structure under excitations are important in order to understand the dynamical behaviour of it. These deflection shapes can be defined as mode shapes and Operating Deflection Shapes (ODS).

Operating Deflection Shapes

Related to mode shape but quite different from it in such a way that, ODS analysis is also an output-only technique for vibration related problems. ODS is generally defined as any forced motion of two or more points on a structure [19]. In vibratory excitations ODS can be called as the deflection of the structure at a particular frequency. ODS can be used to obtain the most deflection with its direction and to make corrective actions in order to reduce vibration levels. In literature, there are studies using this to observe the general motion of a test structure such as a machine [20]. Being similar to mode shapes, ODS has many differences. ODS can be defined at any frequency however mode shapes are defined at resonance frequencies. Mode shapes do not depend on input forces on the other side ODS can change with changing input force. Other differences between mode shapes and ODS are also examined [19] , [21].

Mode Shapes

Mode shape is defined as the characteristic deflection pattern of a structure at its resonance frequencies [4]. In classical modal analysis the mode shapes are scaled since the known inputs are used. However, because of the unknown excitation forces, having a scaled mode shape in OMA is not possible unless some other methods are used. Finite element model (FEM) of the test structure can be used as an auxiliary method with OMA to scale the mode shapes [22]. Without using an auxiliary method scaled mode shapes can be achieved by changing the mass of the structure and repeating the tests [23]. Mass changing method improved by Brincker et al. [24] by driving the scale factors directly from governing equation of motion and reducing the approximation errors in tests. In these scaling methods, addition of too many extra masses to the test structures not only makes the process difficult but also shifts the natural frequencies. New scaling methods are being improved to handle these problems [25] , [26] .

2.4.4 Operational Modal Analysis applications

In literature there are several studies made as applications of OMA which are widely used for modal identification of structures. Moreover, it can be used as a tool for damage identification and numerical modal updating.

OMA applications on aerospace structures

Operational Modal Analysis is widely used in test applications on aerospace structures. Mevel et al. compared input/output and output-only methods within two classes of methods: subspace-based and prediction error [27]. In LMS application note, OMA application on an output-only flight data of a business jet is described [28]. Various sets of data coming from different flight speeds which are read from the limited number of accelerometers on the aircraft structure are processed by SSI techniques and the major dynamic properties are extracted at the end of this process. Camargo et al. applied OMA to a modified helicopter to validate the structural effects of these modifications [29]. OMA is applied during flight to see the modification effects on the existing flight envelope. The downward shifts in natural

frequencies and damping ratios of the helicopter are obtained and then regarding these changes flight procedures and operating profiles for the helicopter are updated. Moreover by using OMA during flight instead of a classical input-output technique on ground, time required for modal survey tests is reduced. Grappasonni et al. applied OMA on a UAV Helicopter under the noise excitation and aerodynamic harmonics [30]. In that particular study, a new method is proposed for detecting harmonic excitation in input loading. The effectiveness of this new method was shown in different flight conditions.

OMA is also used in the fields FEM updating and damage detection of the aerospace structures. Crema et al. investigated the effectiveness of output-only analysis in both frequency estimation and finite element updating of a AB-204 helicopter blade [31]. Parker used output-only methods to detect and track the damage in a wing attachment fitting [32]. Alam et al. conducted numerical and experimental study on output-only modal testing of a on-orbit satellite appendages [33]. The extracted modal parameters results are then compared with those obtained using traditional modal analysis. It is concluded that output-only based on SSI techniques can be used for modal identifications of satellite and space applications.

OMA Applications on Other Types of Structures

OMA is used for the structures other than aerospace structures. Some of these structures are machines, wind turbines and civil structures.

Hermans et al. illustrated three different industrial application of OMA which are modal characterization of a rear suspension system of a family car, flight flutter analysis of a commercial aircraft and identification of modes of a concrete bridge under ambient excitation [34]. Capabilities and limitations of OMA techniques, NExT and SSI, are examined in this particular study. OMA is preferred rather than classical modal analysis when the test structure is very huge and hard to be excited. Wind turbines are good examples for these kind cases. Carne et al. applied OMA to a wind turbine over 100 m tall and extracted modal parameters [35]. It is observed that wind turbines are well excited by the winds in their operating conditions and the quality of modal parameters are ascertained. Tcherniak et al. investigated the

applicability limits of OMA to operational wind turbines [36]. In their study, the limitations of OMA technique are also pointed out and aeroelastic phenomena caused by rotor rotation are denoted as the source of these limitations. OMA is also used for damage identifications due to dynamic behaviour during operation of wind turbines [37].

Health Monitoring and Damage Detection by OMA

Since OMA is a method which makes the use of ambient excitations; health monitoring and damage detection techniques can be applied to test structures without interrupting their operations. Brincker et al. extracted the modal parameters of a highway bridge by using EFDD and observe the change in these parameters [38]. Different types of damages are detected by investigating the frequency, damping and mode shape deviations. Ramos et al. applied EFDD and SSI techniques for verifying damage identification process of a masonry construction using OMA [39]. In their study, classical input-output method is used a reference and adequate results are acquired. In literature, there are different methods being improved to be used for damage detection. Some of these methods are the techniques using MAC [40], Extended Kalman Filter [41] and ODS [42].

Numerical Model Updating by OMA

Finite Element Models are widely used in studies to simulate the dynamic behaviour of the structures. However, to simulate the behaviour of the real structure properly FEM should be updated regarding test results. OMA technique is used in several studies to update the FEMs of the structures [43] , [44].

2.5 Vortex-Induced Vibrations

Vortex-induced vibration is a fluid-interaction problem caused by vortex-shedding from an obstacle under flow. Periodic vortex shedding produces periodic flow forces through the wake region of the obstacle [45]. Buffeting of aircraft structures (such

as vertical tails) is associated with the impact of vortex generated by aircraft at high angles of attack [46]. In literature there are several studies on analysing buffet phenomena [46], [47], [48]. Vortex-shedding of a fixed or flexible cylinder under flow is a typical vortex induced vibration example. Analytical and experimental studies are made on this subject.

2.5.1 Analytical studies

Lienhard summarized the studies on vortex frequency measurements for rigid circular cylinders and improved the available data by examining the effect of Strouhal-Reynolds number relationship [49]. In the same study, the flow regimes behind any bluff body are also described by considering Strouhal Number which varies with vortex shedding frequency, flow speed and the cylinder diameter. Dong et al. presented direct numerical simulations (DNS) for turbulent flows past a rigid cylinder undergoing a forced sinusoidal oscillation in cross-flow direction [50]. Li et al. improved the numerical simulation studies of vortex-induced vibration of a cylinder. They carried out the numerical simulation of a 2-dimensional elastic circular cylinder. The trend of the lift and drag coefficients and the displacements of the cylinder under different oscillating frequencies were examined in their study [45].

2.5.2 Experimental studies

Jauvtis et al. conducted an experimental study on vortex-induced vibration of a cylinder with two degrees of freedom [51]. They constructed an apparatus for the cylinder which allows it to move in-line and transverse to the flow. The responses of the cylinder and the vorticities were then examined. Sarioglu et al. determined vortex sheddings from circular cylinders and rectangular cross-sections experimentally [52]. Spectral density distributions of vortex sheddings in the wake were measured by using a hot film anemometer in the test apparatus in an open wind tunnel. Reynolds and Strouhal numbers effects on vortex sheddings were also examined. Zhan et al. designed a new setup scheme for wind-rain-induced cable vibration experiment [53]. They detected vortex-shedding-induced cable vibration at

very low wind speeds. Zhou et al. examined the vortex-induced vibration phenomena on a bridge [54]. They used a 1:60 model of the real bridge for the wind tunnel tests. In wind tunnel, different flow angles (i.e. angle of attacks) and flow speeds acting on bridge model were used to observe the amplitude of vortex-induced vibrations.

2.6 Summary

In the first part of this chapter, first, application areas of Finite Element Analysis and Classical Modal Analysis are given briefly. Afterwards, Operational Modal Analysis (OMA) is introduced and the application areas of it are presented. Differences between the techniques of OMA which are based on either time or frequency domain are described. Mode shapes and Operating Deflection Shapes (ODS) which are playing important roles in structural dynamics are mentioned. The studies making the use of OMA in the fields numerical model updating and health monitoring are also examined. In the second part of the chapter, vortex-induced vibrations are introduced. Analytical and experimental studies related to this subject are summarised.

CHAPTER 3

FINITE ELEMENT MODELLING AND ANALYSIS OF PLATE-LIKE STRUCTURE

3.1 Introduction

In this chapter, first, general information on plate-like structure is given. Their functions on aircraft are defined. Afterwards, the test structure used in this study which is actually a fin-like structure is defined in terms of material properties and dimensions. Finally, Finite Element Analysis (FEA) for the test structure is conducted.

3.2 General information on plate-like test structure

The test structure used in this study is actually a fin-like structure which can generally be seen in aircraft. General properties and the specifications of the fin-like structure used in this study are given in the following sections.

3.2.1 General properties of fin-like structures

Vertical stabilizers, dorsal and ventral fins and the antennas (i.e. VHF-UHF antennas) can be regarded as fin-like structures in an aircraft.

Vertical stabilizers (See Figure 3.1) are located at the end of fuselage and they prevent yawing (i.e. side-to-side) motion of the aircraft. If lateral stability of the aircraft cannot be satisfied by vertical stabilizers, dorsal and/or ventral fins are used to increase the stability in yawing direction.



Figure 3.1. Vertical stabilizer of Turkish Stars Northrop NF-5

In a structural point of view vertical stabilizers, dorsal and ventral fins are in a cantilevered boundary condition which are excited by the aerodynamic forces over them. UHF and VHF antennas which are used for communication devices in an aircraft are also similar in structural fashion (See Figure 3.2).



Figure 3.2. Antennas of KT-1T Aircraft

Dynamic characteristics of fin-like structures of an aircraft should be well examined in order not to have vibration sourced problems during the service life of aircraft. For instance, the resonance frequencies of fin-like structures should be analysed to

ensure they are not close to the excitation frequencies due to aerodynamic forces during flights.

3.2.2 Geometrical and material properties of fin-like structure

Test structure used in this study is an aluminium plate which has a trapezoid like shape. It is clamped at its root which is the longest side (See Figure 3.3 a)).The thickness of the fin is 2.1 mm and other dimensions are given in Figure 3.3 b).

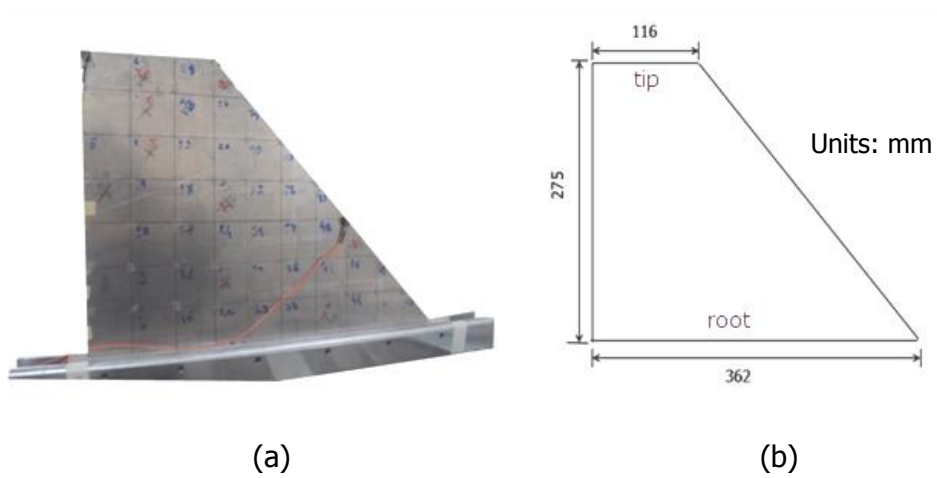


Figure 3.3. (a) Geometry of fin-like structure (b) Dimensions of fin-like structure

The material properties of the fin-like structure is given in Table 3.1

Table 3.1. Material properties for aluminium

Property	Value
Density	2768 kg/m ³
Elastic Modulus	69 GPa
Poisson's Ratio	0.333

3.3 Finite element analysis of fin-like structure

Before starting modal testing of the fin-like structure, FEM is created to obtain the general modal specifications. Package software, MSC[®]/PATRAN 2010-v1, is used for modelling the structure [55]. The model is obtained by using shell elements and the cantilever boundary condition is obtained by fixing 6 degrees of freedoms at the root. Three different mesh sizes are tried for solutions. By considering the run time and the convergence of the natural frequencies, final mesh size is decided for the model (See Appendix A.1). Total number of elements and nodes of this final model are 3024 and 3021, respectively. 2800 of the elements are CQUAD4 type and the remaining 224 are CTRIA type elements. FEM and the boundary condition can be seen in Figure 3.4.

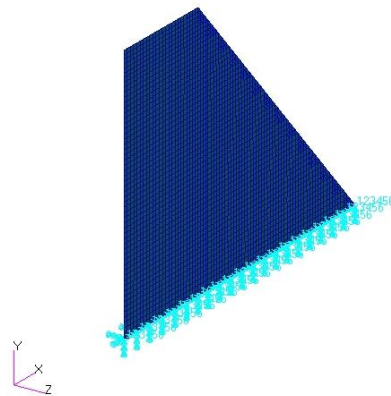


Figure 3.4. Finite element model of the fin-like structure

First five natural frequencies and the corresponding mode shapes of the model are extracted by using Normal Modes (SOL 103) solution type in MSC[®]/NASTRAN 2010-v1 [56]. The natural frequencies obtained from FEA are listed in Table 3.2.

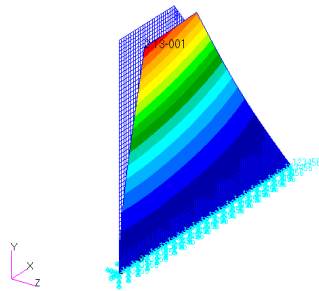
Table 3.2. Natural frequencies of fin-like structure obtained from FEA

Mode	Natural Frequency [Hz]
1 st Bending	27.03
1 st Torsion	89.60
2 nd Bending	144.51
Mixed Mode 1	222.92
Mixed Mode 2	347.33

The shapes of the first five modes of the fin-like structure are given in Figure 3.5.

atran 2010 23-Jul-11 19:15:12

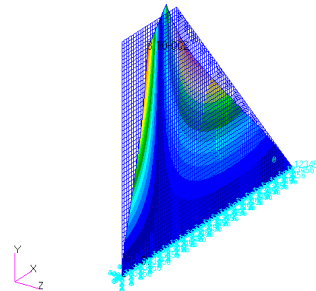
ringe: Default, A1, Mode 1 : Freq. = 27.026, Eigenvectors, Translational, Magnitude, (NON-LAYERED)
eform: Default, A1, Mode 1 : Freq. = 27.026, Eigenvectors, Translational.



(a) Mode 1 (1st Bending)

atran 2010 23-Jul-11 19:23:25

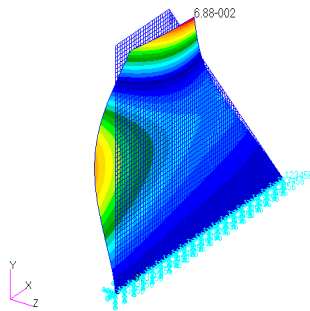
ringe: Default, A1, Mode 2 : Freq. = 89.602, Eigenvectors, Translational, Magnitude, (NON-LAYERED)
eform: Default, A1, Mode 2 : Freq. = 89.602, Eigenvectors, Translational.



(b) Mode 2 (1st Torsion)

Patran 2010 23-Jul-11 19:24:10

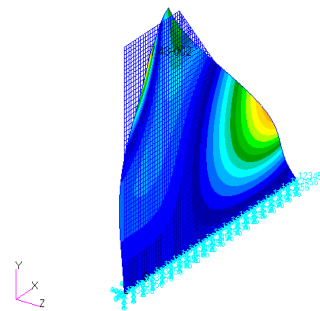
Fringe: Default, A1, Mode 3 : Freq. = 144.51, Eigenvectors, Translational, Magnitude, (NON-LAYERED)
Deform: Default, A1, Mode 3 : Freq. = 144.51, Eigenvectors, Translational.



(c) Mode 3 (2nd Bending)

atran 2010 23-Jul-11 19:24:53

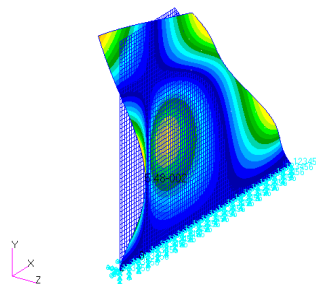
ringe: Default, A1, Mode 4 : Freq. = 222.92, Eigenvectors, Translational, Magnitude, (NON-LAYERED)
eform: Default, A1, Mode 4 : Freq. = 222.92, Eigenvectors, Translational.



(d) Mode 4 (Mixed Mode 1)

atran 2010 23-Jul-11 19:25:42

ringe: Default, A1, Mode 5 : Freq. = 347.33, Eigenvectors, Translational, Magnitude, (NON-LAYERED)
eform: Default, A1, Mode 5 : Freq. = 347.33, Eigenvectors, Translational.



(e) Mode 5 (Mixed Mode 2)

Figure 3.5. First five mode shapes of the fin-like structure extracted from FEA

According to finite element analysis results the first and the third modes are purely out-of-plane bendings whereas the second mode is a purely torsional one. Throughout the study they are referred as 1st Bending, 2nd Bending and 1st Torsion, respectively. As the fourth and the fifth modes comprise bending and torsion couplings (i.e. the first out-of-plane bending - torsion coupling and the second out-of-plane bending - torsion coupling, respectively), throughout the study, they are referred as Mixed Mode 1 and Mixed Mode 2, respectively.

Throughout the experimental modal analysis part of this study, the accelerometers which weigh 1 gram each are used. (Specifications of accelerometers are presented in Section 4.3). To examine the mass effects of accelerometers on natural frequencies of the fin-like structure FEA is repeated by adding accelerometers to the FEA as lumped masses (i.e. CONM2 elements in MSC[®]/NASTRAN). As can be seen in Figure 3.5 top two corners have major deflections in all mode shapes of the model. For this reason two accelerometers are modelled as lumped masses at top two corners of the fin to see their effect on natural frequencies of the model. The resulting natural frequencies of FEA is given in Table 3.3

Table 3.3. Natural frequencies of fin-like structure by adding the mass effects of accelerometers

Mode	Natural Frequency [Hz]
1 st Bending	26.60
1 st Torsion	88.55
2 nd Bending	142.24
Mixed Mode 1	218.11
Mixed Mode 2	342.49

By comparing these results with that of in Table 3.2, it can be seen that the maximum change in natural frequency values due to the mass effect of the accelerometers is approximately 2%.

3.4 Summary

In this chapter, after defining the general properties fin-like structures and the test fin-like structure FEA is conducted for the test structure. Natural frequencies and mode shapes of the fin-like structure are extracted from this analysis. Moreover, mass effects of the accelerometers which will be used in the tests are investigated. It is seen that they have no significant effects on mode shapes and natural frequencies.

CHAPTER 4

MODAL TESTING OF FIN-LIKE STRUCTURE VIA CLASSICAL MODAL ANALYSIS

4.1 Introduction

After conducting FEA of the test structure, modal tests are performed on the fin-like structure to verify the previously obtained numerical model. In this chapter, first the theory of Classical Modal Analysis (CMA) is explained. After introducing test setup and software classical modal analysis tests conducted are given.

4.2 Classical Modal Analysis theory

Modal analysis can be defined as the process of determining inherent dynamic characteristics in forms of natural frequencies, mode shapes and damping ratios and using them for a mathematical model [4]. The classical modal analysis carries out this process by examining input-output relationships of a system.

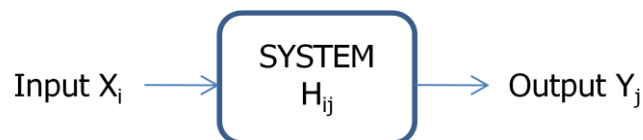


Figure 4.1. Analysis of a system

As shown in Figure 4.1 a system can be defined as a transfer function which is the value of output of a system is divided by the input to a system. It can be shown as:

$$H_{ij} = \frac{Y_j}{X_i} \quad (4.1)$$

In vibration theory, the transfer functions can be defined at each frequency value and called Frequency Response Functions (FRF) [57]. The FRF estimators can be shown as:

$$H_1 = \frac{G_{XY}}{G_{XX}} \quad (4.2)$$

or

$$H_2 = \frac{G_{YY}}{G_{YX}} \quad (4.3)$$

where G_{XY} is the cross-spectrum between input and output signal whereas G_{XX} and G_{YY} are the autospectra of input and output signal, respectively. FRF estimators are complex quantities and functions of frequency. They can be shown in two graphs which are frequency vs. magnitude and frequency vs. phase graphs. The resonance frequencies of a system can be extracted from FRF graphs. Criteria for resonance frequency extraction can be listed as [58]:

- FRF magnitude should be a maximum.
- The imaginary part of FRF should be a maximum or minimum.
- The real part of the FRF should be zero.
- A phase change of 90° should exist.

Damping estimation is also made by using FRF graphs. Modal damping ratios are related to the width of the resonance peak which can be calculated by the method called half-power bandwidth [58]. These damping ratios are also referred as the total damping ratio which comprise both material (or structural) and non-material (or viscous) damping. The remaining modal parameter, mode shapes can also be

extracted from FRFs. The imaginary parts of the FRF curves for different measurements are used for mode shape determination [59].

4.3 Test setup and software for Classical Modal Analysis tests

Test fixture

Test fixture has a significant role in modal testing. Two main concerns should be taken into account to have reliable modal parameters. The first one is the boundary condition of the test structure. The second one is the dynamic characteristics of the test fixture itself. For the first, the fixture should be stiff enough. For the latter, all resonance frequencies of the test fixture should be out of the test frequency range [60].

For the classical modal analysis tests of this study the fin-like structure is fixed between two aluminium sticks along its bottom edge. Assuring the fin-like structure is not allowed to move in any direction between these sticks, the whole structure is attached to a 0.5 m long aluminium bar with 6 bolts. After having the fixed boundary condition at the bottom edge of the fin the bar is fixed to a massive test table. Test fixture is shown in Figure 4.2

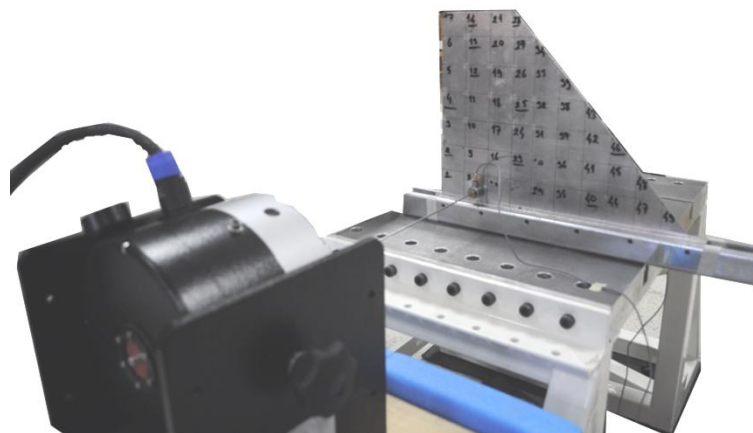


Figure 4.2. Test setup for the classical modal analysis tests

Fixing mechanism of fin to the aluminium bar is given in Figure 4.3

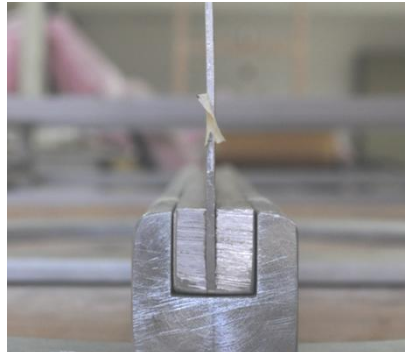


Figure 4.3. Text fixture bar and fixed fin

In addition to checking the boundary condition compliance, the resonance frequencies of test fixture should also be checked. FEA for calculating the resonance frequencies is given in Appendix A.2. At the end of FEA first, natural frequency of the bar is determined at 2673 Hz. Since this value is away from the frequency range of interest of the fin (see Table 3.3) the possibility of interference of the test setup natural frequencies to fin modal analysis is eliminated.

In classical modal analysis tests by using the shaker, input excitation is applied to the structure via stringer attached with the force transducer to the modal shaker. The stringer is attached to a point close to the root of the fin by the help of super glue (See Figure 4.4). The reason to attach the stringer at this position is simply from the fact that the displacements are minor near to root of the fin. In the case of attachment of the stringer near the tip of fin, huge displacements at the tip may affect the damping mechanism. It may also bring additional mass effect and may ultimately cause dismounting problem for the stringer.

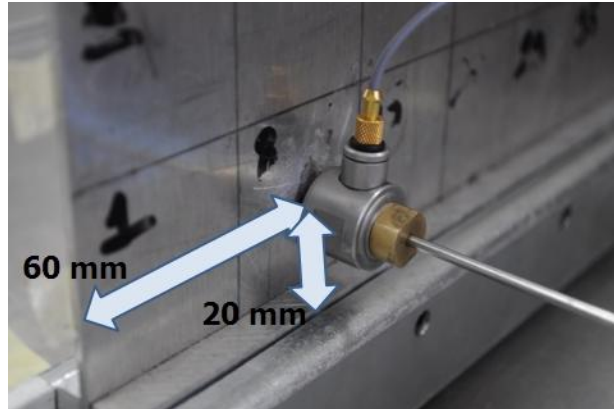


Figure 4.4. Shaker stringer attachment

Test equipments

The main equipments used in Classical Modal Analysis tests are the accelerometers, impact hammer, force transducer and data acquisition system. Brüel & Kjaer (B&K) Type 4517-002 accelerometers are used as response measuring devices [61]. They are miniature type accelerometers which weigh 1 gram. They are attached to the fin by the help of bee wax.

For exciting the system B&K Type 8206 impact hammer is used [62] for the impact hammer tests. The impact hammer has three available tips which have different force spectrums. They are given in Figure 4.5. By considering the interested frequency range for test structure, tip to use in the test is decided.

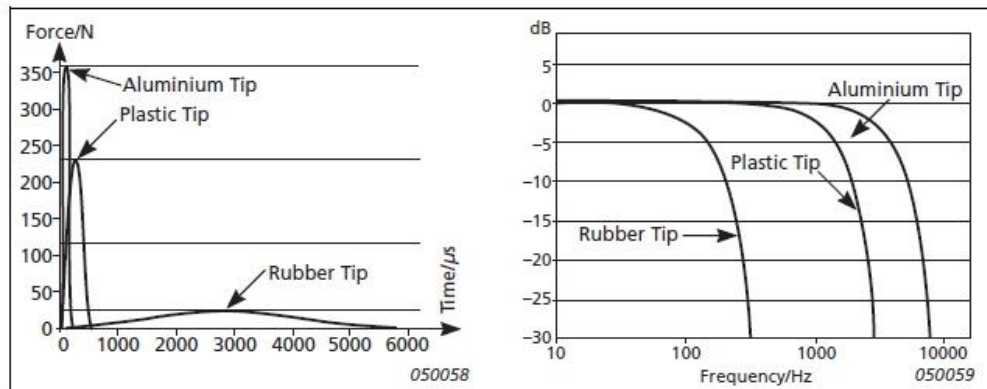


Figure 4.5. Impulse shapes (left) and force spectrums (right) on an aluminium plate for different impact hammer tips [62].

For exciting the system by sine sweep and random noise signals, B&K Type 4825 modal shaker is used [63]. Sine sweep and random noise signals for the excitation is generated by Agilent 33120A Signal Generator [64].

B&K Type 8230-002 DeltaTron[®] force transducer is attached to the impact hammer and shaker stringer to measure the excitation force [65].

Test software

B&K 3560-C PULSE[™] platform is used for data acquisition [66]. It is a 6-channel system and works compatible with the software PULSE[™] Labshop 13.5.0 [67]. In PULSE[™] Labshop, first the accelerometers and force transducer are introduced to the system. Then the measurements locations and the test geometry are defined in Modal Test Consultant (MTC) part of the software Labshop. Before starting test, Fast Fourier Transform (FFT) analysis setting should be made by regarding the number of FFT lines, frequency span and each measurement length. After finishing the measurements, the data are stored and exported to MATLAB[™]. A sample screen for the PULSE[™] Labshop software given in Figure 4.6

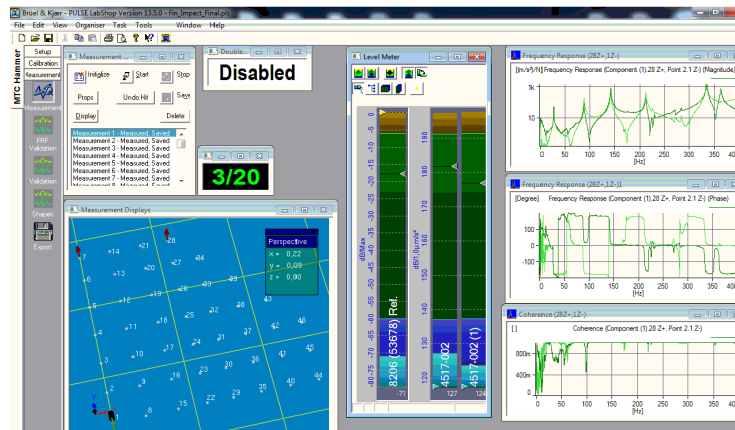


Figure 4.6. Sample screen of PULSE™ Labshop Software

4.4 Classical Modal Analysis tests

In the experimental part of this study first Classical Modal Analysis techniques are used for modal analysis of the fin-like structure. Impact hammer testing is first conducted as one of the classical modal analysis method. Then shaker tests are performed with sine-sweep and random noise input signals. Tests are detailed in following sections.

4.4.1 Impact hammer tests

Impact hammer testing is the most practical way for classical modal testing since it requires a few equipments and relatively shorter measurement times. Moreover, there is no physical attachment of any kind like stringer etc. during the impact hammer excitation therefore it can be a preferable method to compare the results with OMA application on a structure under non-contact ambient excitation.

As described in section 4.3, selection of the tip of the hammer is critical for exciting the desired frequencies during modal testing. By considering the natural frequency results by FEA for the test structure (See Table 3.2 and Table 3.3); a frequency range of 27-347 Hz. should be excited by impact hammer for an adequate modal analysis covering the first five modes of the fin. For this frequency range, a rubber or plastic tip seems to be proper (See Figure 4.5). Plastic tip has wider linear

frequency spectrum for the interested range. However, plastic tip had more double-hit problems in the tests. As a result, the rubber tip is used for the impact hammer tests.

For the FFT analysis, the analysis parameters are setup by regarding the interested frequency range. FFT analysis settings used in software are given in Table 4.1.

Table 4.1. FFT Analysis Settings

Parameter	Value
FFT Lines	3200
Span	0-400 Hz
Measurement time	8 seconds

“FFT lines” is the number of discrete points where the Fast Fourier Transform calculations are taken into account. “Span” is the interval where these calculations are conducted. So, one step unit in frequency range for the FFT process which is called frequency resolution is 0.125 Hz for this test. Measurement time is selected considering the decay of the acceleration output of the test structure. After a few trial runs, it is seen that acceleration output of the fin decays in 8 seconds after hitting by the hammer. A sample acceleration-time history is given in Figure 4.7.

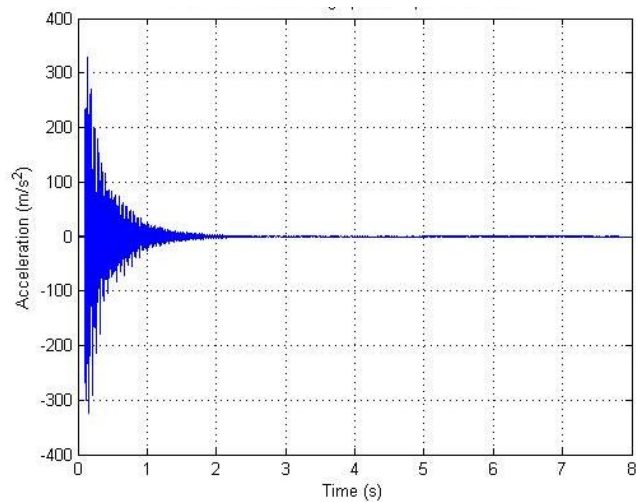


Figure 4.7. A sample acceleration-time history via impact hammer test

Mode shape results from FEA (see Figure 3.5) are also examined to specify the number of measurement points which will represent the first five mode shapes of the fin sufficiently. 49 points over fin are selected in vertical and horizontal directions to excite and/or measure the force and the acceleration data for classical modal analysis. Two miniature accelerometers were placed at the top two corners for monitoring the response of the fin. Principally, one is adequate for the classical modal analysis. The other one was used to double check the results and include the same mass effect of the accelerometers in impact hammer test with OMA tests since OMA tests require at least two accelerometers to be utilized. 49 points over the fin is excited by roving the hammer. The roving sequence and measurement/excitation points are given in Figure 4.8.

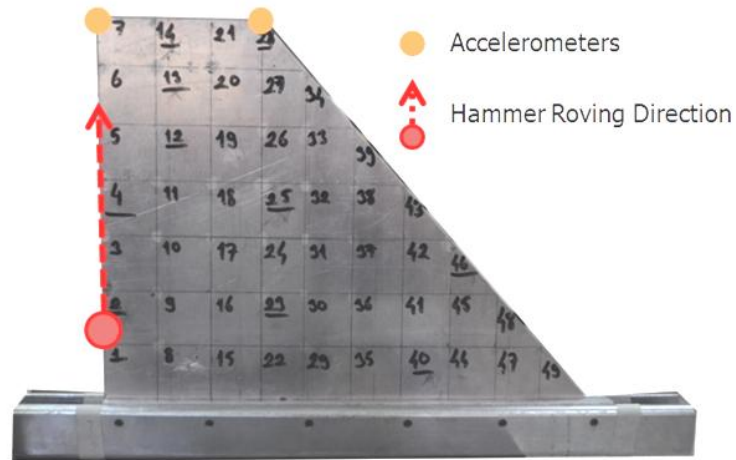


Figure 4.8. Measurement/excitation points over the fin and hammer roving direction

The tests are conducted by using B&K 3560-5 PULSE™ platform for data acquisition. The measured data is post-processed by the help of a MATLAB™ [68] script. Frequency response curves for 49 different measurements are given in Figure 4.9.

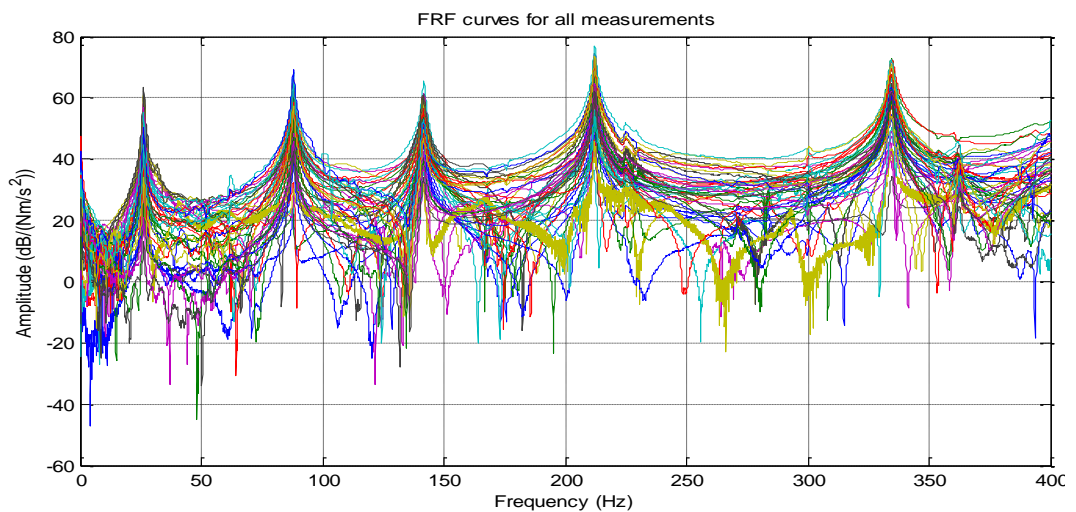


Figure 4.9. Frequency Response Functions from impact hammer test results

In order to achieve a more simplified form of the FRF and to make resonance peaks more observable, magnitudes of all obtained FRFs are summed up in the frequency domain of interest and a so-called "composite FRF" is obtained [5]. The composite FRF is given in dB scale in Figure 4.10.

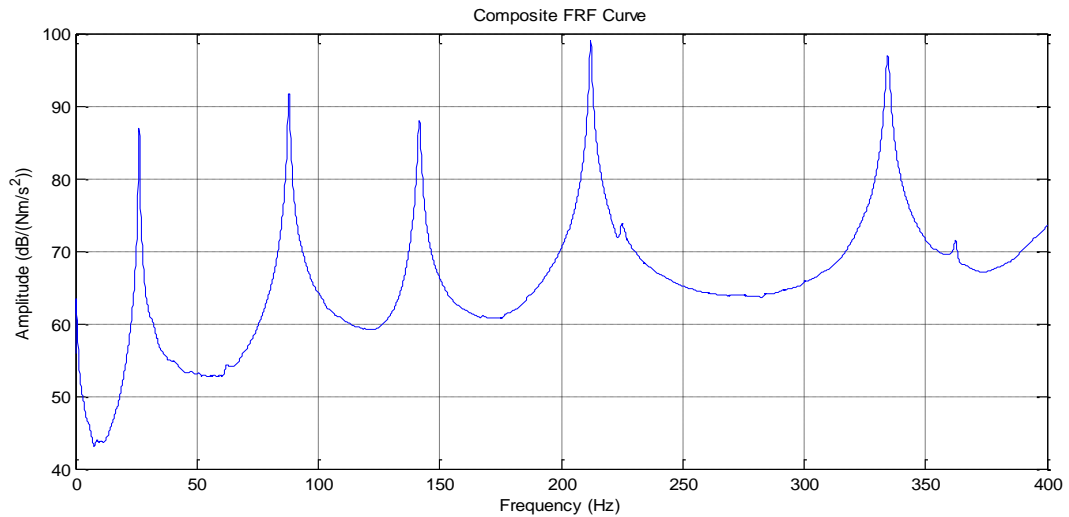


Figure 4.10. Composite FRF curve from the impact hammer test results

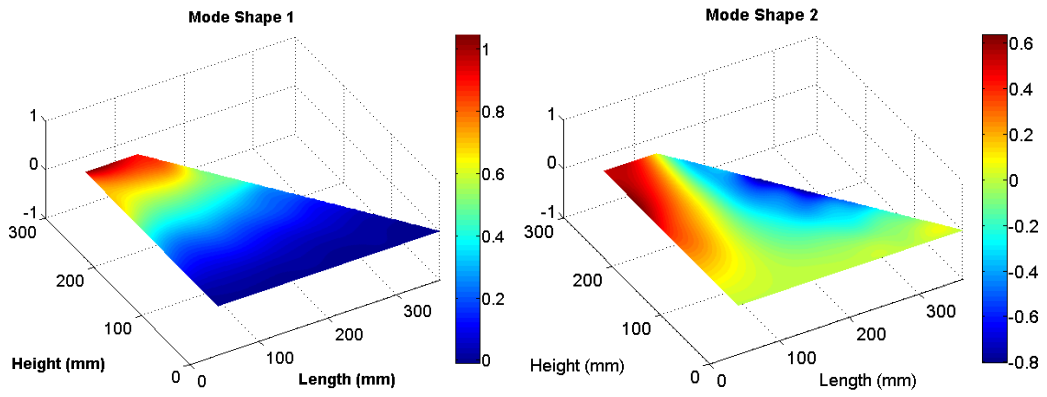
Resonance frequencies and damping ratios of the fin are then calculated for each individual measurement. Resonance frequencies are calculated using simple peak picking method. For damping ratio calculations half-power bandwidth method is used. All corresponding 49 values of both frequencies and damping ratios are averaged to obtain the final values. Standard deviations are also checked to realise any problematical measurements. A few measurements with high standard deviations which seem to be inaccurate are eliminated. The results which are calculated by using the response values from the first accelerometer are compared with that of from the second accelerometer as well. As expected the results are close to each other. The results from the FRF estimators H_1 and H_2 are also compared with each other. There were no significant differences between them in terms of resonance frequencies and damping ratios. Averaged resonance frequencies and damping ratios using H_1 estimator is given in Table 4.2.

Table 4.2. Resonance frequencies and damping ratios of fin-like structure from impact hammer test

Mode	Resonance Frequency [Hz]	Damping Ratio [%]
1 st Bending	26.27	1.44
1 st Torsion	87.93	1.14
2 nd Bending	141.54	0.79
Mixed Mode 1	212.17	0.43
Mixed Mode 2	334.46	0.46

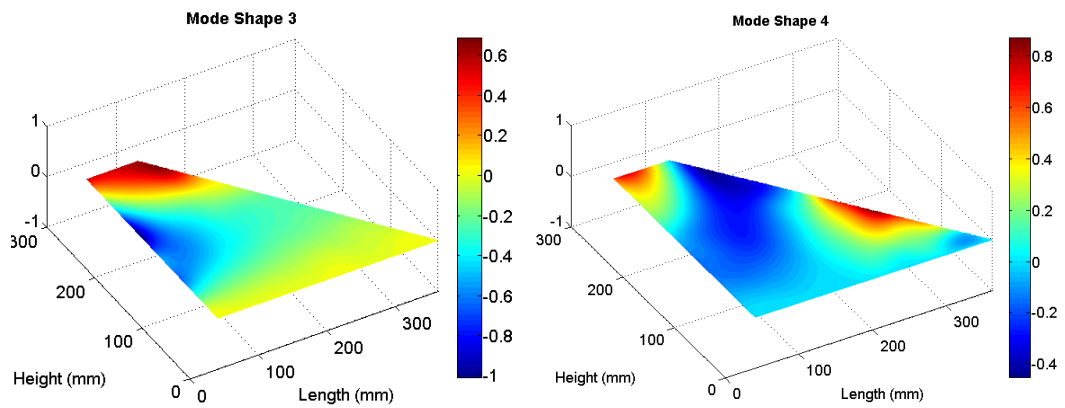
Resonance frequencies extracted from impact hammer test are compared with FEA results in order to validate the reliability of the FEM. The differences in frequencies are 2.81%, 1.86%, 2.06%, 4.82%, and 3.71% for the first five modes respectively.

Mode shapes of the fin are also extracted by the help of the aforementioned script written and shown in Figure 4.11.



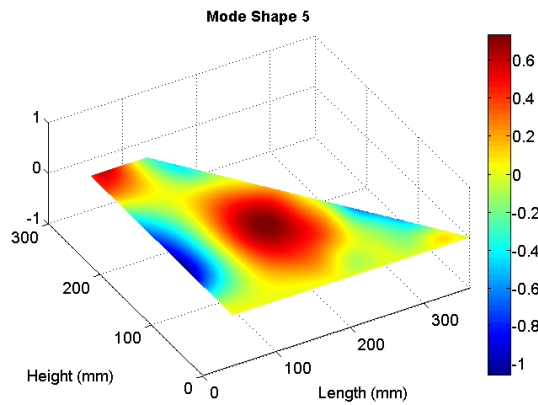
(a) Mode 1 (1st Bending)

(b) Mode 2 (1st Torsion)



(c) Mode 3 (2nd Bending)

(d) Mode 4 (Mixed Mode 1)



(e) Mode 5 (Mixed Mode 2)

Figure 4.11. First five mode shapes of the fin extracted from impact hammer test

These mode shapes are also compared with that of FEA results. Modal Assurance Criteria (MAC) parameter is used for the comparison purposes [40]. First, by the help of a FORTRAN™ script the eigenvectors corresponding to test measurement points are filtered from the FEA results file. Secondly, these mode shape vectors are implemented to MATLAB™ script and compared with mode shape vectors of impact hammer test results by calculating MAC values for the first five modes. The MAC diagram is shown in Figure 4.12 and MAC table is provided in Table 4.3.

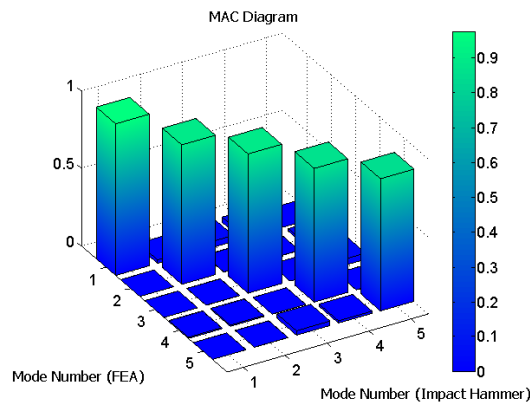


Figure 4.12. MAC diagram for impact hammer test and FEA results

Table 4.3. MAC table for impact hammer test and FEA results

Mode Numbers	1	2	3	4	5
1	0.9737	0.0218	0.0391	0.0337	0.0000
2	0.0001	0.8954	0.0019	0.0008	0.0168
3	0.0003	0.0010	0.8943	0.0000	0.0401
4	0.0073	0.0074	0.0004	0.8584	0.0006
5	0.0003	0.0008	0.0285	0.0143	0.8490

By examining the MAC values, relatively high correlation between FEA and impact hammer test can be noticed for the first mode. For the other modes MAC values which are under the value of 0.90 shows relatively less correlation between FEA and impact hammer test results. As expected the off-diagonal terms in MAC matrix have very small values which indicates that the modes are well matched.

4.4.2 Shaker tests with random noise input

Modal shakers are widely used equipment for modal analysis tests which can have accurate results. Shakers can provide different type of excitations by using different signals from a signal generator. In shaker tests, first random white noise signal is given by the signal generator [63] and applied to the structure via stringer attached with the force transducer to the modal shaker.

In the software (See Section 4.3) after defining the geometry and measurement points the FFT analysis setup is completed and the main parameters used in the analysis are given in Table 4.4.

Table 4.4. FFT analysis setup parameters for random noise shaker test

Parameter	Value
FFT Lines	1600
Span	0-400 Hz
Number of averages	66
Time for one measurement	90.67 s
Overlap	66.67%

“FFT lines” and “Span” parameters are already defined in the impact hammer test section (See Section 4.4.1). “Number of averages” is the parameter for the number of spectra or time records. When the number for the averages is reached during the

measurement process, the process finishes. "Time for one measurement" is given manually by the user or calculated by using the "Number of averages" and "Overlap" parameters. It is the time length for one measurement process. "Overlap" is the parameter which decides the percentage of the overlaps of time record segments. It supplies better amplitude accuracy and prevents the loss of measurement data.

The measurement process is similar to the impact hammer tests however the accelerometer is roved to 49 points shown in Figure 4.8. Measurement results taken from the software are post-processed by the same MATLAB™ script used in impact test results post processing. The FRF plots from 49 measurements and the composite FRF of all are given in Figure 4.13 and Figure 4.14, respectively.

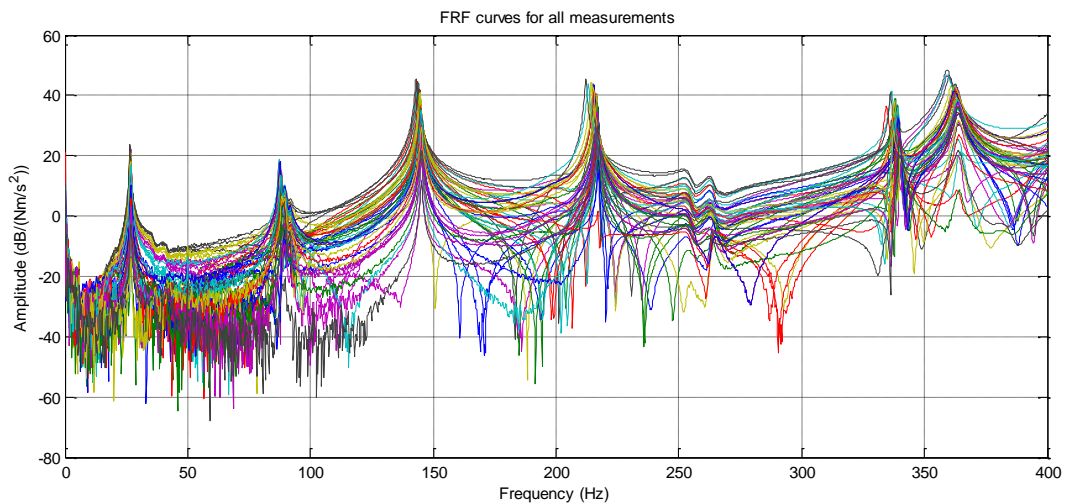


Figure 4.13. FRF plots for shaker test with random noise

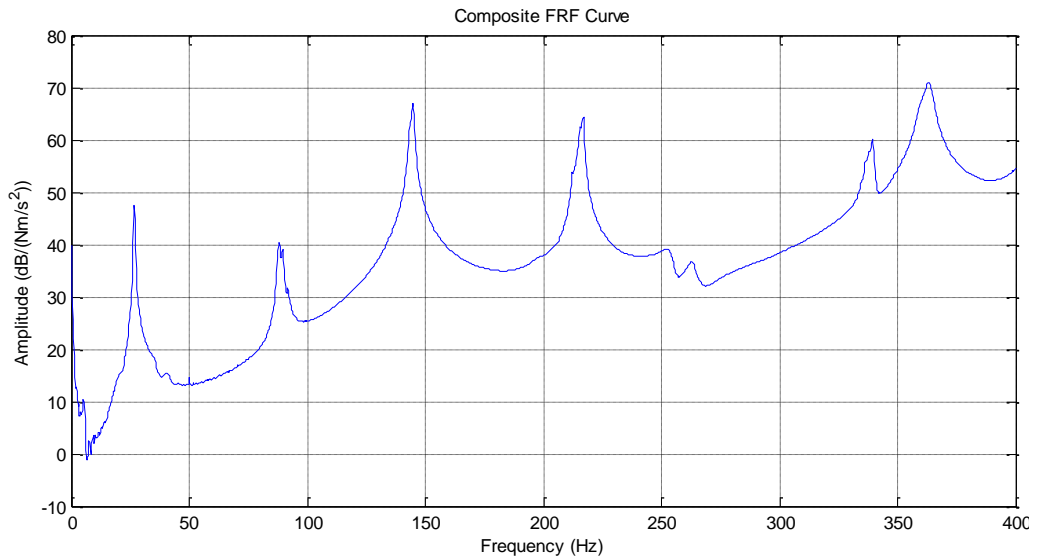


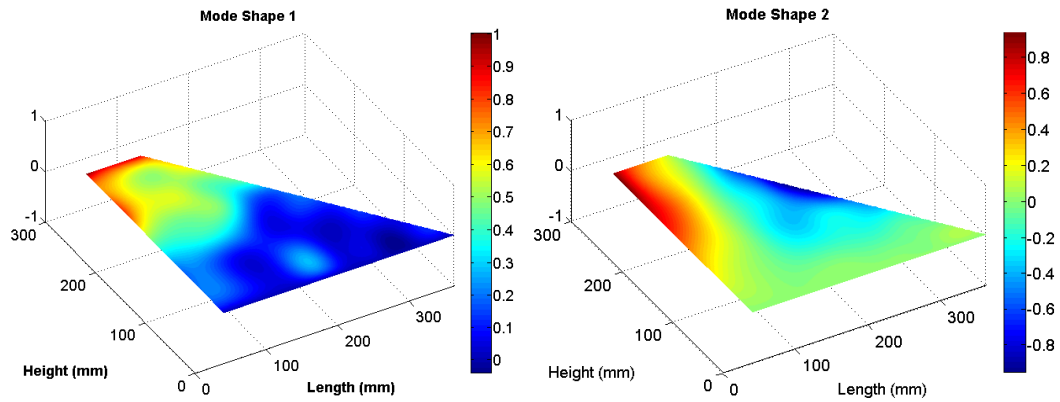
Figure 4.14. Composite FRF plot for shaker test with random noise

As seen from the FRF plots, the resonance peaks could be identified from the random noise input test and corresponding resonance frequencies and damping ratios are given in Table 4.5.

Table 4.5. Resonance frequencies and damping ratios of the fin from random noise shaker test

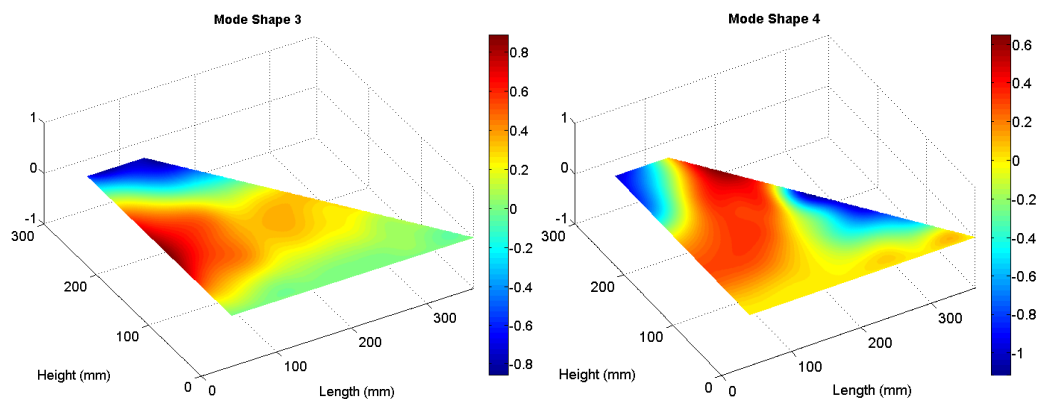
Mode	Resonance Frequency	Damping Ratio
	[Hz]	[%]
1 st Bending	26.72	1.66
1 st Torsion	88.64	1.37
2 nd Bending	144.79	0.5
Mixed Mode 1	216.48	0.30
Mixed Mode 2	338.97	0.32

When these results are compared to those of impact hammer tests, it can be observed that the differences between resonance frequencies are not more than 2%. However, in damping ratios the differences are about 20%-30%. Relatively big amount of differences in damping ratios can be explained by the changing of damping mechanisms within two tests. In impact hammer test there is an impulsive force on the structure and there is no attachment on the surface. However, the stringer attachment in shaker test can result in change of damping ratios for the fin. Mode shapes from the random noise input test are extracted by the same script used in impact hammer test and given in Figure 4.15.



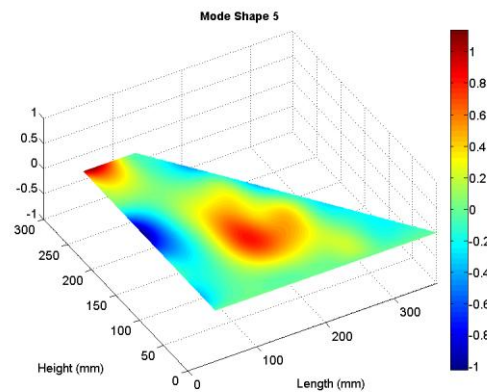
(a) Mode 1 (1st Bending)

(b) Mode 2 (1st Torsion)



(c) Mode 3 (2nd Bending)

(d) Mode 4 (Mixed Mode 1)



(e) Mode 5 (Mixed Mode 2)

Figure 4.15. First five mode shapes of the fin extracted from shaker test with random noise

By using the same procedure applied in impact hammer test, mode shapes extracted from random noise shaker test are then compared with FEA results. Their MAC diagram and table are given in Figure 4.16 and Table 4.6, respectively.

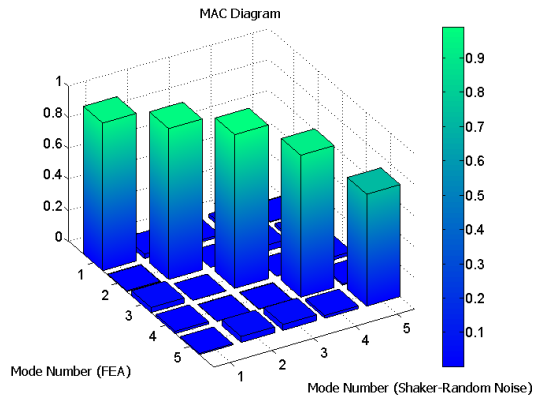


Figure 4.16. MAC diagram for random noise shaker test and FEA results

Table 4.6. MAC table for random noise shaker test and FEA results

Mode Numbers	1	2	3	4	5
1	0.9497	0.0251	0.0134	0.0243	0.0033
2	0.0075	0.9770	0.0000	0.0420	0.0200
3	0.0338	0.0010	0.9890	0.0005	0.0201
4	0.0113	0.0091	0.0018	0.9609	0.0090
5	0.0106	0.0268	0.0353	0.0194	0.7374

By comparing these MAC values with Table 4.3, it can be seen that the correlation between FEA results and test results are improved for modes numbers 2, 3 and 4 in shaker test with random noise. In the first four modes the MAC values are high in

random noise shaker test. However for the fifth mode impact hammer test gives better correlation with FEA results.

4.4.3 Shaker tests with sine sweep input signal

Sine-sweep shaker tests can bring the researcher a well observation for the response of the systems for a given frequency interval. After completing the shaker tests with random noise input, in order to be sure about the modal characteristics of the fin, the shaker is driven by a sine sweep signal by using the same test setup.

For the sine sweep tests first the frequency interval to be excited should be decided. By considering the FEA, impact hammer tests and random noise shaker tests results the frequency interval is selected as 10 Hz - 400 Hz to observe the modal characteristics of the first five modes of the fin. Secondly, the speed of the sine sweep which is a significant parameter for the test is decided. After a few trials in pre-tests, one sweep cycle time is chosen as 60 seconds. These parameters are then provided to the signal generator to drive the modal shaker. Then the FFT analysis setup is rearranged considering these sine-sweep parameters given to the signal generator. To observe the behaviour at least in two complete cycles in the required frequency range the measurement time is selected as 120 seconds. Those parameters are given in Table 4.7.

Table 4.7. FFT analysis setup parameters for sine-sweep shaker test

Parameter	Value
FFT Lines	1600
Span	400 Hz
Number of averages	88
Time for one measurement	120 s
Overlap	66.67%

The measurement procedure is same as random noise test and the results are post-processed in similar fashion by using the same script. All measurement FRFs and the composite FRF for the sine-sweep shaker test are given in Figure 4.17 and Figure 4.18, respectively. Resonance frequencies and damping ratios for the sine-sweep test are also given in Table 4.8.

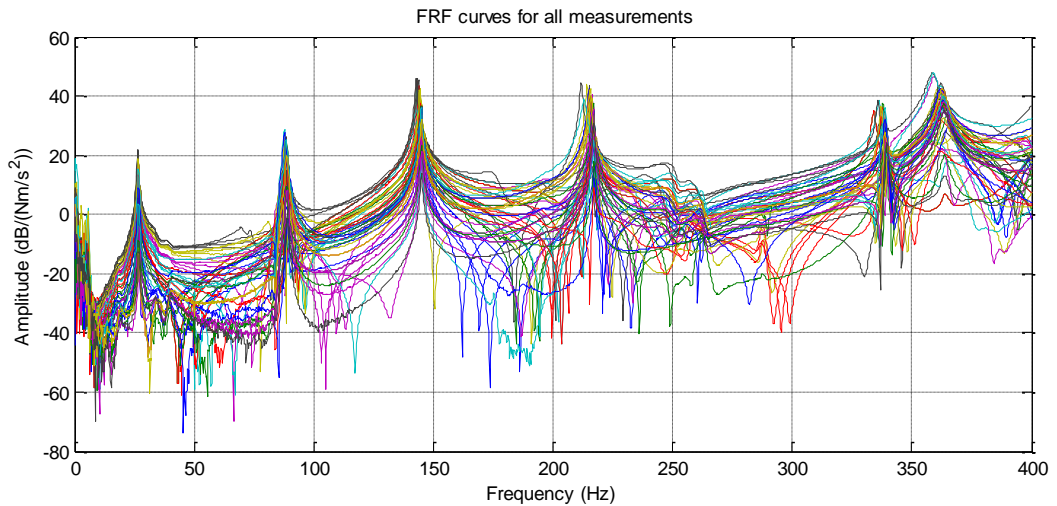


Figure 4.17. FRF plots for shaker test with sine-sweep input

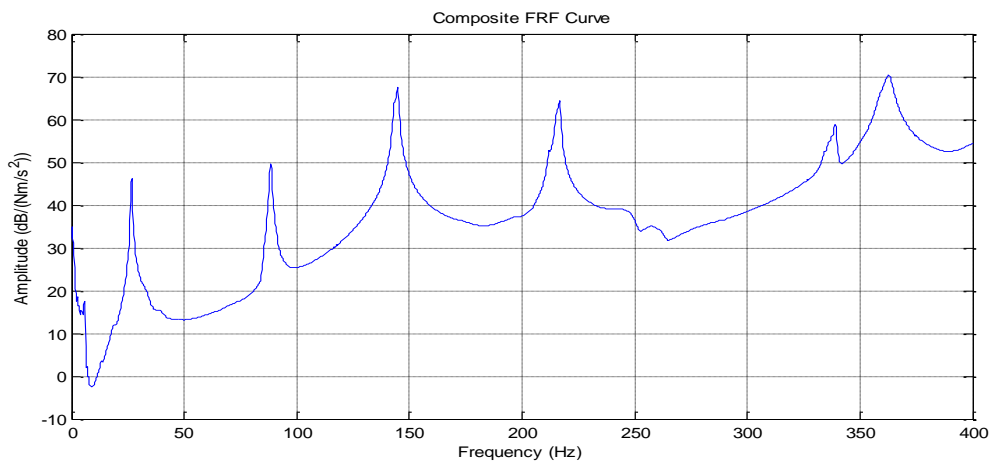


Figure 4.18. Composite FRF plot for shaker test with sine-sweep input

Table 4.8. Resonance frequencies and damping ratios of the fin from sine-sweep shaker test

Mode	Resonance Frequency [Hz]	Damping Ratio [%]
1 st Bending	26.72	2.15
1 st Torsion	88.71	1.05
2 nd Bending	144.63	0.47
Mixed Mode 1	216.36	0.34
Mixed Mode 2	338.59	0.34

It can be observed that the resonance frequencies from shaker test with random noise and sine-sweep inputs are almost the same. However, damping ratios are varying in each run. The shaker test results show maximum 1%- 2% differences with impact hammer test results regarding resonance frequencies. Mode shapes extracted from the sine-sweep tests can be seen in Figure 4.19.

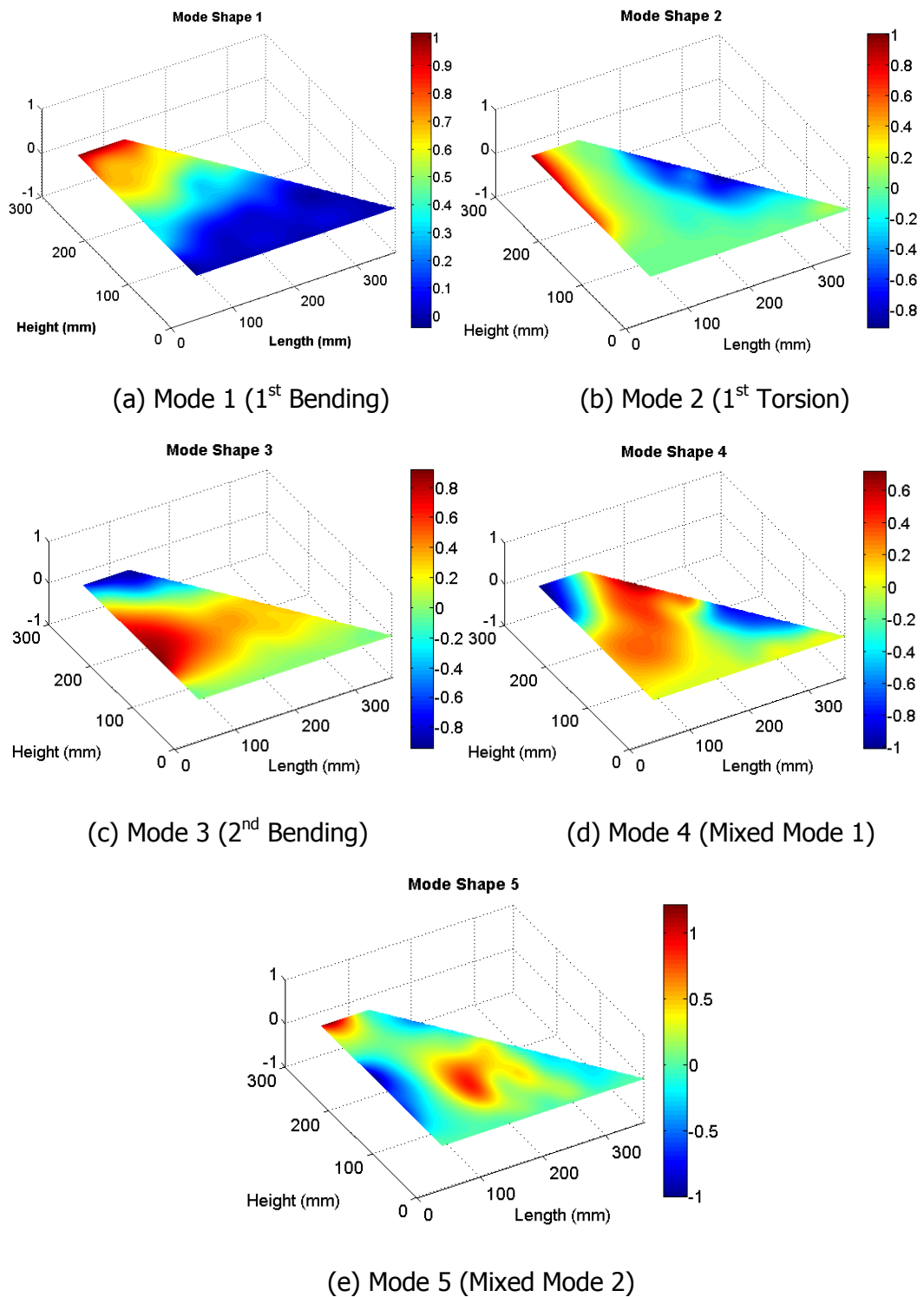


Figure 4.19. First five mode shapes of the fin extracted from shaker test with sine-sweep input

MAC diagram and MAC table constructed for sine-sweep shaker test and FEA results are given in Figure 4.20 and Table 4.9, respectively.

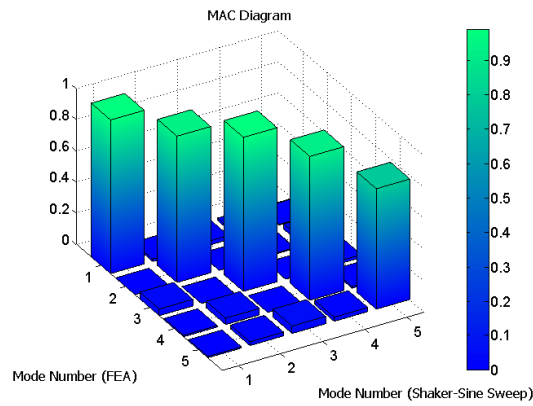


Figure 4.20. MAC diagram for sine-sweep shaker test and FEA results

Table 4.9. MAC table for sine-sweep shaker test and FEA results

Mode Numbers	1	2	3	4	5
1	0.9850	0.0152	0.0262	0.0150	0.0037
2	0.0000	0.9381	0.0000	0.0065	0.0347
3	0.0430	0.0008	0.9875	0.0006	0.0177
4	0.0095	0.0412	0.0000	0.9221	0.0113
5	0.0082	0.0241	0.0473	0.0263	0.7724

Similar to shaker test results with random noise, sine-sweep shaker test results show high correlation with FEA results in mode shapes. Nevertheless, the fifth mode has a smaller MAC value similar to one obtained in random noise shaker tests. The poor correlation for the fifth mode in both shaker tests can be explained by the attachment point of the shaker. When the mode shapes for the FEA results are

examined in a detailed way it can be observed that the attachment point of the shaker actually corresponds to a nodal point of the fifth mode. Since the magnitudes of the output are very small for that nodal point in the fifth mode, the output signal cannot be measured appropriately for an adequate modal analysis. As the hammer test results provide sufficient correlation in the fifth mode with FEA results and changing the position for shaker attachment can cause problems in the other modes, the shaker tests are not performed for the fifth mode again.

4.5 Summary

In this chapter impact hammer and shaker tests (with random noise and sine-sweep inputs) are conducted on fin-like structure to extract resonance frequencies and corresponding mode shapes. These results are compared with the FEA results calculated in the previous chapter. The natural frequencies calculated via FEA and the resonance frequencies from the classical modal analysis tests are summarised in Table 4.10. It can be seen from Table 4.10, all frequency values extracted from FEA and classical modal analysis tests are in close agreement.

Table 4.10. Comparison of FEA and Classical Modal Analysis tests results for the fin-like structure

Mode Numbers	Frequencies [Hz]			
	FEA	Impact Hammer Test	Shaker Test with Random Noise Input	Shaker Test with Sine-Sweep Input
1	27.03	26.27	26.72	26.72
2	89.60	87.93	88.64	88.71
3	144.51	141.54	144.79	144.63
4	222.92	212.17	216.48	216.36
5	347.33	334.46	338.97	338.59

CHAPTER 5

MODAL TESTING OF FIN-LIKE STRUCTURE VIA OPERATIONAL MODAL ANALYSIS IN IN-VACUO CONDITIONS

5.1 Introduction

After conducting Finite Element Analysis and Experimental Classical Modal Analysis for the fin-like structure, this chapter introduces Operational Modal Analysis (OMA) performed in in-vacuo laboratory conditions.

5.2 Operational Modal Analysis Theory

In Operational Modal Analysis, the modal identification is conducted without using the input excitation. Therefore, the modal parameters are determined by processing the output signal. The theory of OMA in frequency domain is based on Frequency Domain Decomposition (FDD) [9]. FDD provides resonance frequencies and the corresponding mode shapes of the test structure via simple peak picking [8]. To express the FDD procedure the starting point could be the input-output relation for a system. As shown in Classical Modal Analysis part of this study (see Eqn. 3.1) the relation between input and output can be shown for a linear, time invariant system as:

$$Y(j\omega) = H(j\omega)X(j\omega) \quad (5.1)$$

Where $H(j\omega)$ is the Frequency Response Function (FRF) matrix; $Y(j\omega)$ and $X(j\omega)$ are the output and input to the system. Post-multiplying by their transpose:

$$Y(j\omega)^T = X(j\omega)^T H(j\omega)^T \quad (5.2)$$

yields:

$$Y(j\omega)Y(j\omega)^T = H(j\omega)X(j\omega)X(j\omega)^T H(j\omega)^T \quad (5.3)$$

By replacing:

$$G_{yy}(j\omega) = Y(j\omega)Y(j\omega)^T \quad (5.4)$$

$$G_{xx}(j\omega) = X(j\omega)X(j\omega)^T \quad (5.5)$$

And averaging; the equation can be expressed in terms of spectral density matrices of input and output of a system as:

$$G_{yy}(j\omega) = H(j\omega)^* G_{xx}(j\omega) H(j\omega)^T \quad (5.6)$$

Where $G_{xx}(j\omega)$ and $G_{yy}(j\omega)$ are Power Spectral Density (PSD) matrices of input and output, respectively. "*" and "T" denote the complex conjugate and transpose of the matrix, respectively. In this equation, input is assumed as white noise and input PSD is equal to a constant. This relation can be shown as:

$$G_{yy}(j\omega) = H(j\omega)^* [I] H(j\omega)^T \quad (5.7)$$

By this relation it can be concluded that output PSD matrix holds the dynamic properties of a system in case of white noise assumption for input PSD matrix. By using partial fraction expansion FRF of the system can be expressed as:

$$H(j\omega) = \sum_{k=1}^N \frac{R_k}{j\omega - \lambda_k} + \frac{R_k^*}{j\omega - \lambda_k^*} \quad (5.8)$$

where λ_k is the pole location used in the determination of resonance frequency and the residue, R_k is:

$$R_k = \gamma_k \phi_k \quad (5.9)$$

where ϕ_k is the mode shape vector and γ_k is the modal participation vector.

By using the equations 3.10 and 3.11, for a lightly damped structure the output PSD function in a partial fraction can be rewritten as:

$$G_{yy}(j\omega) = \sum_{k \in Sub(\omega)} \frac{d_k \phi_k \phi_k^T}{j\omega - \lambda_k} + \frac{d_k^* \phi_k^* \phi_k^{T*}}{j\omega - \lambda_k^*} \quad (5.10)$$

where d_k is a scalar constant for the k^{th} mode and $Sub(\omega)$ is the set of modes contributing at the particular frequency, ω .

To obtain Single Degree of Freedom (SDOF) systems from output PSD function, Singular Value Decomposition (SVD) is conducted to the final form of the output PSD at discrete frequencies as follows:

$$G_{yy}(j\omega) = U_i S_i U_i^T \quad (5.11)$$

where S_i is a diagonal matrix holding the singular values and U_i is another matrix holding singular vectors. Singular values are used to estimate resonance frequencies whereas singular vectors contain mode shape information.

SVD process is applied for each frequency ω and each measurement. A sample SVD plot obtained during operational modal testing is given in Figure 5.1

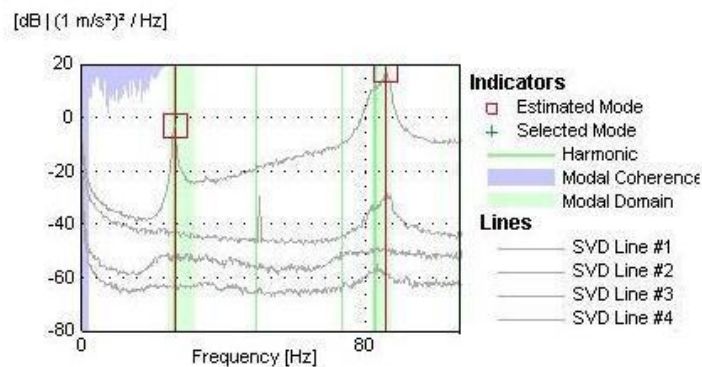


Figure 5.1. Sample SVD Plot

In SVD plots, the number of SVD lines is equal to the measurements at each run. In other words, number of transducers (except the reference one) used for output signal measuring determines the number of SVD lines.

An improved version of FDD, called Enhanced Frequency Domain Decomposition (EFDD), has the ability of estimating damping ratios in addition to resonance frequencies and mode shapes. In EFDD method, Single Degree of Freedom (SDOF) PSD function identified around a resonance peak is transformed to time domain using Inverse Discrete Fourier Transform (IDFT) [69]. This process is represented in Figure 5.2.

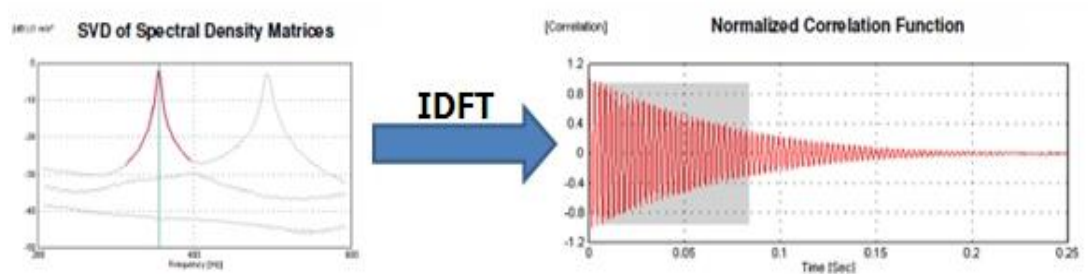


Figure 5.2. Inverse Discrete Fourier Transform(IDFT) process for EFDD method

The resonance frequency is calculated by the zero-crossings of this function in time domain. Damping calculation is conducted by using logarithmic decrement. Sample natural frequency and damping calculation are shown in Figure 5.3.

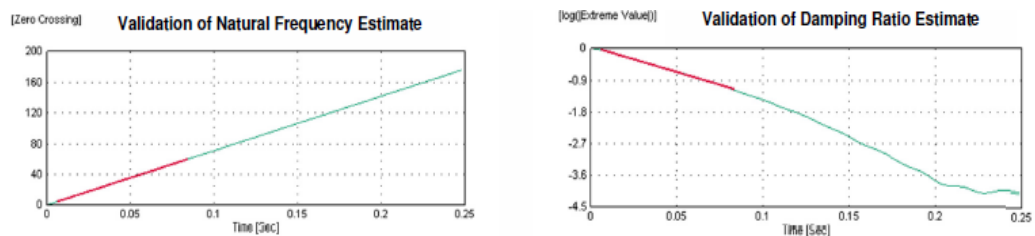


Figure 5.3. Natural frequency(left) and damping ratio(right) calculation in EFDD method

The formulation for damping calculation in EFDD method can be shown as [9]:

$$\delta_k = \frac{2}{k} \ln \left(\frac{r_0}{r_k} \right) \quad (5.12)$$

where δ_k is the logarithmic decrement, r_0 is the initial value of correlation function and r_k is the k^{th} extreme. Then, the damping ratio can be given as:

$$\zeta = \frac{\delta}{\sqrt{\delta^2 + 4\pi^2}} \quad (5.13)$$

Another type of OMA methods is Curve-fit Frequency Domain Decomposition (CFDD) which estimates not only the natural frequency and mode shapes but also the damping ratios. It is an improved version of FDD like EFDD however; it calculates the modal parameters by curve-fitting SDOF functions in frequency domain. Since it works in frequency domain it is more appropriate method than EFDD when the SVD plots are noisy. For the reason that, the back-transform process in EFDD method can decrease the accuracy while using noisy data in frequency domain [11].

To summarize the methods used in OMA; FDD is a method which estimates the natural frequencies and mode shapes by snapping to the peaks. Therefore, it is a fast and easy method. The ability snap to the frequency values other than resonance peaks, gives better understanding of structural behaviour. The disadvantages of FDD method is the lack of damping estimation and limited frequency resolution [70].

EFDD method is an improved version of FDD method which estimates damping in addition to FDD estimates. By using all SVD lines in calculations it calculates standard deviations of frequency and damping ratios. One disadvantage of EFDD method can rise when the resonance peaks cannot be distinguished for all data sets (i.e. SVD lines) [70].

CFDD method can calculate the same modal parameters which can be calculated by EFDD method but in a different way. CFDD method directly fits SDOF functions in frequency domain instead of transforming them into time domain.

In this study both three types of OMA techniques are applied in tests. For all types of OMA tests, if a few conditions are satisfied then the OMA can provide better results. Those conditions are listed below [70]:

- Input forces should be broadband and smooth.
- Input forces should be un- or weakly correlated.
- Entire structure should be excited by the forces all over it.

5.3 Test setup and software for Operational Modal Analysis tests

Test fixture

The fixture designed for Classical Modal Analysis tests is also used (See Section 4.3) for in-vacuo Operational Modal Analysis tests.

Test equipments

In in-vacuo OMA tests, same miniature accelerometers and the data acquisition system is used as in the Classical Modal Analysis cases (See Section 4.3). OMA tests conducted in in-vacuo conditions are in two types. In the first test, the fin is excited via the shaker by using a random noise. In the second one on the other hand, it is excited by an acoustic noise given by the speakers. For the OMA test with random noise, the input excitation is given to the system by the modal shaker which is also used in CMA part of this study (See Section 4.3). Signal generator used for random noise signal generation is also same with the CMA part (See Section 4.3). For the OMA tests using acoustic noise excitation Philips™ SPA-1300 multimedia speakers are used. They are positioned just back to the fin and the white noise sound signal is generated by the software MATLAB™. The placement of the speakers and the fin is given in Figure 5.4.

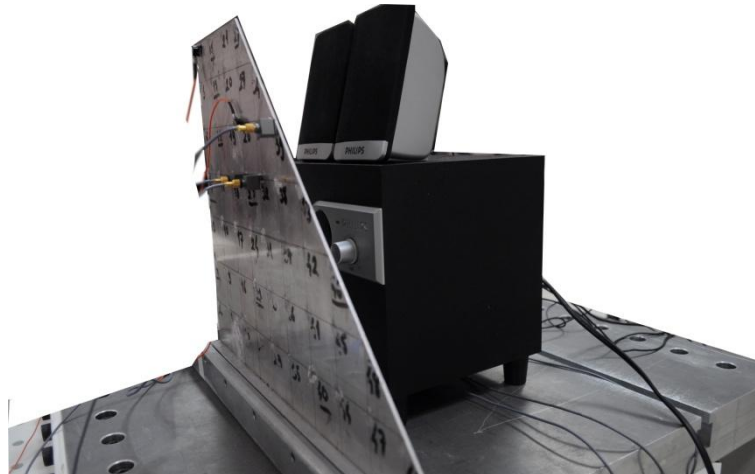


Figure 5.4. Acoustic noise excitation equipments and placements

Test software

The measurements in OMA tests are recorded and stored in the lab computer by the help of the PULSE™ Modal Test Consultant software which is also used in the Classical Modal Analysis of this study (See Section 4.3). For the post-process of the measurements Type 7760 PULSE™ OMA software is used [11]. After importing measurement data, analysing options for OMA is set. The values defined here are used for automatic mode extraction which is a feature of the software that automatically peaks the resonance frequencies by using the limits defined. The software also allows adding modes manually. Analysing options screen and the related parameters are given in Figure 5.5.

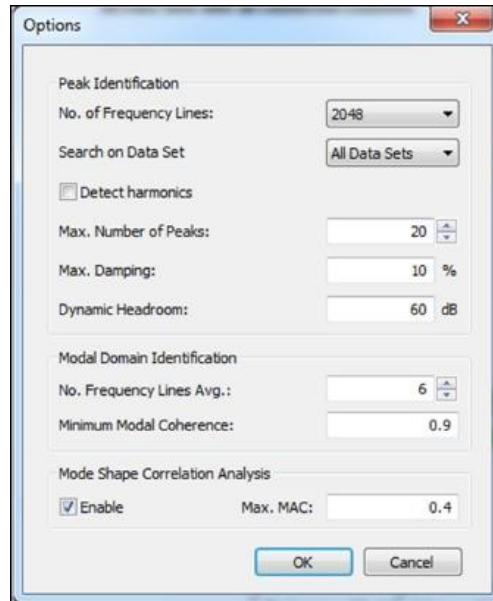


Figure 5.5. OMA Software analysis options screen

The definitions of the significant parameters in analysing options are as follows:

No. of frequency lines

Number of frequency lines that is used for sampling the measurement data set is defined here.

Max. Number of Peaks

This value is defined to limit the number of identified modes.

Max. Damping

To eliminate unrealistic modes upper limit for the damping ratio can be defined here.

Dynamic Headroom

Difference between the nominal and the maximum value of the output.

No. of Frequency Lines Avg.

Number of frequency lines to include in a moving average is defined here. For closely coupled modes this parameter should be bigger. For high frequency resolutions higher values can be used.

Minimum Modal Coherence

For the defined number of frequency lines for averaging, singular vectors are averaged according to the formula:

$$d_1(f_0) = \frac{1}{N} \sum_{n=1}^N u_1(f_n)^T u_1(f_0) \quad (5.14)$$

where N is the number of frequency lines averaging and $u_1(f)$ is the singular vectors as a function of frequency. If the value $d_1(f_0)$ (i.e. modal coherence) is greater than the number defined as the minimum mode coherence, a modal domain is satisfied for the region around the peaks.

Max. MAC

This value is given to the software to eliminate the duplicate modes. Modes having bigger correlation value than Max. MAC are reduced to one mode in automatic mode extraction.

Detect Harmonics

If the box is checked in this part, the harmonic components detected in OMA are marked on the SVD line screen.

The values defined in "Analysis Options" window are just to help the researcher by accelerating the modal analysis by analysing the modes and extracting them automatically. However, the right choices for the values require sufficient experience on the test structure and Operational Modal Analysis software.

After defining those parameters for automatic mode extraction the SVD plots are obtained and shown in the next screen of the software. In this part some of the

modes can be deleted and some of them can be added manually by selecting the desired frequency from the SVD plot. For FDD analysis resonance frequencies are given in the list below the screen. In EFDD analysis, damping ratios are also listed in addition to the frequency values. Moreover, the standard deviation values for both resonance frequencies and damping ratios are listed. To visualise a mode shape, first the desired mode is selected from the table then it is animated on the screen. The sample screen for mode extraction is given in Figure 5.6.

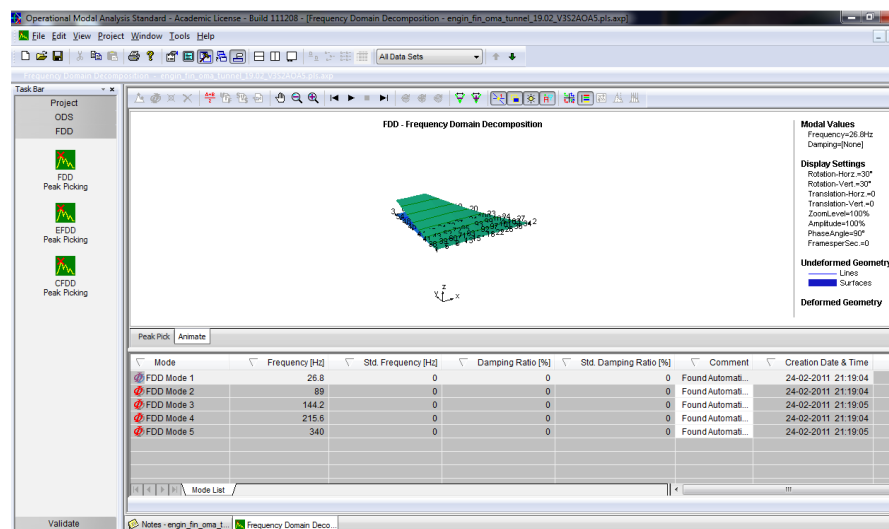


Figure 5.6. Sample screen for mode extraction in OMA software

To check the correlation between the mode shapes between two different test measurements, MAC matrix can be calculated and indicated by graphs in OMA software. This tool can also be used for AutoMAC calculations for one test measurement.

5.4 Operational Modal Analysis tests in in-vacuo conditions

After conducting Finite Element Analysis and verifying the results by Classical Modal Analysis tests, in the same laboratory environment Operational Modal Analysis and tests are then performed. First, the fin-like structure is excited by the shaker (See

Section 5.3) with white noise input and analyzed by using OMA. Secondly, the fin is excited by acoustic noise given by the speakers (See Section 5.3) and the modal parameters are extracted using OMA technique.

5.4.1 Operational Modal Analysis by using shaker excitation with random noise input signal

Broadband input excitation is one of the main requirements for OMA method to apply it for dynamic property estimation (See Section 5.2). To satisfy this condition, white noise excitation is given to the fin by shaker via a stringer. Stringer is attached to the same position as in Classical Modal Analysis (CMA) part (See Figure 4.4). By examining the previous results from CMA tests and FEA, the magnitude of the displacements for all measurement points are calculated for the first five modes. It is observed that the rear-top corner of the fin (Point 7, in Figure 4.8) is experiencing significant deflections in all modes. As a result, the reference accelerometer which is a must in OMA is attached to this point. The other accelerometer is roved to 48 positions over the fin to extract modal parameters.

By considering the first resonance frequency of the fin, in data acquisition software (i.e. PULSE™ MTC) the lowest frequency of interest is selected as 5 Hz. After a few trials and checking the measured data, 100 cycles of the period is selected as measurement time parameter. Therefore, duration of one measurement is resulted as 20 seconds.

At the end of the post processing of the measured data by PULSE™ OMA software, SVD plots are extracted. The average SVD from all measurements is given in Figure 5.7 and the peaks corresponding to the resonance frequencies of the fin are also pointed out.

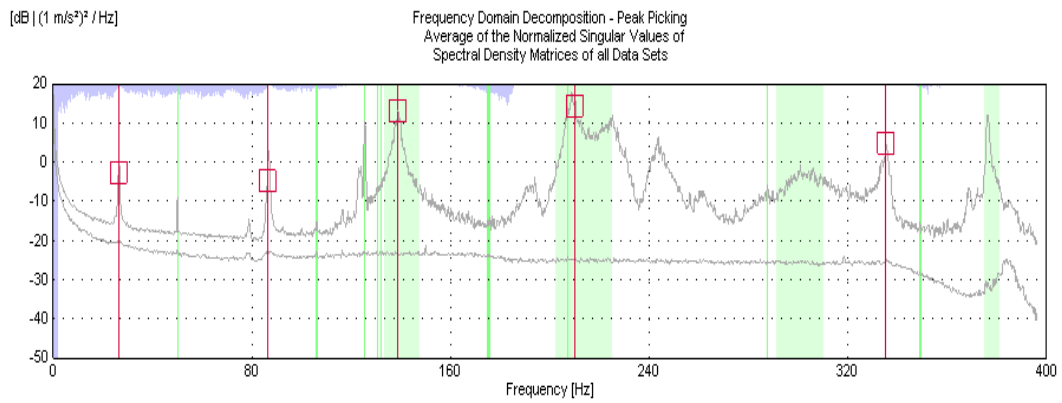


Figure 5.7. Average SVD plot from shaker random noise OMA test

As seen from the figure that there are also peaks in SVD plot other than the resonance frequencies. To check whether those peaks correspond to any mode or not, the mode shapes are animated at those frequencies by using the software. It is observed that they do not belong to any mode of the fin. The first five resonance frequencies extracted by FDD method and their percentage differences from the shaker random noise test (See Table 4.5) are given in Table 5.1.

Table 5.1. Resonance frequencies by OMA-FDD method and differences from CMA random noise shaker test

Mode	Resonance Frequency by FDD in OMA [Hz]	Differences from random noise input shaker test (CMA) [%]
1 st Bending	26.20	1.95
1 st Torsion	86.20	2.75
2 nd Bending	138.80	4.14
Mixed Mode 1	209.80	3.09
Mixed Mode 2	335.20	1.11

As it can be seen from the table, the resonance frequencies are in a close agreement for the same input type for CMA and OMA.

As also explained in Section 5.2, the damping ratios are calculated by using both methods of EFDD and CFDD in OMA. Damping ratios resulted from these methods and damping ratios from CMA by shaker test with noise input are given in Table 5.2.

Table 5.2. Damping ratios by OMA and CMA for shaker test with random noise input

Mode	Damping ratios by EFDD [%]	Damping ratios by CFDD [%]	Damping ratios from CMA(shaker test with random noise) [%]
1 st Bending	0.59	0.66	1.66
1 st Torsion	0.22	0.18	1.37
2 nd Bending	0.48	0.62	0.50
Mixed Mode 1	0.53	0.73	0.30
Mixed Mode 2	0.07	0.20	0.32

Damping ratios calculated from OMA with two methods are close to each other whereas their differences with CMA results are relatively high.

Mode shapes extracted from OMA are given in Figure 5.8.

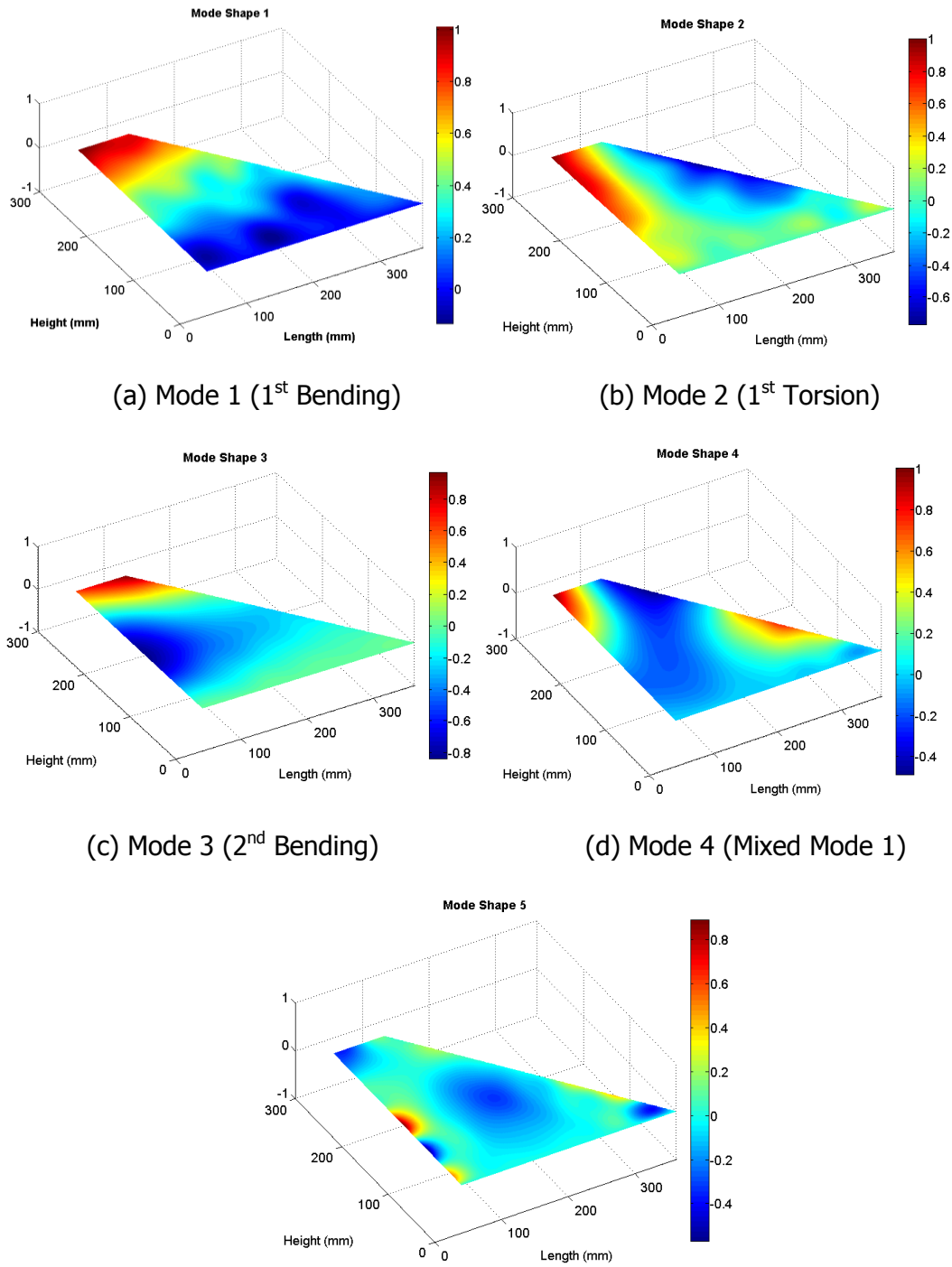


Figure 5.8. First five mode shapes of the fin extracted from shaker test with random noise input by OMA

Mode shapes extracted with OMA are also compared with the CMA results by the same input type. MAC diagram and MAC table are given in Figure 5.9 and Table 5.3, respectively.

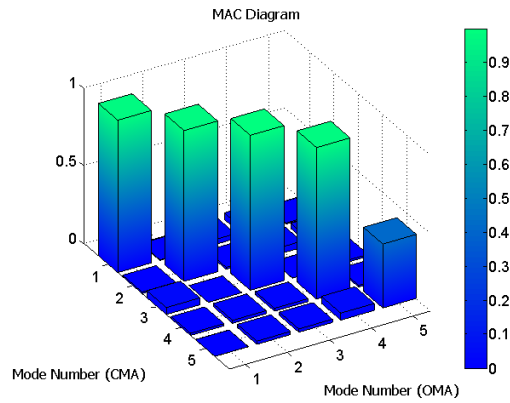


Figure 5.9. MAC diagram for OMA and CMA with random noise shaker input

Table 5.3. MAC table for OMA and CMA with random noise shaker input

Mode Numbers	1	2	3	4	5
1	0.9246	0.0387	0.0133	0.0176	0.0002
2	0.0035	0.9318	0.0004	0.0221	0.0133
3	0.0208	0.0109	0.9827	0.0219	0.0225
4	0.0309	0.0063	0.0001	0.9214	0.0405
5	0.0036	0.0477	0.0354	0.0094	0.4014

As it is observed from Table 5.3, there is a high correlation in the first four modes between OMA and CMA regarding the same type of input. However, the fifth mode provides the lowest MAC value. As it can also be seen from Table 4.6, the correlation between CMA with random noise shaker input and FEA is quite low. For

that reason, in order to be sure about the accuracy of estimation of the fifth mode shape, OMA result is also compared with FEA ones in terms of MAC values. The result is given in Table 5.4.

Table 5.4. MAC table OMA with random noise shaker input and FEA

Mode Numbers	1	2	3	4	5
1	0.9793	0.0099	0.0445	0.0139	0.0008
2	0.0038	0.9691	0.0006	0.0193	0.0203
3	0.0318	0.0127	0.9962	0.0190	0.0210
4	0.0423	0.0401	0.0010	0.9742	0.0450
5	0.0069	0.0330	0.0130	0.0114	0.4110

Very high MAC values can be observed for the first four modes although the fifth mode has a very low MAC value again. The very low MAC value for the fifth mode can be explained by the single excitation point on the fin. When the mode shapes extracted from FEA and impact hammer tests are examined, it is realised that the excitation point was a nodal point for the fifth mode. This means, the fin could not be excited properly in the fifth mode since the modal deflections are close to zero there.

5.4.2 Operational Modal Analysis by using acoustic noise excitation

After conducting OMA test with random noise shaker input, to eliminate the influence of the attachment of the input excitation, a non-contact type excitation is selected for the input. The non-contact input is given as acoustic noise by the help of the speakers (See Section 5.3). Same measurement settings with the OMA test with random noise shaker input (See Section 5.4.1) are used and a measurement time is selected as 20 seconds again.

Reducing the number of measurement points

To have time saving in tests and to check the resonance frequencies in a faster way, the number measurement points is reduced. The reduction process is performed by examining the mode shape data from CMA results. The points which have significant deflection in all modes are selected first. Then, to have better information from all over the fin structure some of the neighbouring points are eliminated and some other points are added to the measuring test matrix. At the end of this selection process, 49 measurement points are reduced down to 11 including the reference accelerometer. The positions of these points are given in Figure 5.10.

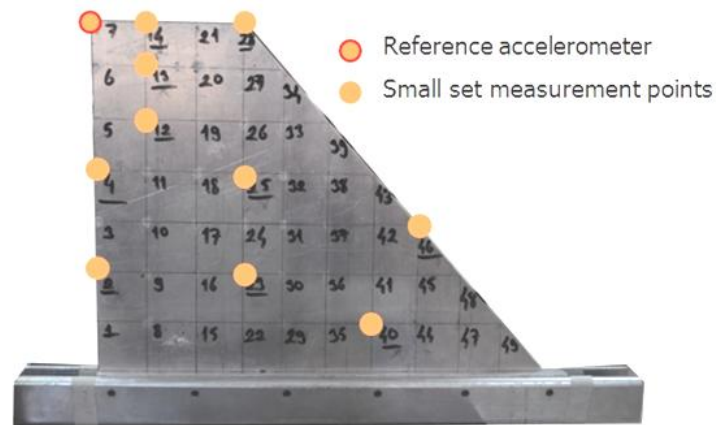


Figure 5.10. Reduced set of measurement points for OMA tests

The fixed reference accelerometer is attached to the upper rear corner of the fin and the other accelerometer is moved on to 10 different points under the excitation of the acoustic noise to conduct OMA tests. Resulting SVD is given in Figure 5.11.

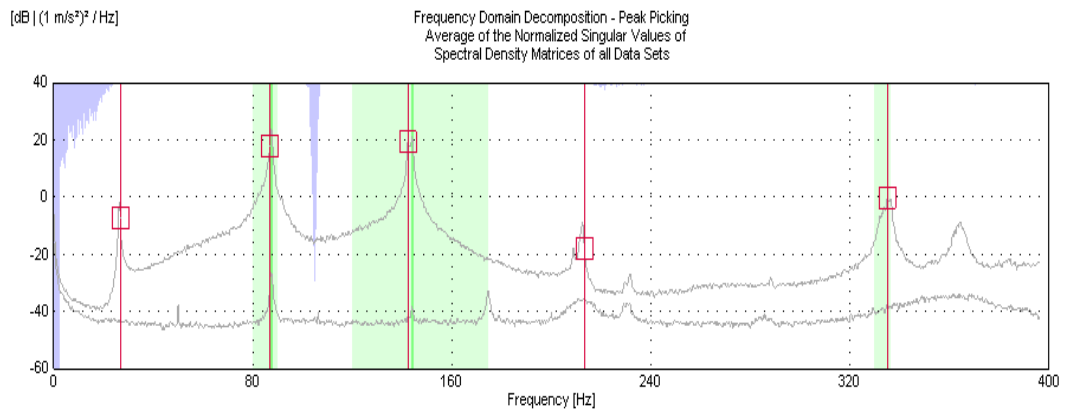


Figure 5.11. Average SVD plot for OMA test with acoustic noise input

If the SVD plot in Figure 5.11 is compared to the one in Figure 5.7, it can be observed that the acoustic input in OMA gives more clear SVD plots than that of in the random noise input which is given by an attached shaker. The resonance peaks in SVD plots for OMA with acoustic noise input are also determined well. The frequency values corresponding to these peaks are given in Table 5.5 .

Table 5.5. Resonance frequencies by OMA-FDD method with acoustic noise input and differences from impact hammer test result

Mode	Resonance Frequency by FDD in OMA [Hz]	Differences from impact hammer test (CMA) [%]
1 st Bending	26.75	1.79
1 st Torsion	86.75	1.36
2 nd Bending	142.25	0.46
Mixed Mode 1	213.25	0.48
Mixed Mode 2	335.00	0.16

As it is seen from Table 5.5, resonance frequencies from non-contact input OMA tests are very close to the results from impact hammer test which is a CMA method which has no attached excitation mechanism to the test structure.

Damping ratios calculated by OMA methods (i.e. EFDD and CFDD) are given with the impact hammer test damping ratio results in Table 5.6.

Table 5.6. Damping ratios by OMA with acoustic noise input and impact hammer test

Mode	Damping ratios by EFDD [%]	Damping ratios by CFDD [%]	Damping ratios from CMA(impact hammer test) [%]
1 st Bending	0.74	0.68	1.44
1 st Torsion	0.76	0.65	1.14
2 nd Bending	0.32	0.30	0.79
Mixed Mode 1	0.25	0.24	0.43
Mixed Mode 2	0.19	0.19	0.46

EFDD and CFDD method gives similar damping ratios for this test whereas they are far from impact hammer test results. PULSE™ OMA software calculates the damping ratios by taking the average of the results from each data set. Standard deviations of the results are also given as outputs. The standard deviations of the damping ratios are around 80% for both OMA-EFDD and OMA-CFDD methods. These high numbers of deviations can be caused due to the low level of excitation and less number of measurement devices which affects the correlations between the measurements for each data set.

CASE STUDY: Increasing the number of accelerometers in OMA

In this thesis study, two accelerometers are used for all OMA tests. To investigate the effect of increasing the number of accelerometers in OMA, 3 accelerometers are added. These three accelerometers are B&K Type 4508B [71] and each weighs 8 grams. Same test setup with the previous acoustic noise OMA test is used for this case study as well. The new added accelerometers are also attached to the fin by the help of bee wax. For the measurement process, one of the lighter accelerometers is placed as a reference accelerometer at exactly the same point with the previous OMA tests. Other four accelerometers are moved over the fin in each measurement. To minimise the mass effect of the accelerometers the lighter accelerometer is always positioned in upper regions (i.e. closer to the free end of the structure) whereas the heavier ones are tried to be located in lower regions (i.e. closer to the clamped end of the structure). A sample accelerometer position is given in Figure 5.12.

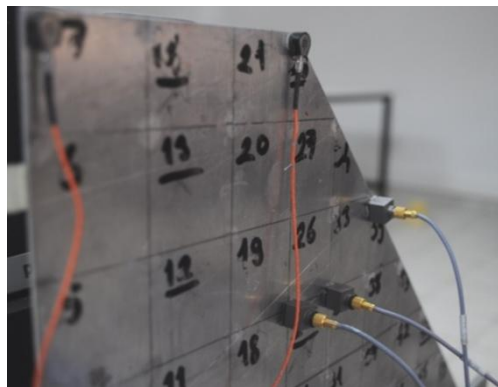


Figure 5.12. A sample position for five accelerometers

By moving the accelerometer set containing four accelerometers to different positions over the fin, all 48 points to measure are covered in seven successive measurement operations. The analyser settings are held same with the previous tests and the resulting average SVD plot is given in Figure 5.13.

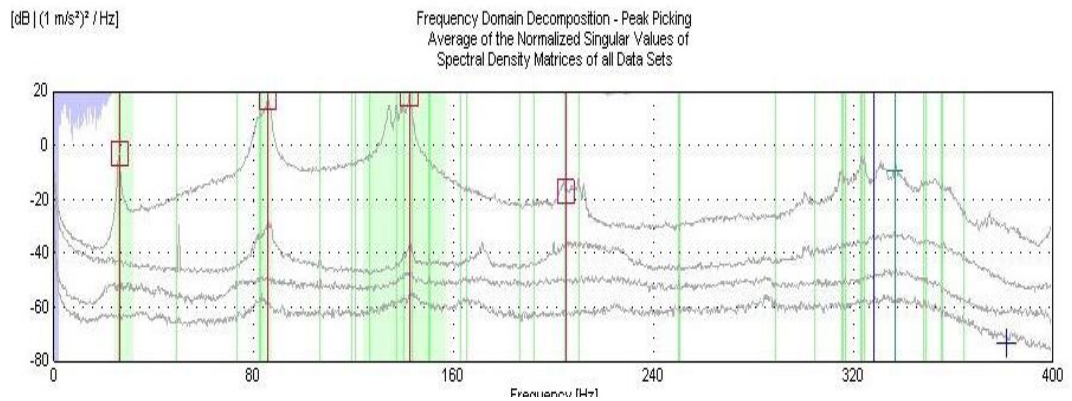


Figure 5.13. Average SVD plot for OMA acoustic noise test with 5 accelerometers set

Since there are four accelerometers for the measurement other than the reference one it can be observed from Figure 5.13 that there are 4 SVD lines for the results. Another thing to observe in SVD plots are the mass effects of the accelerometers. Except first two modes in all other modes the SVD plots have a few peaks around the resonance region. This phenomenon is caused due to the changing the effective mass of the fin by changing positions of the accelerometers. The resonance frequencies extracted at the end of OMA analysis and comparison of these values with those of in previous acoustic noise OMA tests are given in Table 5.7.

Table 5.7. Resonance frequencies extracted by OMA-FDD method using different number of accelerometers

Mode	Resonance Frequency from case study with five accelerometers by FDD in OMA	Differences from acoustic noise OMA test with two accelerometers
	[Hz]	[%]
1 st Bending	26.20	2.10
1 st Torsion	85.40	1.58
2 nd Bending	142.20	0.00
Mixed Mode 1	N/A	N/A
Mixed Mode 2	N/A	N/A

As it is observed from Figure 5.13, the resonance peaks around Modes 4 and 5 are not very clear and therefore the OMA software cannot automatically detect the modes. In fact, they can be added manually but for an unknown test structure it is not easy task to determine the modes around those several peaks. So, in this case study, the fin is treated as if its dynamic properties are not known through other tests as a result of that the frequency values are considered to be not estimated.

The first three modes shapes of the fin extracted from this test are given in Figure 5.14.

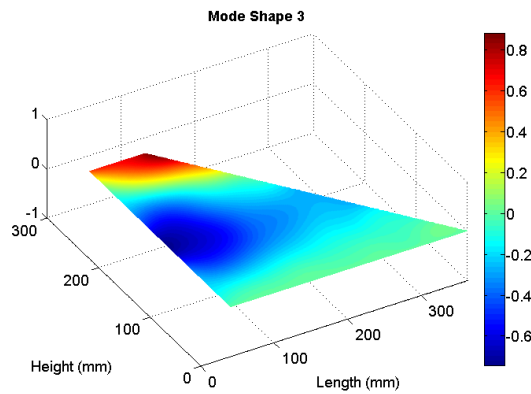
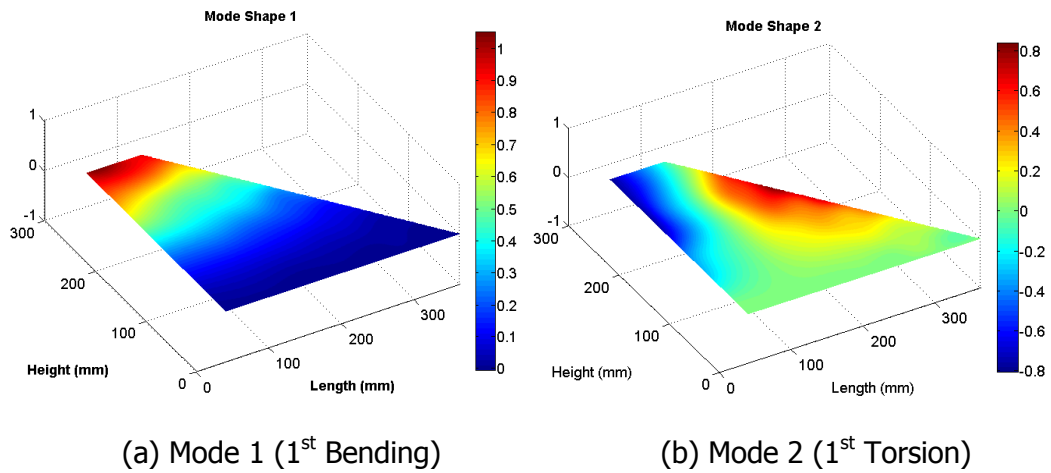


Figure 5.14. The first three mode shapes of the fin extracted from OMA test with acoustic noise input (five accelerometer case)

Since the first three of mode shapes are estimated in a greater accuracy they are shown in Figure 5.14 and their correlation with impact hammer test results are given as a MAC diagram in Figure 5.15 and tabulated form in Table 5.8 respectively.

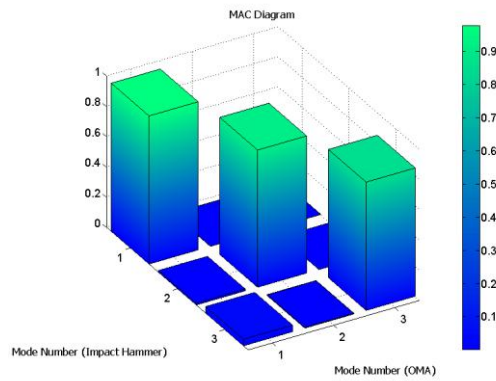


Figure 5.15. MAC diagram for OMA acoustic noise (five accelerometers case) and impact tests results

Table 5.8. MAC table for OMA acoustic noise (five accelerometers case) and impact tests results

Mode Numbers	1	2	3
1	0.9768	0.0013	0.0009
2	0.0115	0.9044	0.0003
3	0.0431	0.0049	0.8458

Similar to SVD plots, mass effect of the accelerometers can also be observed in MAC table and MAC diagram for this case study. In the first mode, there is a high correlation between acoustic noise input OMA test and impact test. However in the second and third ones, the MAC values are relatively low due the mass effect of accelerometers on the mode shapes.

5.5 Summary

In this chapter, modal parameters of the fin are extracted by Operational Modal Analysis in the laboratory environment of having similar conditions with the tests

performed via Classical Modal Analysis. First, the shaker setup is used to excite the fin by white noise signal. Resonance frequencies extracted at the end of this test are generally in close agreement with the CMA test having the same excitation input. On the other hand, SVD plot obtained by the OMA is noisy which makes the resonance frequency picking process difficult. Exciting the fin only from one point seems to violate the general requirements for a satisfactory OMA. This exciting condition results as a noisy SVD plot.

Mode shapes extracted from this test are also in close agreement with CMA and FEA results in the first four modes. The low MAC value obtained in the fifth mode is due to the excitation point which is a nodal point. As a second OMA test in this chapter, fin is excited with acoustic noise input given by speakers. Compared to the test results with shaker noise input, SVD plots are appeared to be clearer in this test. Resonance frequencies of this test results are then compared with those of impact hammer tests and observed to be very close to each other. Damping ratios extracted from both OMA tests are observed to be close agreement with each other although they are relatively different from the results of CMA.

As a particular case study, number of accelerometers is increased and the accuracy of the results of OMA is checked. Additional mass effect of the accelerometers is observed in SVD plots and due to this effect, the fourth and the fifth modes could not be extracted. Whereas, the obtained values of resonance frequencies and mode shapes are close to the results of impact hammer test in the first three modes.

CHAPTER 6

MODAL TESTING OF FIN-LIKE STRUCTURE VIA OPERATIONAL MODAL ANALYSIS IN WIND TUNNEL CONDITIONS

6.1 Introduction

The test structure used in this study is a fin-like structure which is generally used in aircraft. The main loading on these types of structures is aerodynamic load and those loads can be simulated in wind tunnels. It is stated that wind loading fulfils the requirements for the OMA input forces [70]. Because wind forces are not only broadband and smooth but also act all over the structures.

In this chapter OMA is applied to the fin which is excited by the wind loading in wind tunnel. Effects of different flow angles and disturbances through the flow on modal parameters are examined.

6.2 Wind tunnel and test setup

Wind Tunnel

Wind tunnels are frequently used to simulate the acting forces on aircraft structures. The wind tunnel used in this study is an open-loop blow-down wind tunnel which has $0.6 \times 0.6 \text{ m}^2$ square cross-section fully transparent test section located in the Department of Aerospace Engineering, METU. Sections and dimensions of the wind tunnel are given in Figure 6.1 [72].

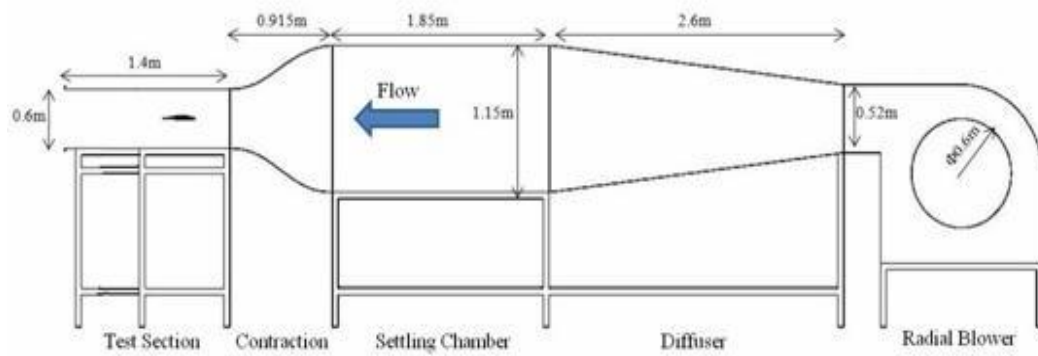


Figure 6.1. Wind tunnel sections and dimensions

The tunnel is operating by a frequency controlled electrical motor. The speed of the wind tunnel is set by the help of an interface module for setting the operating frequency of this motor. The motor frequencies and corresponding flow speeds are given in Appendix B.1. Minimum and maximum operating speeds of the tunnel are 4.78 m/s and 15.39 m/s, respectively.

Test fixture

For the wind tunnel tests, a mounting frame which is located at the exit of the wind tunnel is used to hold the fin. The mounting frame location is shown in Figure 6.2.

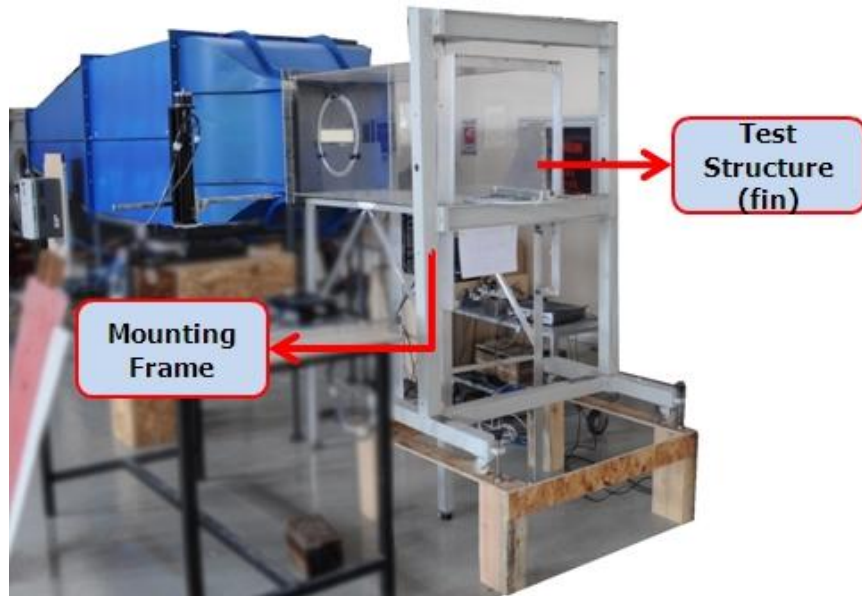


Figure 6.2. Fin mounting frame location for wind tunnel tests

Fin is located on a base which is attached to the mounting frame. The base is designed as heavy and stiff ring of aluminium which allows fixing the test structure in different positions. These fixing positions provide four different angles of incoming flow with respect to fin-like structure (so-called angle of attacks) of 0, 5, 10 and 15 degrees. First, fin is mounted to the aluminium bar (See Section 4.3), and then both the bar and the fin are attached to the aluminium ring in the desired position. Test base (i.e. both bar and ring together) with the fin is attached to the mounting frame. Test base location on mounting frame and top view of test base are given in Figure 6.3 (a) and Figure 6.3 (b), respectively.



Figure 6.3. (a) Test base location on mounting frame (b) Test base top view

As performed in CMA part (See Section 4.3), resonance frequencies of the test base are also checked in order to guarantee that there won't be any interference with the dynamic characteristics of the fin structure. The analysis procedure is given in Appendix A.3. At the end of the modal analysis of the test base, the fundamental natural frequency is found as 414 Hz which is well outside of the frequency range of interest of the fin regarding the first five modes (See Table 3.3).

6.3 Operational Modal Analysis tests in wind tunnel

For OMA tests in wind tunnel, the dynamic properties are extracted first under the flow condition where there is no disturbance on the flow over the fin. The effect of different flow speeds and flow angles are investigated for the flow condition without vortex generator. For the second part of the tests the vortices are generated just before the fin. The effect of the position of the vortex generator is examined and the modal analysis is conducted under this turbulent flow conditions as well.

6.3.1 Tests by OMA in wind tunnel without vortex generator

The fin is located on the test base with an angle of zero degree (See Figure 6.3 (a)). The speed of the electrical motor is selected as 2 Hz which corresponds to a flow speed, 4.78 m/s (See Table B.1). The reference accelerometer is placed at the same location used in in-vacuo tests of OMA. Since there are quite a few runs to be performed in the wind tunnel, in order to save time the aforementioned reduced measurement set (See Figure 5.10) is used. To analyse the modal properties of the fin in a faster way in various conditions (i.e. angle of attack and flow speed combinations) which will be given in following sections, the Automatic Mode Extraction property of the PULSE™ OMA software is set. The automatic mode extraction parameters are defined in Section 5.3. After a few trial runs they are identified as in Table 6.1 for all OMA tests in wind tunnel.

Table 6.1. Automatic Mode Extraction parameters for OMA wind tunnel tests

Parameter	Value
Maximum number of peaks	10
Max. Damping	5%
Dynamic Headroom	100 dB
No. Frequency Lines Avg.	10
Minimum Modal Coherence	0.99
Max. MAC for Mode Shape correlation	0.99

The value for minimum modal coherence is taken as very high and the frequency number of lines for averaging is stated relatively low to avoid from any peaks which is not a structural mode. Other parameters are also decided in a way which increases the performance of automatic mode estimation.

Before starting OMA post-process, the settings for frequency interval are also conducted in the software. Frequency range to be analyzed in OMA software is

selected as 0-512 Hz and the number of FFT lines is selected as 2048. As a result, the frequency resolution for the results is 0.25 Hz.

At the end of the post-process of the measurements the resulting SVD plot is given in Figure 6.4.

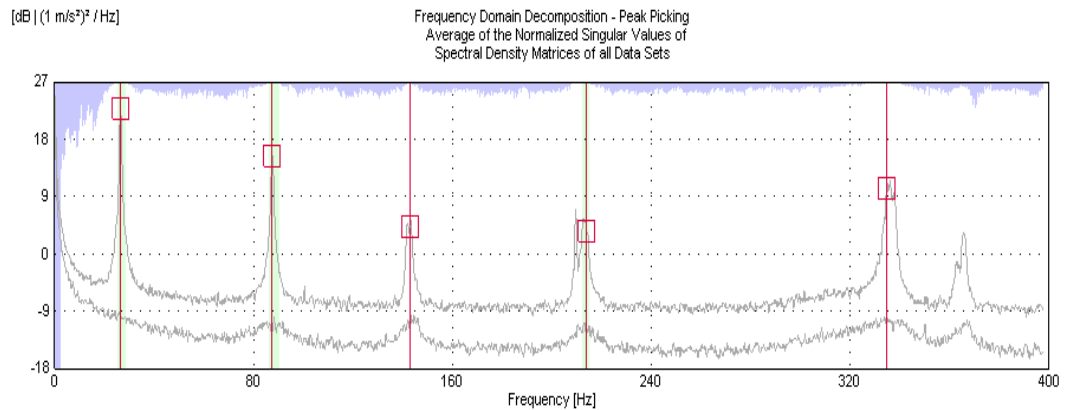


Figure 6.4. SVD plot for OMA test in tunnel with flow speed=4.78 m/s

As it can be seen from the above SVD plot the resonance peaks of the fin exist in the resulting SVD. However, the modal domains (shown with light green colour and appear either side of the resonance peaks) are not clear. On the other hand, the modal coherence regions i.e. the noise domains for the analysis are distinguishable at the top of the graph. The reason for these to be appeared in SVD plots may possibly be due to the low level of excitation forces.

The resonance frequencies and damping ratios extracted from this test are summarised in Table 6.2.

Table 6.2. Resonance frequencies and damping ratios extracted from OMA wind tunnel test with flow speed=4.78 m/s

Mode	Resonance Frequency via OMA (FDD) [Hz]	Damping Ratio via OMA (EFDD) [%]
1 st Bending	26.50	0.75
1 st Torsion	87.50	0.36
2 nd Bending	143.00	0.43
Mixed Mode 1	214.00	0.37
Mixed Mode 2	334.50	0.21

The resonance frequencies extracted in this test are in a close agreement with those of CMA tests and OMA in in vacuo conditions. However, the damping ratios are not close to the results extracted by CMA. On the other hand, they are quite close to the damping ratio values extracted by OMA in in-vacuo conditions.

After conducting OMA test for the flow speed 4.78 m/s, the test is repeated for the increased flow speeds. By the same procedure the resonance frequencies and damping ratios are extracted for the flow speeds 7.06 m/s and 9.06 m/s. The results for these two tests and the first test are given in Table 6.3 for resonance frequencies and in Table 6.4 for damping ratios.

Table 6.3. Resonance frequencies extracted by OMA for different flow speeds in wind tunnel

Mode	Resonance Frequency via OMA (FDD) $V_{\text{flow}} = 4.78 \text{ m/s}$	Resonance Frequency via OMA (FDD) $V_{\text{flow}} = 7.06 \text{ m/s}$	Resonance Frequency via OMA (FDD) $V_{\text{flow}} = 9.06 \text{ m/s}$
	[Hz]	[Hz]	[Hz]
1 st Bending	26.50	26.50	26.50
1 st Torsion	87.50	87.50	87.50
2 nd Bending	143.00	142.75	141.75
Mixed Mode 1	214.00	213.50	214.00
Mixed Mode 2	334.50	334.75	335.00

Table 6.4. Damping ratios extracted by OMA for different flow speeds in wind tunnel

Mode	Damping ratios via OMA (EFDD) $V_{\text{flow}} = 4.78 \text{ m/s}$	Damping ratios via OMA (EFDD) $V_{\text{flow}} = 7.06 \text{ m/s}$	Damping ratios via OMA (EFDD) $V_{\text{flow}} = 9.06 \text{ m/s}$
	[%]	[%]	[%]
1 st Bending	0.75	0.93	1.14
1 st Torsion	0.36	0.55	0.89
2 nd Bending	0.43	0.50	0.65
Mixed Mode 1	0.37	0.34	0.33
Mixed Mode 2	0.21	0.11	0.28

As it can be seen from the above tables, regarding the first five modes there are no significant changes in resonance frequencies with the increased flow speeds. On the other hand, there is a significant increasing trend in damping ratios for the first three modes of the fin with the increased flow speeds. Standard deviations of the extracted damping ratios of these tests by OMA-EFDD method are given in Table 6.5.

Table 6.5. Standard deviations of damping ratios extracted by OMA-EFDD for different flow speed conditions

Mode	Standard deviations of damping ratios via OMA (EFDD) $V_{\text{flow}} = 4.78 \text{ m/s}$	Standard deviations of damping ratios via OMA (EFDD) $V_{\text{flow}} = 7.06 \text{ m/s}$	Standard deviations of damping ratios via OMA (EFDD) $V_{\text{flow}} = 9.06 \text{ m/s}$
	[%]	[%]	[%]
1 st Bending	85.16	86.15	77.34
1 st Torsion	77.51	45.15	59.55
2 nd Bending	38.26	51.02	59.25
Mixed Mode 1	66.38	73.56	76.90
Mixed Mode 2	45.43	54.24	72.78

The standard deviations are considered to be relatively high for the damping ratios. The reason for this is the correlation between the outputs for each data set which is affected by the number of measurement sets and measuring devices.

So as to observe the effect of high flow speed on the test results, an OMA test with the highest speed of the tunnel is also conducted. The flow speed, 14.79 m/s, is set as the maximum test speed which is considered to be safest for the test structure and the test equipment. The resulting SVD obtained at the end of the test is given in Figure 6.5.

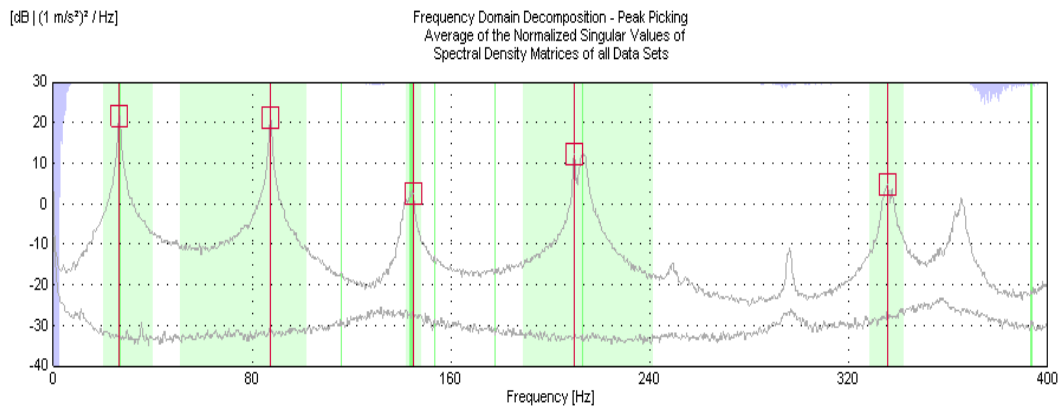


Figure 6.5. SVD plot for the OMA test in wind tunnel with flow speed=14.79m/s

When the above SVD plot is compared with the one extracted for the flow speed of 4.78 m/s (See Figure 6.4) it can easily be seen that the modal domains are more distinguishable for the highest speed case. Additionally, the noise domains diminish for this case as well. This result is due to the strength of the input excitation which directly affects the vibration levels of the fin. The resonance frequencies and damping ratios extracted from this highest flow speed test are given in Table 6.6.

Table 6.6. Resonance frequencies and damping ratios extracted from OMA wind tunnel test with flow speed=14.79 m/s

Mode	Resonance Frequency via OMA (FDD)	Damping Ratio via OMA (EFDD)
	[Hz]	[%]
1 st Bending	26.50	1.41
1 st Torsion	87.25	0.99
2 nd Bending	144.70	0.87
Mixed Mode 1	209.50	0.61
Mixed Mode 2	335.50	0.44

As it is seen from the table that the resonance frequencies extracted for the highest flow speed are still close to the values of the other flow speeds which are relatively low. Those resonance frequencies are also close to the ones extracted by CMA and OMA in in-vacuo conditions.

On the other hand, the increasing behaviour in damping ratios with increased flow speeds can also be observed in this case. For all the modes extracted, damping ratios are higher than the results which are extracted for the lower flow speeds. The standard deviations for the damping ratios extracted by the software are also given in Table 6.7.

Table 6.7. Standard deviations for damping ratios extracted by OMA-EFDD for the wind tunnel test with flow speed=14.79 m/s

Mode	Standard deviations for damping ratios via OMA (EFDD) [%]
1 st Bending	58.78
1 st Torsion	34.20
2 nd Bending	44.12
Mixed Mode 1	10.45
Mixed Mode 2	4.49

If the above standard deviations are compared with those given in Table 6.5, the decreasing trend in the deviations can easily be observed. These decrements is said to be related to the increasing correlation between the measurements for each data set.

Another important point to stress is the differences between the damping ratios of this particular test and impact hammer one. Since the impact hammer test is performed with no attachment to the fin and this ultimately results no change in

damping mechanism, the impact hammer tests results are selected and compared with the CMA tests. Damping ratios obtained via impact hammer test and OMA test with high flow speeds and their percentage differences are tabulated in Table 6.8.

Table 6.8. Damping ratios of impact hammer test and OMA test in wind tunnel with high speed and their differences

Mode	Damping ratios extracted from impact hammer test [%]	Damping ratios extracted from OMA $V_{\text{flow}} = 14.79 \text{ m/s}$ [%]	Differences [%]
1 st Bending	1.44	1.41	2.00
1 st Torsion	1.14	0.99	14.62
2 nd Bending	0.79	0.87	9.11
Mixed Mode 1	0.43	0.61	29.36
Mixed Mode 2	0.46	0.44	5.26

The damping ratios for the high speed OMA test in wind tunnel are generally in close agreement with impact hammer test results. Moreover, it can be realised that these values are the closest values between CMA and OMA tests regarding the damping ratios. In order to examine the effect of the flow speed on the vibratory motion of the fin, several speeds in the wind tunnel operating interval are swept and PSD functions are extracted by using only the output of the reference accelerometer located on the fin. PSD curves are given in Figure 6.6 for the flow speeds from 5 m/s to 15 m/s with 2 m/s increment. As it can be observed from the below figure, the vibration levels are in increasing trend with the increased flow speeds.

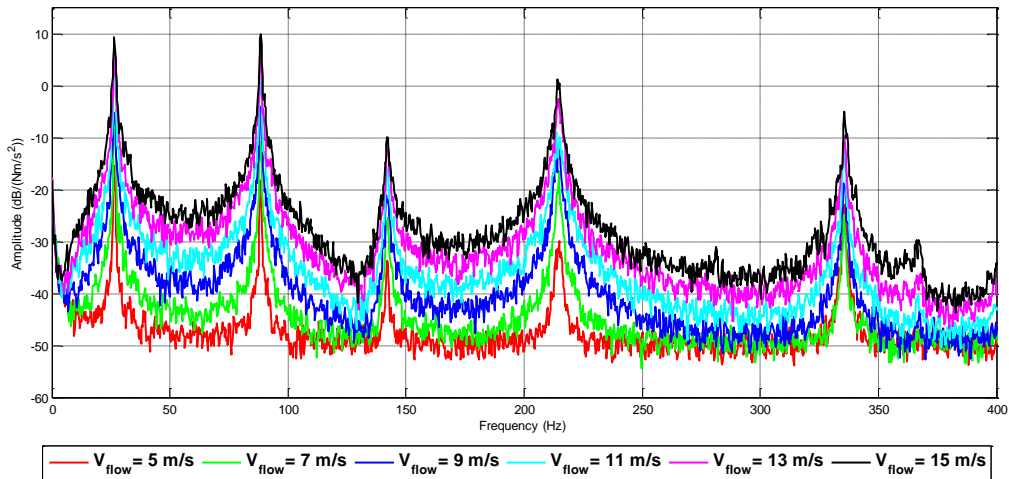


Figure 6.6. Output PSD curves for the fin under different flow speed conditions in wind tunnel

Investigating the flow angle (angle of attack) effect on modal parameters

After completing the OMA tests in wind tunnel for zero angle of attack, various tests are repeated for different angle of attacks. By using the fixing points on the test base, fin is positioned in 3 different angles of attacks (AOA) which are 5, 10 and 15 degrees. For each and every angle, the flow speed is taken as 4.78 m/s. The test results obtained under these conditions regarding the resonance frequencies and the damping ratios are given in Table 6.9 and Table 6.10, respectively.

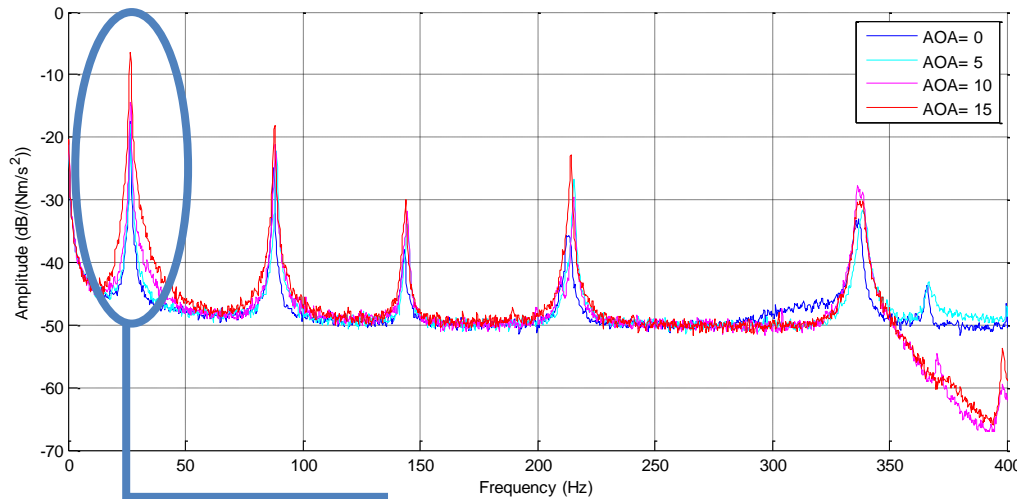
Table 6.9. Resonance frequencies extracted from OMA wind tunnel test for different angle of attacks with flow speed=4.78 m/s

Mode	Resonance Frequency via OMA(FDD) AOA=0°	Resonance Frequency via OMA(FDD) AOA=5°	Resonance Frequency via OMA(FDD) AOA=10°	Resonance Frequency via OMA(FDD) AOA=15°
	[Hz]	[Hz]	[Hz]	[Hz]
1 st Bending	26.50	26.75	26.50	26.50
1 st Torsion	87.50	88.75	88.25	88.00
2 nd Bending	143.00	144.00	145.25	144.00
Mixed Mode 1	214.00	215.75	215.50	214.50
Mixed Mode 2	334.50	337.50	336.25	336.50

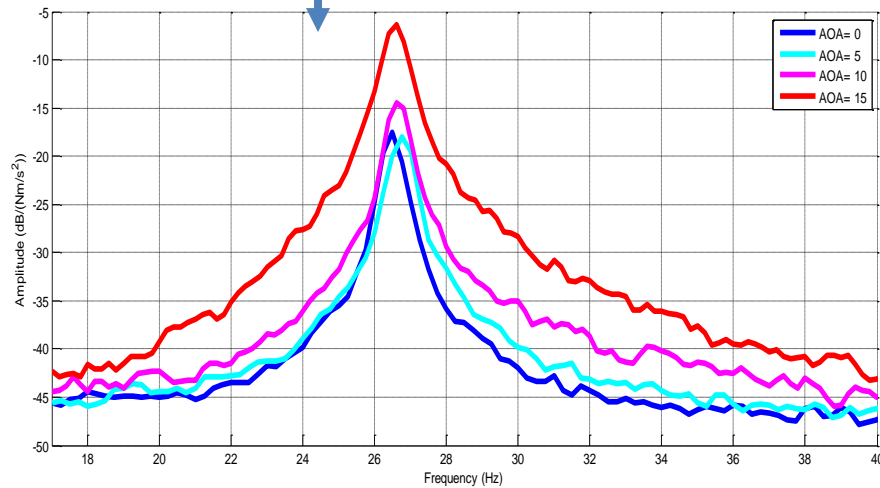
Table 6.10. Damping ratios extracted from OMA wind tunnel test for different angle of attacks with flow speed=4.78 m/s

Mode	Damping Ratio via OMA(EFDD) AOA=0°	Damping Ratio via OMA(EFDD) AOA=5°	Damping Ratio via OMA(EFDD) AOA=10°	Damping Ratio via OMA(EFDD) AOA=15°
	[%]	[%]	[%]	[%]
1 st Bending	0.75	0.94	0.89	1.00
1 st Torsion	0.36	0.33	0.33	0.32
2 nd Bending	0.43	0.20	0.18	0.22
Mixed Mode 1	0.37	0.10	0.27	0.10
Mixed Mode 2	0.21	0.22	0.16	0.19

The resonance frequencies of the fin obtained under constant flow speeds do not vary significantly by changing the angle of attack. On the other hand, the value of the damping ratio in the first mode increases slightly with the increasing angle of attacks. Damping ratios of the other four modes generally do not show regular trends in damping ratios with the variations in angle of attack. In the previous part of this section, the vibration levels of the fin are determined by examining the output PSD functions of the reference accelerometer for the increasing flow speed conditions. By following the same procedure the vibration levels of the fin with increased angle of attacks is examined. The average PSD functions for different angle of attacks are given in Figure 6.7 (a) and Figure 6.7 (b)



(a)



(b)

Figure 6.7. Output PSD curves for the fin for changing angle of attack (a) All modes (b) First mode

It can be observed from the above figures that the increasing angle of attack does not cause a major increase in vibration levels but it increases the amplitude of the resonance peaks for some of the modes especially in the first mode. For the first mode, the amplitude of the peak is nearly same for the angles of 0 and 5 degree. The peak for the angle of attack of 10 degree is higher than them. 15 degree angle

of attack condition has the maximum amplitude peak in the first mode of the fin. It can be observed for the examined values that the change of angle of attack is not as dominant as the flow speed variations on the vibration levels of the fin. In order to examine the values of the resonance frequencies and the damping ratios of the fin for different combinations of flow speeds and angle of attacks, the final test is repeated in the flow speed conditions of the previous test and the resonance frequencies and the damping ratios are extracted by using the same procedure. Those tabulated results are given in Table 6.11.

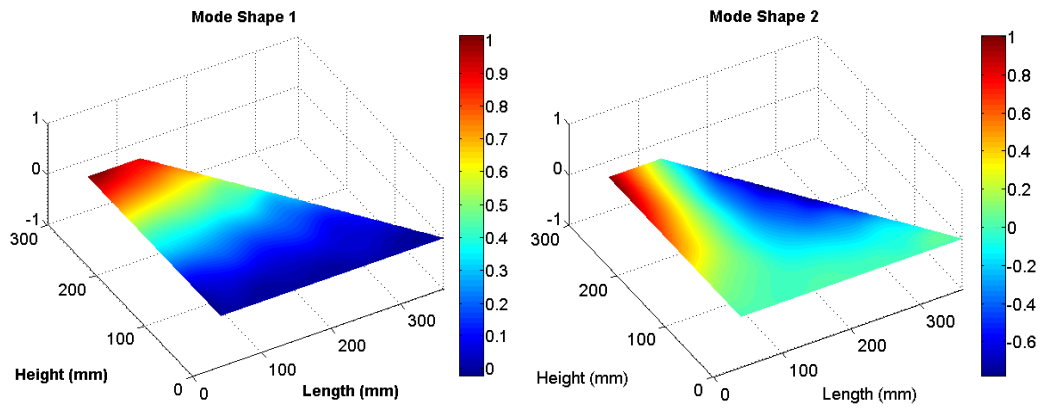
Table 6.11. Resonance frequencies and damping ratios of the fin extracted from the tunnel tests with different flow speed and angle of attack combinations

Angle of Attack [degree]	Tunnel Speed [m/s]	1 st Bending		1 st Torsion		2 nd Bending	
		Freq. [Hz]	Damping Ratio [%]	Freq. [Hz]	Damping Ratio [%]	Freq. [Hz]	Damping Ratio [%]
0	4.78	26.50	0.75	87.50	0.36	143.00	0.43
	7.06	26.50	0.93	87.50	0.55	142.75	0.50
	9.06	26.50	1.14	87.50	0.89	141.75	0.65
5	4.78	26.75	0.94	88.75	0.33	144.00	0.20
	7.06	26.75	1.11	89.00	0.58	145.00	0.22
	9.06	26.75	1.01	88.75	0.81	145.00	0.35
10	4.78	26.50	0.89	88.25	0.33	145.25	0.18
	7.06	26.50	0.99	88.50	0.58	145.00	0.27
	9.06	26.75	1.05	88.25	0.85	144.75	0.46
15	4.78	26.50	1.00	88.00	0.32	144.00	0.22
	7.06	26.50	1.02	88.25	0.75	144.50	0.40
	9.06	26.50	0.96	88.25	0.98	144.00	0.54

Angle of Attack [degree]	Tunnel Speed [m/s]	Mixed Mode 1		Mixed Mode 2	
		Freq. [Hz]	Damping Ratio [%]	Freq. [Hz]	Damping Ratio [%]
0	4.78	214.00	0.37	334.50	0.21
	7.06	213.50	0.34	334.75	0.11
	9.06	214.00	0.33	335.00	0.28
5	4.78	215.75	0.10	337.50	0.22
	7.06	215.75	0.15	337.25	0.18
	9.06	215.75	0.14	337.25	0.21
10	4.78	215.50	0.27	336.25	0.16
	7.06	215.75	0.34	336.25	0.20
	9.06	215.50	0.25	336.50	0.20
15	4.78	214.50	0.10	336.50	0.19
	7.06	214.50	0.14	335.50	0.21
	9.06	214.50	0.25	335.75	0.20

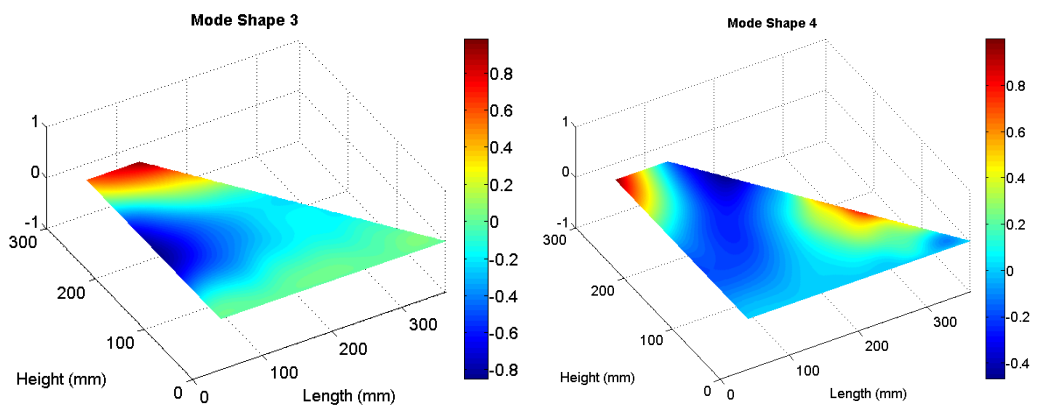
It is observed from the table that the increasing trend of the damping ratios by increasing speed is also present for the angle of attacks other than zero. On the other hand, the damping ratios do not show regular variations for the increasing angle of attack for the flow speeds of higher than 4.78 m/s.

The deflections of the fin (at the measured reduced set of points) in the first five modes shapes are examined by PULSE™ OMA software for all conditions given in Table 6.11 and similar mode shapes are also observed. Due to this reason, one of these conditions is selected and the measurement process is repeated for the whole measurement points (i.e. 49 points) over the fin to extract mode shapes for the whole geometry. The first five mode shapes of the fin for the condition of $V_{\text{flow}}=4.78$ m/s and $\text{AOA}=5^\circ$ is given in Figure 6.8. To examine the correlation of these mode shapes with the FEA results, MAC values are also calculated. MAC diagram and its tabulated form are given in Figure 6.9 and Table 6.12, respectively.



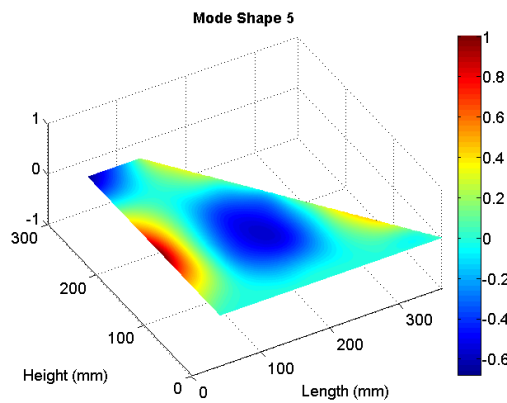
(a) Mode 1 (1st Bending)

(b) Mode 2 (1st Torsion)



(c) Mode 3 (2nd Bending)

(d) Mode 4 (Mixed Mode 1)



(e) Mode 5 (Mixed Mode 2)

Figure 6.8. First five mode shapes of the fin extracted from OMA in wind tunnel for the condition $V_{\text{flow}} = 4.78 \text{ m/s}$ and $\text{AOA} = 5^\circ$

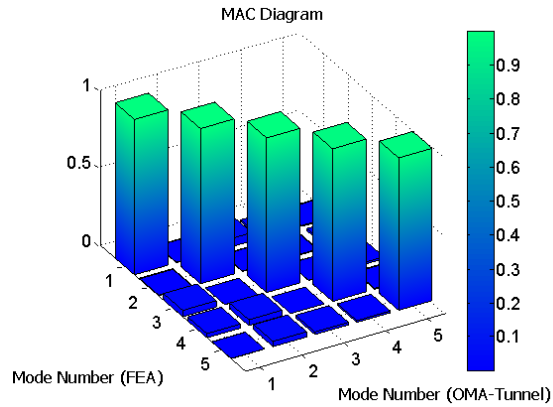


Figure 6.9. MAC diagram for OMA in wind tunnel and FEA results

Table 6.12. MAC table for OMA in wind tunnel and FEA results

Mode Numbers	1	2	3	4	5
1	0.9983	0.0050	0.0411	0.0263	0.0015
2	0.0031	0.9968	0.0005	0.0379	0.0334
3	0.0532	0.0038	0.9935	0.0000	0.0161
4	0.0122	0.0046	0.0015	0.9809	0.0115
5	0.0058	0.0131	0.0113	0.0064	0.9793

As it can be seen from the above MAC diagram and its table that the mode shapes obtained from OMA test performed in the wind tunnel are highly correlated with the ones found from FEA for the examined condition. It can also be concluded that as the software provide similar deflection results for the mode shapes extracted from all conditions examined in the wind tunnel, the mode shapes extracted from all conditions will be well correlated with the FEA results.

6.3.2 Tests by OMA in wind tunnel with vortex generator

For a flow condition if the motion of the fluid elements is very irregular and tortuous then this flow condition is called turbulent flow [73]. In wake regions of the obstacles, vortices generated by them can turn the flow from laminar to turbulent and this condition can sometimes cause problems. For example, buffeting is a phenomenon associated with the impact of vortical flows (i.e. vortex sheddings) generated by the aircraft on the structures such as vertical tail [46]. Vertical tail buffeting has an important role on fatigue life of an aircraft as well. Frequency of vortex shedding from the fuselage or wing of an aircraft which will have an influence on the vertical tail should be analysed for a proper design in terms of fatigue life. If the vortex shedding frequency is close to the primary resonance frequencies of the vertical tail, this condition may be treated as a critical design. The wind tunnel tests in this part of the study are performed by using vortex generators in front of the fin which may represent a buffeting scenario for the fin. The aim is to generate vortices which have a frequency equal to primary resonance frequencies (i.e. the first out-of-plane bending and the first torsional mode resonance frequencies separately) of the fin. A circular cylinder is selected as the vortex generator and the diameter of it is selected according to the below formula [74] :

$$St = \frac{f_s D}{\bar{U}} \quad (6.1)$$

where f_s is the vortex shedding frequency in Hz, D is the diameter of the circular cylinder vortex generator and \bar{U} is the speed of the air flow and St is the Strouhal number (St) which depends on the Reynolds number (Re). Relationship between Reynolds and Strouhal number is given in Figure 6.10 [75]

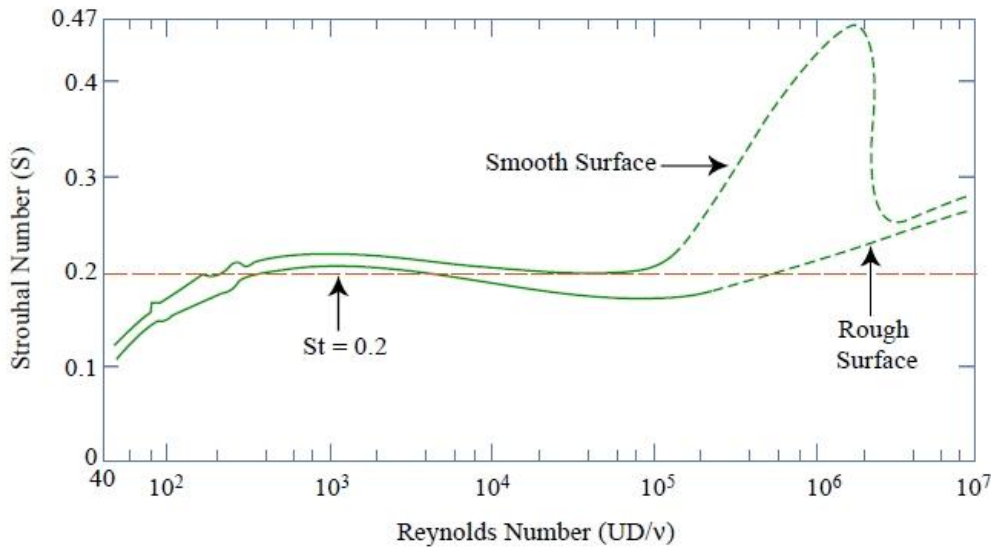


Figure 6.10. Reynolds Number (Re) vs Strouhal Number (St) [75]

It can be observed from the figure for the subcritical flow ($Re < 10^5$), St can be taken as 0.2. For the test condition, the flow is assumed to be subcritical and the St is also taken as 0.2. For the first test case, the vortex shedding frequency is at 26.50 Hz which is the first bending frequency of the fin obtained from previous OMA test results. Among various flow speed-cylinder diameter combinations, the one where the cylinder (i.e. vortex generator 1) diameter of 0.05 m and the flow speed of 6.625 m/s is selected. At this stage the subcritical flow assumption is checked by calculating the Re according to the formula given below [73]:

$$Re = \frac{\rho \bar{U} D}{\mu} \quad (6.2)$$

where ρ denotes the air density which is 1.225 kg/m^3 , \bar{U} is the speed of the air flow which is selected as 6.625 m/s, D is the characteristic cross-wind dimension in the flow and for this test the diameter of the cylinder, 0.05 m and μ is the dynamic viscosity which is equal to $1.79 \times 10^{-5} \text{ kg/(m.s)}$. The resulting Reynolds number is 2.27×10^4 which is less than 10^5 and corresponds to a Strouhal number around 0.2 (See Figure 6.10). So the subcritical assumption is cleared with this calculation.

After selecting the diameter for the vortex generator and the flow speed, the effect of the vortex generator position on the vibration levels of the fin are investigated. By examining the previous results of the studies on the vortex shedding frequency amplitudes [52] a few locations are tried for the cylinder and the one providing the maximum amplitude is selected for further studies. Position of the vortex generator and the fin is given in Figure 6.11 and the coordinate definition for the vortex generator location is given in Figure 6.12.

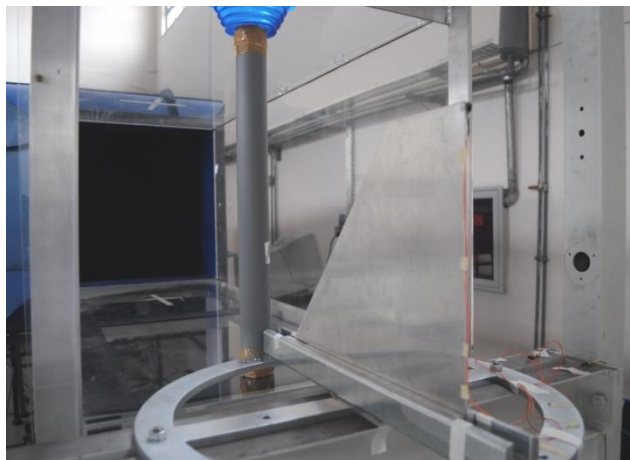


Figure 6.11. Position of the vortex generator and the fin

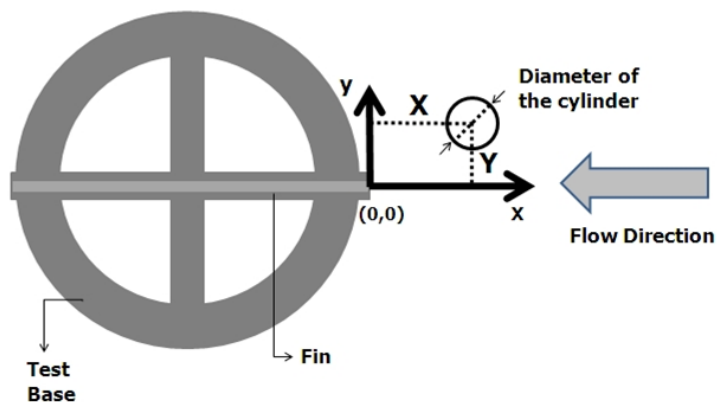


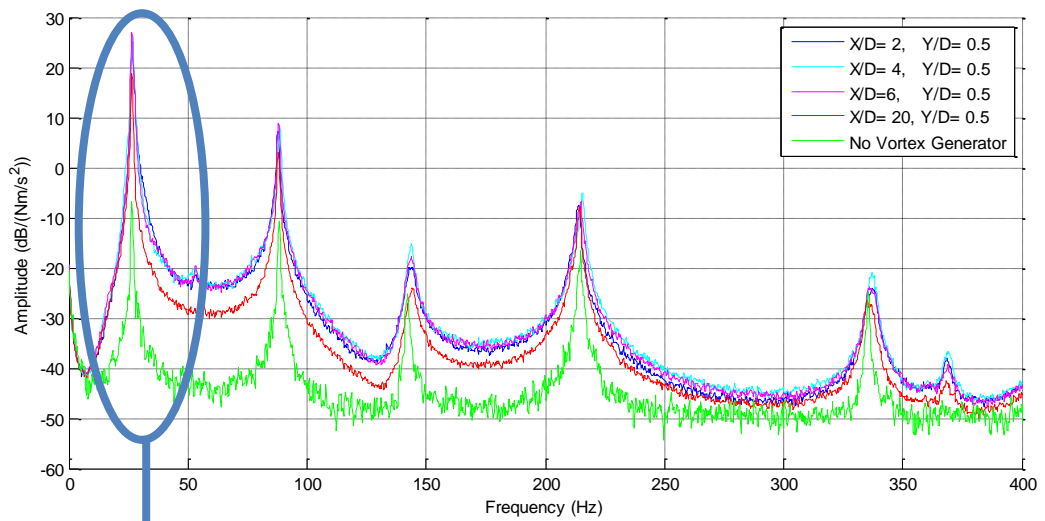
Figure 6.12. Coordinate definition for the vortex generator position in wind tunnel

It is known from the previous studies that [52] vortex sheddings lose their strength outside for the region $Y/D=1.5$. After a few trial runs under the value 1.5, it is seen that the vibration levels are close to each other for changing directions along y axis. Therefore, the position of the cylinder along y axis is taken constant as 0.5 and different locations along x axis are tried. Positions for the circular cylinder are given in Table 6.13.

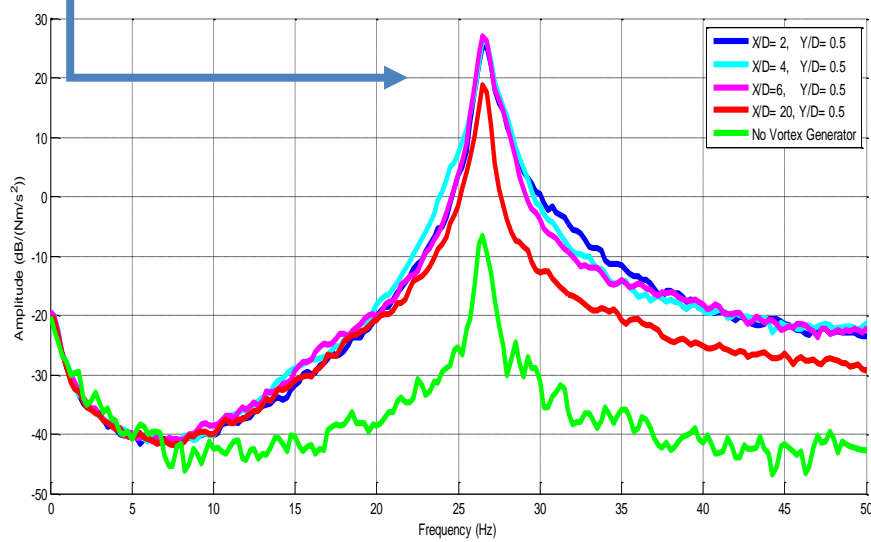
Table 6.13. Circular cylinder positions for the vibration levels investigation

Position	Diameter of the circular cylinder- D [m]	X location [m]	Y location [m]	X/D	Y/D
1	0.05	0.1	0.025	2	0.5
2	0.05	0.2	0.025	4	0.5
3	0.05	0.3	0.025	6	0.5
4	0.05	1	0.025	20	0.5

For each position of the cylinder, measurements on the fin are taken by the same process with previous OMA tests. To determine the cylinder position effect on the vibration levels, the measured data from the reference accelerometer is used. Average PSD functions for each position of the cylinder around the first resonance frequency are given in Figure 6.13.



(a)



(b)

Figure 6.13. Average PSD functions from reference accelerometer for different positions of the vortex generator 1 (a) For all modes (b) For the first mode

As it can be seen from the above figures that the vibration levels in the test with vortex generator are significantly higher than those of the tests performed without

vortex generator. For the position $X/D=20$, the vibration levels are higher than the tests results obtained without vortex generator 1. However for the positions X/D is equal to 2, 4 and 6 the levels are higher than the $X/D=20$ case and they are also close to each other. Since the diameter of the vortex generator 1 and the flow speed are selected to excite the first mode, the vibration level changes to due vortex generator are significant for the first mode.

For the conditions examined above resonance frequencies and damping ratios of the fin are also extracted by OMA. They are given in Table 6.14 and Table 6.15.

Table 6.14. Resonance frequencies extracted by OMA for different positions of vortex generator 1

Mode	Resonance Frequency via OMA(FDD) for the position $X/D=2$ [Hz]	Resonance Frequency via OMA(FDD) for the position $X/D=4$ [Hz]	Resonance Frequency via OMA(FDD) for the position $X/D=6$ [Hz]	Resonance Frequency via OMA(FDD) for the position $X/D=20$ [Hz]
1 st Bending	26.00	26.75	26.00	26.00
1 st Torsion	87.25	88.50	88.00	88.25
2 nd Bending	142.75	142.50	143.00	142.75
Mixed Mode 1	214.25	215.75	215.00	214.50
Mixed Mode 2	335.25	335.75	335.25	334.75

Table 6.15. Damping ratios extracted by OMA for different positions of vortex generator 1

Mode	Damping Ratio via OMA(EFDD) for the position X/D=2 [%]	Damping Ratio via OMA(EFDD) for the position X/D=4 [%]	Damping Ratio via OMA(EFDD) for the position X/D=6 [%]	Damping Ratio via OMA(EFDD) for the position X/D=20 [%]
1 st Bending	2.52	2.20	2.34	2.02
1 st Torsion	1.97	1.84	1.80	1.54
2 nd Bending	1.30	0.85	1.13	1.14
Mixed Mode 1	0.42	0.50	0.47	0.36
Mixed Mode 2	0.21	0.19	0.27	0.22

Standard deviations of the damping ratios are also extracted and found around %80 for the first mode for different positions of the vortex generators.

It can be observed from the above tables that the change in vortex generator 1 position does not have a significant effect on the resonance frequencies on the fin. Whereas, damping ratios for the first two modes of the fin generally increases by the decreasing distance between the fin and the vortex generator. Other three modes show no regular trend for the changing of the position of the vortex generator.

After finalising the tests for exciting the first mode, different diameter and flow speed combinations are determined for the second mode as well. The frequency required to excite the second mode is taken as 87.50 Hz from previous OMA test results. By using Equation 6.1, the air flow speed is found as 7.875 m/s and the diameter of the circular cylinder (i.e. vortex generator 2) is taken as 0.018 m. In this equation Strouhal number is taken as 0.2 again by the subcritical flow assumption. This assumption is also cleared by calculating the Reynolds number as

9.70×10^3 by using the Equation 6.2 with the flow speed and vortex generator diameter selected for this case. For the position of the vortex generator 2, X/D is taken as 6 which is the position that provides the maximum vibration level for the vortex generator 1. Y/D ratio is taken as 0.5 which is also used in the first case. Vibration levels for the second mode excitation case are given with the first mode excitation and no vortex generator conditions in Figure 6.14 (a) and Figure 6.14 (b).

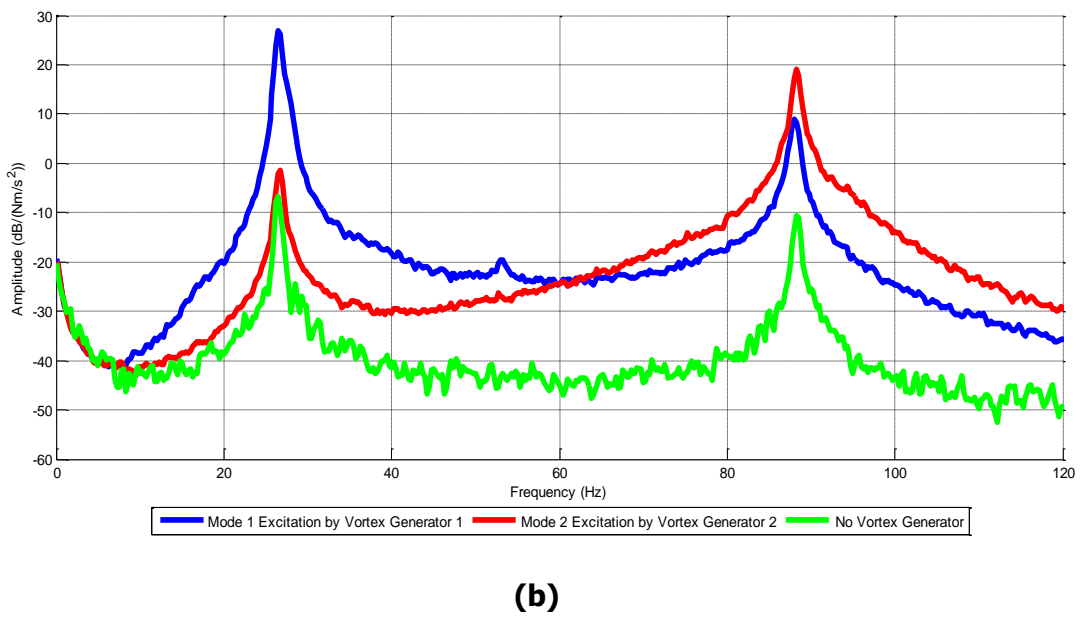
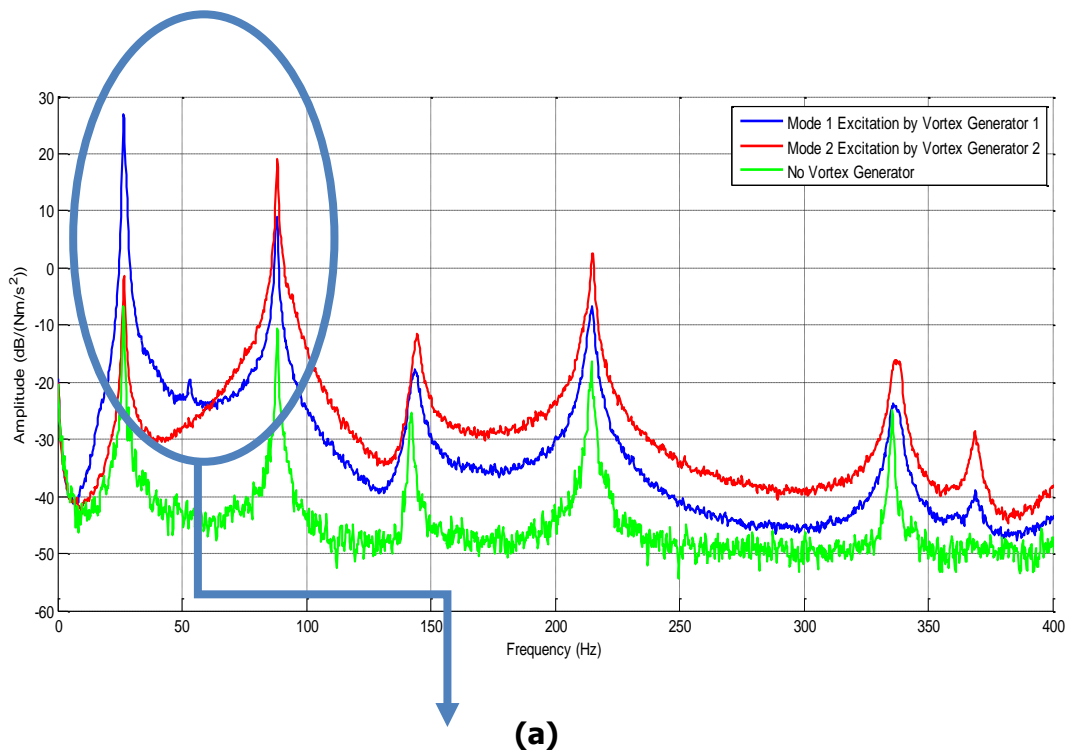


Figure 6.14. Average PSD functions for first and second mode excitation by vortex generators (a) For all modes (b) For the first two modes

The above figures show that the vibration levels are significantly higher in the case with vortex generator 2 than the case without vortex generator. The vibration levels for the second vortex generator case are also higher than the first vortex generator case except in the first mode. This is due to the higher flow speed in the second vortex generator case. On the other hand, the well excitation conditions in the first two modes can be seen in Figure 6.14 (b). The resonance frequencies and the damping ratios are also extracted by OMA for the second vortex generator case. They are given in Table 6.16 and Table 6.17 with the results of the first vortex generator and no vortex generator cases. The vortex generator positions are $X/D=6$ and $Y/D=0.5$ for both vortex generator cases. For no vortex generator case, the closest flow speed to the cases with vortex generators is taken from the previous tests for comparison purposes.

Table 6.16. Resonance frequencies extracted from the OMA tests with and without vortex generators

Mode	Resonance Frequency via OMA(FDD) for the Vortex Generator 1 case	Resonance Frequency via OMA(FDD) for the Vortex Generator 2 case	Resonance Frequency via OMA(FDD) for No Vortex Generator case
	$V_{\text{flow}}=6.63 \text{ m/s}$ [Hz]	$V_{\text{flow}}=7.88 \text{ m/s}$ [Hz]	$V_{\text{flow}}=7.06 \text{ m/s}$ [Hz]
1 st Bending	26.00	26.75	26.50
1 st Torsion	88.00	88.25	87.50
2 nd Bending	143.00	144.50	142.75
Mixed Mode 1	215.00	215.00	213.50
Mixed Mode 2	335.25	338.75	334.75

Table 6.17. Damping ratios extracted from the OMA tests with and without vortex generators

Mode	Damping Ratio via OMA(EFDD) for the Vortex Generator 1 case	Damping Ratio via OMA(EFDD) for the Vortex Generator 2 case	Damping Ratio via OMA(EFDD) for No Vortex Generator case
	$V_{\text{flow}}=6.63 \text{ m/s}$ [Hz]	$V_{\text{flow}}=7.88 \text{ m/s}$ [Hz]	$V_{\text{flow}}=7.06 \text{ m/s}$ [Hz]
1 st Bending	2.34	0.54	0.93
1 st Torsion	1.80	0.33	0.55
2 nd Bending	1.13	0.50	0.50
Mixed Mode 1	0.47	0.25	0.34
Mixed Mode 2	0.27	0.23	0.11

The above tables indicate that the resonance frequencies remain nearly same for different vortex generators cases and the case with no vortex generator. The damping ratio values extracted by using the first vortex generator condition are higher than the results obtained from the other conditions where second vortex generator and no vortex generator are used. On the other hand, the damping ratio values extracted for the second vortex generator case are generally lower than other two conditions.

Since the cases with vortex generators are examined in order to check the effects of the vortex generators on the excitation of selected primary modes (i.e. first two modes of the fin) a whole mode shape extraction process is not conducted. Nevertheless, the deflections for the reduced measurement set in the first five modes of the fins are then compared by using MAC calculations between the cases

with vortex generators and FEA results. The resulting MAC tables are given in Table 6.18 and Table 6.19.

Table 6.18. MAC table for the condition with vortex generator 1 in wind tunnel and FEA results (For reduced measurement point set)

Mode Numbers	1	2	3	4	5
1	0.9988	0.3004	0.2173	0.1569	0.0042
2	0.3023	0.9989	0.0077	0.1446	0.0654
3	0.2124	0.0071	0.9981	0.0306	0.0876
4	0.2179	0.2060	0.0487	0.9930	0.0686
5	0.0192	0.0931	0.1388	0.0780	0.9898

Table 6.19. MAC table for the condition with vortex generator 2 in wind tunnel and FEA results (For reduced measurement point set)

Mode Numbers	1	2	3	4	5
1	0.9994	0.2960	0.2090	0.1535	0.0021
2	0.3065	0.9976	0.0096	0.1364	0.0527
3	0.2098	0.0091	0.9961	0.0319	0.1004
4	0.2127	0.2121	0.0513	0.9905	0.0597
5	0.0181	0.0914	0.1475	0.0771	0.9902

As seen from the above tables, the mode shapes (for the reduced measurement point set) extracted from the OMA tests in wind tunnel with vortex generators are highly correlated with the FEA mode shapes results.

6.4 Summary

In this chapter, OMA is applied to the fin in wind tunnel conditions. First, the flow condition without vortex generator is examined. For three different speeds, the resonance frequencies and the damping ratios of the fin are then extracted. It is observed that the higher the speed, the higher the damping ratios. On the other hand, there are no significant differences for the resonance frequencies with increased speeds. Additionally, the resonance frequency values are similar to the ones obtained via CMA and OMA in in-vacuo conditions.

After examining the flow speed effect on the extracted modal parameters, the effect of different angle of attacks are also investigated. It is found that the angle of attack variation does not have significant influence on the modal parameters as much as the flow speeds.

The effect of the combinations of different angle of attack and flow speeds are also investigated and tabulated in this chapter. The vibration levels of the fin for different flow speed and angle of attack conditions are also examined. Additionally, increase in vibration levels are observed for the increasing flow speed. The angle of attack has smaller influence of the vibration levels of the fin.

After conducting the tests without vortex generator, the vortex generator is located in front of the flow and the effects of the turbulence flow are also examined. By selecting appropriate vortex generator diameter and flow speed combinations, the first two modes of the fin are excited separately. The excitations are clearly observed by examining the output PSD functions of the fin. The effect of the vortex generator position on the vibration levels and the extracted modal parameters of the fin are also examined.

For both flow conditions (i.e. with and without vortex generator), the mode shapes of the fin are extracted and found to be highly correlated with the results of FEA.

CHAPTER 7

CONCLUSIONS

7.1 General conclusions

The main objective of this thesis is to investigate the dynamic characteristics of a plate-like structure (i.e. a fin) by using different modal analysis methods and verify the modal parameters extracted by the finite element modelling and analysis.

In the first part of the study, the finite element model of the fin is generated and then the natural frequencies and the corresponding mode shapes are extracted. The mass and the stiffness effect of both the measuring devices and the test equipment on these modal parameters are modelled, investigated and found to be negligible. Having taken the finite element analysis results as a benchmark, various types of modal tests are performed. First, the impact hammer test which brings no physical attachment to the test structure is applied and the resonance frequencies, mode shapes and the damping ratios of the fin are extracted. Secondly, the modal shaker tests with random noise and sweep sine inputs are performed. The resonance frequencies obtained from all types of classical modal testing methods are found to be correlated with each other with some expectable deviations. Moreover, the first five mode shapes of the fin show good correlation with each other and the finite element analysis results except the fifth mode which is heavily affected by the position of the attachment point of the shaker.

In the second part of the thesis, Operational Modal Analysis tests are conducted under mechanical (i.e via modal shaker) and acoustical types of excitations in the same laboratory environment. Since Operational Modal Analysis does not require

any information of input forcing, the fin is excited via modal shaker under random noise but without measuring the given input and providing it to the analysis software. As a second type of input, the acoustical noise is used to excite the fin and Operational Modal Analysis and testing procedure is repeated. The results regarding the extracted modal parameters of the fin are improved compared to the previous tests conducted by mechanical input. In this part, in order to investigate the effect of increasing number of accelerometers on Operational Modal Analysis, the process is also performed as a case study. Consistent results from Operational Modal Analysis are observed in the first three modes of the fin whereas the adverse mass effect of the added accelerometers resulted as poor estimations in the fourth and the fifth modes.

In the final part of the study, the fin is excited by an air flow under different conditions in the wind tunnel simulating its real operating environment. First, the effect of the flow speeds on the dynamic properties of the fin is examined. The consistency and good correlation in the resonance frequencies with the previous Classical Modal Test results are achieved. However, an increasing trend is observed in the measured total damping ratios (i.e. both material and non-material damping) of the fin with the increasing flow speeds. Secondly, the effects of the flow angle (i.e. the angle of attack) on the test results are examined. The effect of the angle of attack is found not to be as dominant as the flow speed in the estimation of the modal parameters when Operational Modal Analysis is used as a modal parameter extraction tool. Having completed the wind tunnel tests without vortex generator, the fin is excited under various turbulent flows. By placing designed vortex generators in front of the fin, the first two modes of the fin are tried to be excited separately. The excitations are clearly observed by examining the vibration levels of both conditions. The resonance frequencies obtained by Operational Modal Analysis under these conditions are found to be correlated with the tests without vortex generator although this is not the case regarding the damping ratios. The mode shapes of the fin extracted under both flow conditions with and without vortex generator are found to be highly correlated with each other and finite element results.

7.2 Recommendations for future works

In this thesis, Finite Element Analysis, Classical Modal Analysis and Operational Modal Analysis methods are applied to the fin structure to extract its dynamic characteristics.

The recommendations for future works of this study can be listed as follows:

- As the test structure used in this study is a 2-D plate-like isotropic structure. Test structures of composite 3-D models could be used.
- Wind tunnel testing part of this study is conducted in a limited flow speed range and test section region. By using a wind tunnel capable of providing higher flow speeds with a larger test section, a wing model of an aircraft could be tested. The test fixture capabilities should also be improved for these types of structures as well.
- With the improved wind tunnel tests, the aeroelastic effects on the test structure could also be analysed and taken into account in the determination of the dynamic characteristics of the test specimen.
- By using the advantages of output-only modal identification of Operational Modal Analysis in the modal testing area, both structural health monitoring and damage detection studies could also be conducted.

REFERENCES

1. **Rieger, N. F.** *The Relationship Between Finite Element Analysis and Modal Analysis*. New York : Journal of Sound & Vibration, 1986.
2. **Buehrle R. D., Fleming G. A., Pappa R. S., Ferdinand W. G.** *Finite Element Model Development and Validation for Aircraft Fuselage Structures*. San Antonio, Texas : 18th International Modal Analysis Conference, 2000.
3. **Pickrel, C. R.** *Airplane Ground Vibration Testing - Correlation with Nominal Modal Model*. s.l. : Proceedings of IMAC XX, 2002.
4. **He J., Fu Z. F.** *Modal Analysis*. s.l. : Butterworth Heinemann, 2001. 0 7506 5079 6.
5. **Ewins, D.J.** *Modal Testing: Theory and Practice*. s.l. : Research Studies Press Ltd. , 1995.
6. **Peeters B., Hendricx W. , Debille J., Climent H.** *Modern solutions for Ground Vibration Testing of large aircraft*. s.l. : Sound and Vibration Magazine, 2009.
7. **Pickrel C. R., White P. J.** *Flight Flutter Testing of Transport Aircraft: In-Flight Modal Analysis*. s.l. : Proceedings of IMAC XXI, 2003.
8. **Brincker, R., Zhang, L. and Andersen, P.** *Modal Identification of Output-Only Systems using Frequency Domain Decomposition*. s.l. : Smart Materials and Structures, 2001. p. 441. Vol. 10.
9. **Brincker, R, Zhang, L. Andersen.** *Damping Estimation by Frequency Domain Decomposition*. s.l. : Proceedings of the 19th International Modal Analysis Conference (IMAC), p 698-703, 2001.
10. **Gade S., Møller N. B., Herlufsen H. , Hansen H. K.** *Frequency Domain Techniques for Operational Modal Analysis*. s.l. : IMAC-XXIV: Conference & Exposition on Structural Dynamics, 2006.
11. **Brüel&Kjaer.** *Operational Modal Analysis — Type 7760 Software Product Data*. s.l. : Brüel&Kjaer, 2008.

12. **James G. H., Carne T.G., Lauffer J.P.** *The Natural Excitation Technique (NExT) for Modal Parameter Extraction From Operating Wind Turbines*. California : Sandia National Laboratories, 1993.
13. **Buke, F.** *An Investigation on the Application of Operational Model Analysis*. s.l. : METU Master Thesis, 2006.
14. **Jacobsen, N.J.** *Identifying Harmonic Components in Operational Modal Analysis*. Lisbon : Twelfth International Congress, 2005.
15. **Jacobsen N.J., Andersen P. ,Brincker R.** *Eliminating the Influence of Harmonic Components in Operational Modal Analysis*. s.l. : Proceedings of IMAC XXV, 2007.
16. **Jacobsen N. J., Andersen P. , Brincker R.** *Applications of Frequency Domain Curve-fitting in the EFDD Technique*. s.l. : Proceedings of IMAC XXV, 2007.
17. **Johansson J., Samuelsson H.,Jacobsen N.J.,Angantyr A.** *Operational Modal Analysis of Large 2-Pole Rotating Machinery*. s.l. : Proceedings of III IOMAC, 2009.
18. **Gade S., Schlombs R.,Hundeck C. , Fenselau C.** *Operational Modal Analysis on a Wind Turbine Gearbox*. s.l. : Proceedings of IMAC XXVII, 2009.
19. **Schwarz B. J., Richardson M.H.** *Introduction to Operating Deflection Shapes*. Orlando : CSI Reliability Week, 1999.
20. **Heaton, R.,S. Hewitt.** *The use of Operating Deflection Shapes (ODS) to model the vibration of sanders and polishers*. Derbyshire : Health and Safety Laboratory, 2006.
21. **Richardson, M. H.** *Is It a Mode Shape, or an Operating Deflection Shape?* s.l. : Sound & Vibration Magazine 30th Anniversary Issue, 1997.
22. **Doebling S. W., Farrar C. R.** *Computation of Structural Flexibility for Bridge Health Monitoring Using Ambient Modal Data*. s.l. : Proceedings of 11th ASCE Engineering Mechanics Conference, 1996.
23. **Parloo E., Verboven P., Guillaume P. Overmeire , M. V.** *Sensitivity-based Operational Mode Shape Normalisation*. s.l. : Mechanical Systems and Signal Processing (2002) 16(5), 757–767, 2002.
24. **Brincker R., Andersen P.** *A Way of Getting Scaled Mode Shapes*. s.l. : IMAC-XXI: Conference & Exposition on Structural Dynamics, 2003.

25. **Khatibi M.M., Ashory M.R., Malekjafarian A.** *Scaling of operational mode shapes using mass-cancellation methods.* Istanbul : Proceedings of 4th IOMAC Conference, 2011.
26. **Khatibi M.M., Ashory M. R., .Albooyeh A.R.** *A new formula for optimum magnitude of additive mass in.* Istanbul : Proceedings of 4th IOMAC Conference, 2011.
27. **Mevel L., Benveniste A., Basseville M.,Goursat M.,Peeters B., Auweraer H.V., Vecchio A.** *Input/output versus output-only data processing for structural identificationidentification-Application to in-flight data analysis.* s.l. : Journal of Sound and Vibration, 2006.
28. **LMS, Application Note.** *Automatic modal analysis reality or myth?* s.l. : LMS International.
29. **Camargo E., Jacobsen N.J., Strafacci D.** *Operational Modal Analysis on a Modified Helicopter.* Istanbul : Proceedings of 4th IOMAC, 2011.
30. **Grappasonni C., Coppotelli G. , Agneni A.** *Operational Modal Analysis of a Helicopter UAV from Flight Tests.* Istanbul : Proceedings of 4th IOMAC Conference, 2011.
31. **Crema L. B., Coppotelli G.** *Output-Only Approach for Finite Element Model Updating of AB-204 Helicopter Blade.* Texas : 46th AIAA/ASME/ASCE/AHS/ASC Structures, Structural Dynamics & Materials Conference, 2005.
32. **Parker, L. D.** *Optimal design, detection and tracking of damage in a wing attachment fitting.* Istanbul : Proceesings of 4th IOMAC Conference, 2011.
33. **Alam M., Sedaghat R.,Soucy Y.,Rama B.** *Analytical and Experimental Study Using Output-Only Modal Testing for On-Orbit Satellite Appendages.* s.l. : Advances in Acoustics and Vibration, 2009.
34. **Hermans L., Auweraer H.V.D.** *Modal testing and analysis of structures under operational conditions : Industrial applications.* s.l. : Mechanical Systems and Signal Processing, 1999.
35. **Carne T.G., James G.H.** *The inception of OMA in the development of modal testing technology for wind turbines.* s.l. : Mechanical Systems and Signal Processing, 2010.

36. **Tcherniak D., Basurko J.,Salgado O.,Urresti I.** *Application of OMA to operational wind turbine.* s.l. : Proceesings of 4th IOMAC Conference, 2011.
37. **Pelayo F., López-Aenlle M.,Fernández-Canteli A.,Cantieni R.** *Operational modal analysis of two wind turbines with foundation problems.* s.l. : Proceedings of 4th IOMAC Conference, 2011.
38. **Brincker R., Andersen P.,Cantieni R.** *Identification and Level 1 Damage Detection of the Z24 Highway Bridge by Frequency Domain Decomposition.* s.l. : Structural Testing Series, 2001.
39. **Ramos L. F, Costa A. C., Lourenco P.B.** *Operational Modal Analysis for damage detection of a masonry construction.* s.l. : Proceedings of 1st IOMAC Conference, 2005.
40. **Rehman A.U., Worden K.,Rongong J.A.** *Experimental investigation of the MAC based crack detection technique for repeating structures.* Istanbul : Proceedings of 4th IOMAC Conference, 2011.
41. **Bulut Y., Bernal D.** *Online Damage Detection by Fictive Parameter Updating.* Istanbul : Proceedings of 4th IOMAC Conference, 2011.
42. **Bakhshizade A., Ashory M.R.,Ghoshchian H.,Akbari M.** *A new criterion for structural damage detection using operational modal analysis.* Istanbul : Proceedings of 4th IOMAC Conference, 2011.
43. **Cantieni R., Brehm M., Zabel V.** *Ambient Testing and Model Updating of a Bridge for High-Speed Trains.* s.l. : Proceedings of IMAC XXVI, 2008.
44. **MacMillan B., Batel M.,Dascotte E.** *OMA testing by SLDV with FEM Pre and Post-test Analysis.* s.l. : Proceedings of IMAC XXII, 2004.
45. **Li T., Zhang J.Y.,Zhang W.H. and Zhu M.H.** *Vortex-Induced Vibration Characteristics of an Elastic Circular Cylinder.* s.l. : World Academy of Science, Engineering and Technology, 2009.
46. **Lee, B. H. K.** *Vertical tail buffeting of fighter aircraft.* s.l. : Progress in Aerospace Sciences Volume 36,Issues 3-4, p. 193-279, 2000.
47. **Pototzky A.S., Moses R.W.** *A Method to Analyze Tail Buffet Loads of Aircraft.* s.l. : NASA Langley Research Center, 2009.

48. **Chen Y., Ulker F.D.,Nalbantoglu V.,Yaman Y.** *Active Control of Smart Fin Model for Aircraft Buffeting Load Alleviation Applications.* s.l. : JOURNAL OF AIRCRAFT, 2009.
49. **H., Lienhard J.** *Synopsis of lift, drag, and vortex frequency data for rigid circular cylinders.* Pullman : Technical Extension Service, Washington State University, 1966.
50. **Dong S., Karniadakis G.E.** *DNS of flow past a stationary and oscillatingcylinder at Re=10000.* s.l. : Journal of Fluids and Structures, 2005.
51. **Jauvtis N., Williamson C.H.K.** *Vortex-induced vibration of a cylinder with two degrees of freedom.* s.l. : Mechanical and Aerospace Engineering,Upson Hall, Cornell University, 2003.
52. **Sarioglu M., Yavuz T.** *Vortex Shedding From Circular and Rectangular Cylinders Placed Horizontally in a Turbulent Flow.* s.l. : Turkish Journal of Engineering 24:p.217-228, 2000.
53. **Zhan S., Xu Y.L.,Zhou H.J.,Shum K.M.** *Experimental study of wind– rain-induced cable vibration using a new model setup scheme.* s.l. : Journal of Wind Engineering and Industrial Aerodynamics, 2008.
54. **Zhou L., Ge Y.** *Wind Tunnel Test for Vortex-induced Vibration of Vehicle-bridge System Section Mode.* s.l. : Journal of the Brazilian Society of Mechanical Sciences and Engineering, 2008.
55. **MSC.** *PATRAN 2010-v1 User's Guide.* s.l. : MSC, 2010.
56. —. *MSC Nastran Quick Reference Guide.* s.l. : MSC, 2010.
57. **H., Herlufsen.** *Modal Analysis using Multi-reference and Multiple-Input Multiple-Output Techniques.* s.l. : Brüel&Kjaer Application Note, 2002.
58. **Agilent.** *The Fundamentals of Modal Testing-Application Note.* s.l. : Agilent Technologies, 2000.
59. **P., Avitabile.** *Modal Space-In our own little world.* s.l. : University of Massachusetts Lowell, 2001.
60. **Brüel&Kjaer.** *Vibration Testing.* s.l. : Brüel&Kjaer Technical Booklet.
61. —. *Miniature DeltaTron® Accelerometers Types 4517 and 4517-002 Product Data.* s.l. : Brüel & Kjaer, 2005.

62. —. *Impact Hammers — Types 8206, 8206-001, 8206-002 and 8206-003 Product Data*. s.l. : Brüel&Kjaer, 2005.
63. —. *Modal Exciters Types 4825 and 4826-Product Data*. s.l. : Brüel&Kjaer, 2006.
64. **Agilent**. *Agilent 33120A Function/Arbitrary Waveform Generator Data Sheet*. s.l. : Agilent Technologies, 2004.
65. **Brüel&Kjaer**. *DeltaTron® Force Transducers Types 8230, 8230-001, 8230-002 and 8230-003 Product Data*. s.l. : Brüel&Kjaer, 2005.
66. —. *IDAe Hardware Configurations for PULSE- Types 3560-B, 3560-C, 3560-D and 3560-E System Data*. s.l. : Brüel&Kjaer, 2008.
67. —. *PULSE Labshop Software Help*. s.l. : Brüel&Kjaer.
68. **Mathworks**. *MATLAB 7 Getting Started Guide*. s.l. : Mathworks, 2011.
69. **M., Batel**. *Operational Modal Analysis –Another Way of Doing Modal Testing*. Georgia : SOUND AND VIBRATION, 2002.
70. **Gade S., Ventura C.** *Operational Modal Analysis-Pre-conference course notes-4th IOMAC*. Istanbul : Brüel&Kjaer, 2011.
71. **Brüel&Kjaer**. *Miniature DeltaTron Accelerometers Types 4507 and 4508 Product Data*. s.l. : Brüel&Kjaer, 2004.
72. **Mercan B., Ostovan Y., Dogan E., Uzol O.** *Effect of Chordwise Modulated Waveform Tip Injection on the Characteristics of the Tip Vortex*. s.l. : 40th Fluid Dynamics Conference and Exhibit, 2010.
73. **Anderson, J.D.** *Fundamentals of Aerodynamics*. s.l. : McGraw Hill, 2001. 0-07-237335-0.
74. **Dalton, C.** *Fundamentals of Vortex Induced Vibration- Lecture Notes*. s.l. : University of Houston, 1990.
75. **Techet, A.H.** *Vortex Induced Vibration- Lecture Notes*. s.l. : Massachusetts Institute of Technology, 2005.
76. **Buehrle R. D., Fleming G. A., Pappa R. S., Ferdinand W. G.** *Finite Element Model Development and Validation for Aircraft Fuselage Structures*. San Antonio, Texas : 18th International Modal Analysis Conference, 2000.
77. **Brüel & Kjaer, Product Data**. *Operational Modal Analysis — Type 7760 Software*. 2008.

APPENDIX A

ADDITIONAL ANALYSES

A.1. Mesh independency check for Finite Element Analysis(FEA)

Three different mesh densities are used for the Finite Element Model (FEM) of the fin to check the dependence of natural frequencies to the mesh densities. First five natural frequencies of the fin for these different mesh densities are given in Table A.1.

Table A.1. First five natural frequencies of the fin for different mesh densities

Mesh Number	Node Number	Element Number	Natural Frequencies [Hz]				
			Mode 1	Mode 2	Mode 3	Mode 4	Mode 5
1	210	189	28.96	92.99	152.63	229.85	351.38
2	783	756	28.10	91.76	148.99	227.82	351.97
3	3021	3024	27.03	89.60	144.51	222.92	347.33

A.2. Finite Element Analysis(FEA) for the fixture bar used in Classical Modal Analysis tests

The aluminium bar on which the fin-like structure is attached is also modelled in MSC®/PATRAN 2010-v1 as a 1-D beam element. Cross-sectional properties of the bar are also given to the program as shown in Figure A.1

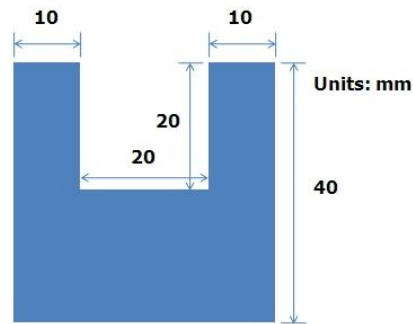


Figure A.1. Test fixture bar cross-section

In test setup the aluminium bar is fixed to test table at three points (i.e. at two ends and middle) with bolts. This boundary condition is simulated in FEM by restraining translations and rotations at all directions for the corresponding FEM nodes. At the end of the modal analysis by MSC®/NASTRAN 2010-v1 the first natural frequency of

the bar is determined at 2673 Hz. The mode shape for the first natural frequency is given in Figure A.2

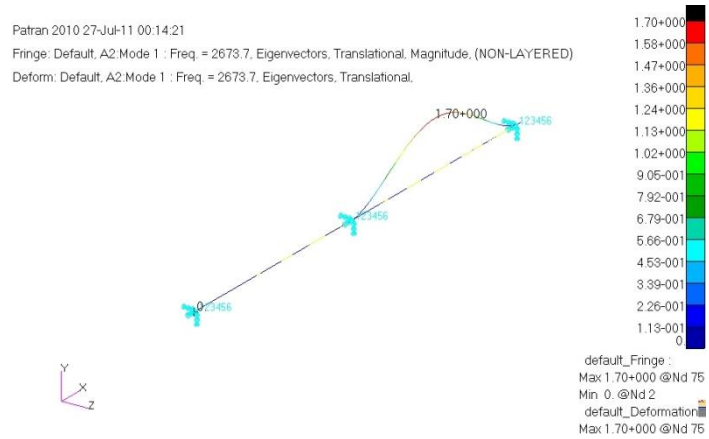


Figure A.2. Text fixture bar FEA result for the first mode

Since this value is away from the frequency range of interest of the fin (see Table 3.3) the possibility of interference of the test setup natural frequencies to fin modal analysis is eliminated.

A.3. Finite Element Analysis(FEA) for the test base used in Operational Modal Analysis tests

Test base where the fin is attached in wind tunnel tests includes the ring and the bar defined in Section 6.2. The dimensions of the test base are given Figure A.3.

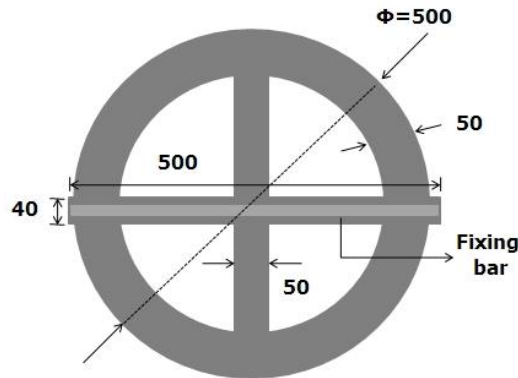


Figure A.3. Dimensions of the test base

Test base ring and the bar are modelled as shell elements in MSC[®]/PATRAN 2010-v1. Normal Modes (SOL 103) solution type in MSC[®]/NASTRAN 2010-v1 is to extract the natural frequencies of the test base. The first natural frequency of the test base is found as 414 Hz which is outside of the frequency range of interest of the fin regarding the first five modes (See Table 3.3). The first mode shape of the test base is given in Figure A.4.

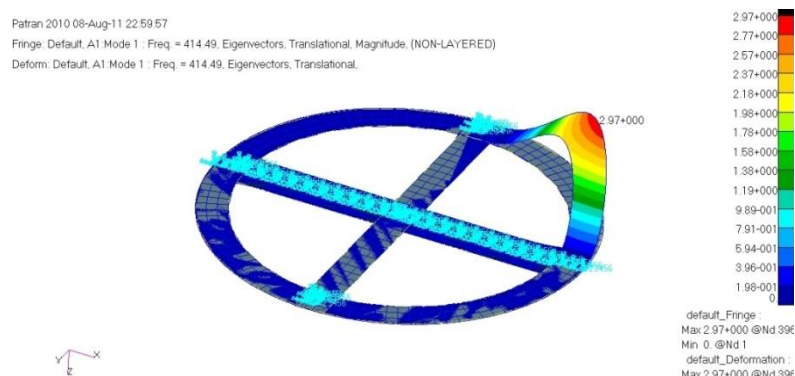


Figure A.4. The first mode shape of the test base

APPENDIX B

ADDITIONAL INFORMATIONS

B.1. Wind tunnel radial blower rotational speed vs. flow speeds

Table B.1. Blower motor rotational speed vs. flow speed table

Blower Motor Rotational Speed [Hz]	Flow Velocity [m/s]
2	4.78
3	7.06
4	9.06
5	10.99
6	12.57
7	13.96
8	14.79
9	15.39

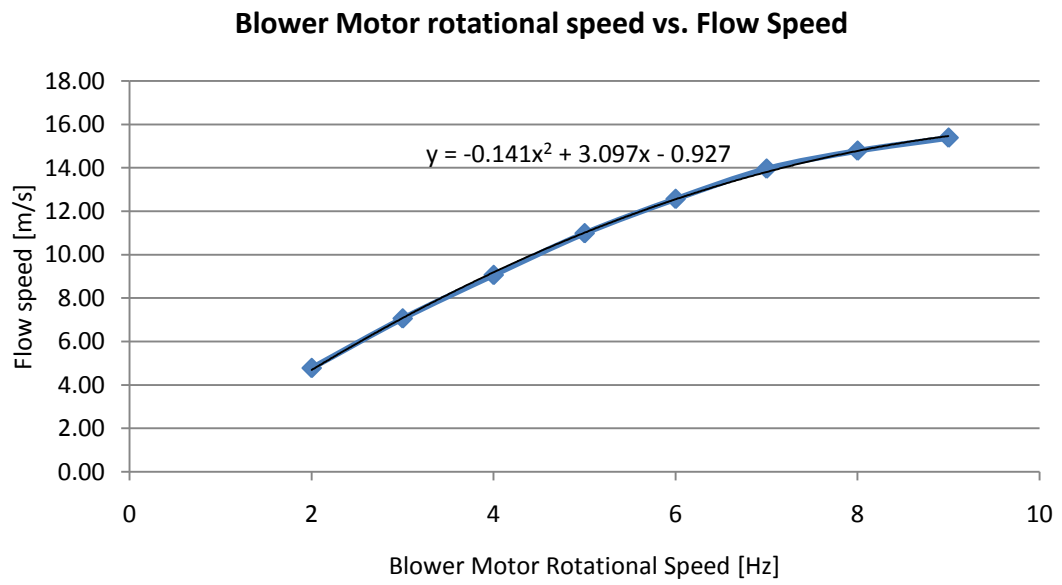


Figure B.1. Blower motor rotational speed vs. flow speed graph and fitted curve